Defense Nuclear Agency
Alexandria, VA 22310-3398

DNA-TR-88-37

Atomic and Molecular Collision Aspects of Thermospheric Uranium-Vapor Releases

Daniel A. Hamlin
Sciences Applications International Corporation
10260 Campus Point Drive
San Diego, CA 92121-1522

May 1990

Technical Report

DTIC
ELECTE
JUN 0 9 1990
D

90 05 09 154

Director
Defense Nuclear Agency
ATTN. TITL
Washington. DC 20305-1000

REPORT DOCUMENTATION PAGE

Public reporting burden for this collection of information is estimated to average 1 hour per response, including the time for reviewing instructions, searching existing data sources gathering and maintaining the data needed, and completing and reviewing the collection of information. Send comments regarding this burden estimate or any other aspect of this collection of information including suggestions for reducing this burden, to Washington Headquarters Services, Directorate for Information Operations and Reports, 1215 Jefferson Davis Highway, Suite 1204, Arlington, VA 22202-4302 and to the Office of Management and Budget. Paperwork Reduction Project (0704-0188) Washington DC 20503

1 AGENCY USE ONLY *(Leave blank)*	2. REPORT DATE 900501	3. REPORT TYPE AND DATES COVERED 821123 - Technical 800215-821130 & 851231

4 TITLE AND SUBTITLE
Atomic and Molecular Collision Aspects of Thermospheric Uranium-Vapor Releases

5 FUNDING NUMBERS
C - DNA 001-83-C-0055
  DNA 001-80-C-0137
PE - 62715H
PR - S99QMXB
  S99QAXH
TA - C
WU - DH006531

6 AUTHOR(S)
Daniel A. Hamlin

7 PERFORMING ORGANIZATION NAME(S) AND ADDRESS(ES)
Science Applications International Corporation
10260 Campus Point Drive
San Diego, CA 92121-1522

8 PERFORMING ORGANIZATION REPORT NUMBER
SAIC-89/1483

9 SPONSORING/MONITORING AGENCY NAME(S) AND ADDRESS(ES)
Defense Nuclear Agency
6801 Telegraph Road
Alexandria, VA 22310-3398

RAEE/Schwartz

10. SPONSORING/MONITORING AGENCY REPORT NUMBER
DNA-TR-88-37

11 SUPPLEMENTARY NOTES
This work was sponsored by Defense Nuclear Agency under RDT&E RMSS Codes B3220 83466 S99QMXBC 00068 H2590D, B3220 80464 S99QAXHC 30106 H2590D, B3220 84466 S99QMXBC 00104 H2590D, B3220 81466 S99QAXHC 00006 H2590D, B3220 84466 S99QMXBC

12a DISTRIBUTION/AVAILABILITY STATEMENT
Approved for public release; distribution is unlimited.

12b. DISTRIBUTION CODE

13. ABSTRACT *(Maximum 200 words)*
The DNA Uranium (Oxides) LWIR Review Committee considered the effectiveness of field measurements of the LWIR from uranium oxides produced by (hypothetical) controlled releases of uranium vapor from rockets in the thermosphere. Collated here is the writer's work supporting the committee on atomic and molecular collision aspects of such releases. Included is an essential auxiliary study to (a) understand, in terms of atomic and molecular parameters, coefficients for Ba^+ diffusion along the magnetic field as measured and predicted for Ba-release events and (b) apply that (limited) understanding to U-release studies. For (UO_n^{m+}) particles colliding with neutral atmospheric species, several interaction potentials are used to compute velocity-dependent momentum-transfer cross sections, stopping power and range versus energy, and diffusion coefficients. The momentum-transfer cross sections are also compared with cross sections for certain uranium oxide reactions specially atom-transfer reactions. Finally, rate coefficients are derived for selected uranium oxide reactions for which velocity-dependent cross sections are either known or assumed, based on extrapolations and/or averaged values of measurements.

14 SUBJECT TERMS
Nuclear Explosions
Nuclear Explosion Simulation
Infrared Backgrounds
Uranium Releases

15. NUMBER OF PAGES 138

16 PRICE CODE

17 SECURITY CLASSIFICATION OF REPORT	18 SECURITY CLASSIFICATION OF THIS PAGE	19 SECURITY CLASSIFICATION OF ABSTRACT	20 LIMITATION OF ABSTRACT
UNCLASSIFIED	UNCLASSIFIED	UNCLASSIFIED	SAR

CLASSIFIED BY

N/A since Unclassified

DECLASSIFY ON
N/A since Unclassified

11. SUPPLEMENTARY NOTES (Continued)

00105 H2590D, B3220 82466 S99QAXHC 00038 H2590D.

Accession For	
NTIS GRA&I	X
DTIC TAB	☐
Unannounced	☐
Justification	
By	
Distribution/	
Availability Codes	
	Avail and/or
Dist	Special
A-1	

CONVERSION TABLE

Conversion factors for U.S. Customary to metric (SI) units of measurement

MULTIPLY ──────────────► BY ──────────────► TO GET

TO GET ◄────────────── BY ◄────────────── DIVIDE

MULTIPLY / TO GET	BY	TO GET / DIVIDE
angstrom	1.000000 × E -10	meters (m)
atmosphere (normal)	1.01325 × E +2	kilo pascal (kPa)
bar	1.000000 × E +2	kilo pascal (kPa)
barn	1.000000 × E -28	meter² (m²)
British thermal unit (thermochemical)	1.054350 × E +3	joule (J)
calorie (thermochemical)	4.184000	joule (J)
cal (thermochemical) / cm²	4.184000 × E -2	mega joule/m² (MJ/m²)
curie	3.700000 × E +1	*giga becquerel (GBq)
degree (angle)	1.745329 × E -2	radian (rad)
degree Farenheit	$t_K = (t_F + 459.67)/1.8$	degree kelvin (K)
electron volt	1.60219 × E -19	joule (J)
erg	1.000000 × E -7	joule (J)
erg/second	1.000000 × E -7	watt (W)
foot	3.048000 × E -1	meter (m)
foot-pound-force	1.355818	joule (J)
gallon (U.S. liquid)	3.785412 × E -3	meter³ (m³)
inch	2.540000 × E -2	meter (m)
jerk	1.000000 × E +9	joule (J)
joule/kilogram (J/kg) (radiation dose absorbed)	1.000000	Gray (Gy)
kilotons	4.183	terajoules
kip (1000 lbf)	4.448222 × E +3	newton (N)
kip/inch² (ksi)	6.894757 × E +3	kilo pascal (kPa)
ktap	1.000000 × E +2	newton-second/m² (N-s/m²)
micron	1.000000 × E -6	meter (m)
mil	2.540000 × E -5	meter (m)
mile (international)	1.609344 × E +3	meter (m)
ounce	2.834952 × E -2	kilogram (kg)
pound-force (lbs avoirdupois)	4.448222	newton (N)
pound-force inch	1.129848 × E -1	newton-meter (N.m)
pound-force/inch	1.751268 × E +2	newton/meter (N/m)
pound-force/foot²	4.788026 × E -2	kilo pascal (kPa)
pound-force/inch² (psi)	6.894757	kilo pascal (kPa)
pound-mass (lbm avoirdupois)	4.535924 × E -1	kilogram (kg)
pound-mass-foot² (moment of inertia)	4.214011 × E -2	kilogram-meter² (kg m²)
pound-mass/foot³	1.601846 × E +1	kilogram/meter³ (kg/m³)
rad (radiation dose absorbed)	1.000000 × E -2	**Gray (Gy)
roentgen	2.579760 × E -4	coulomb/kilogram (C/kg)
shake	1.000000 × E -8	second (s)
slug	1.459390 × E +1	kilogram (kg)
torr (mm Hg, 0° C)	1.333220 × E -1	kilo pascal (kPa)

*The becquerel (Bq) is the SI unit of radioactivity; 1 Bq = 1 event/s.
**The Gray (Gy) is the SI unit of absorbed radiation.

TABLE OF CONTENTS

TABLE OF CONTENTS (Continued)

Appendices   Page

TABLE OF CONTENTS (Concluded)

LIST OF TABLES (Concluded)

SECTION 1

INTRODUCTION AND SUMMARY

1.1 BACKGROUND.

In the early 1980s the Defense Nuclear Agency began to investigate the long wavelength infrared backgrounds expected to result from high-altitude nuclear detonations. The gamut of activities included theoretical efforts, laboratory measurements of spectra and fluorescence efficiency, predictive computer codes, and research toward an upper atmospheric uranium-release simulation. In October 1982, H. C. Fitz, Jr. [Chief, Atmospheric Effects Division (RAAE)] established a six-member working group [Uranium (Oxides) LWIR Review Committee, chaired by I. L Kofsky of PhotoMetrics] to formally review all the technical aspects of that LWIR program. One major function of that committee was to consider the effectiveness of field measurements of the LWIR from uranium oxides produced by controlled releases of uranium vapor from rockets in the thermosphere. Reports of the committee reviews were provided in detailed memoranda by the chairperson to the RAAE program manager. An excellent overview of the committee's activities and the then-current status of the uranium oxides radiation program was prepared by Kofsky [Ref. 40; Section 2 & Appendix]. More recently, a report [Ref. 60] by Visidyne, Inc. personnel describes efforts directed principally to the design of an experiment for the release of uranium vapor in the upper atmosphere in sufficient quantity to permit an evaluation of the impact of high-altitude nuclear weapon debris emissions on advanced space systems.

1.2 SUMMARY.

In addition to the formal meetings of the Uranium (Oxide) LWIR Review Committee, the writer's more extended support of the committee was the preparation of numerous informal working memoranda on relatively narrow-in-scope technical issues which had been raised. Those selected topics involved aspects of neutral-neutral and ion-neutral atomic and molecular collisions for U-release conditions, i.e., velocity-dependent momentum-transfer cross-sections, stopping power and range versus energy, scattering angles, diffusion coefficients, and reaction rate coefficients. This information would ultimately be used to make improved estimates of the geometrical extent of the LWIR radiating region for U-release conditions. Those memoranda have been extensively reorganized and synthesized into the body of this report.

In Section 2 we consider the topic which is basic to the other sections, i.e., momentum-transfer cross-sections. Initially our general approach was (a) to consider some general formulas for atom-atom and ion-atom collisions, (b) to

apply and extend those formulas to [(O,O$^+$)+(O,N$_2$,O$_2$)]-collisions, since there is more known about such collisions than those for uranium species, and (c) to consider procedures for uranium-species collisions

More specifically, for atom-atom collisions at low velocities, we obtain velocity-dependent momentum-transfer cross-sections from the work of Hirshfelder, Bird, and Spatz [Ref. 31] by fitting the Lennard-Jones (12,6)-potential to the ground-state potential of the molecule corresponding to the colliding atoms. This cross section is then extended to lower relative velocities by using the asymptotic results of Monchick and Mason [Ref. 59] and of Kihara, Taylor, and Hirshfelder [Ref. 38] for an attractive (r^{-6})-potential. Thus, there are procedures available for computing momentum-transfer cross-sections for (O+O)- and (U+O)-collisions based on the (r^{-6})-potential.

The situation is more complicated for atom-molecule collisions. Our approach, for lack of a recognized simple alternative, is to consider collision-integrals, which are momentum-transfer cross-sections averaged over the relative velocity distributions in a Maxwellian gas at temperature T. We appeal to collision-integral results in the literature for [O+(O,N$_2$,O$_2$)]-collisions, from which we infer an approximate scaling factor to relate [O+(N$_2$,O$_2$)]-collisions to (O+O)-collisions. That same scaling factor is then applied to (U+O)-collisions to get cross sections for [U+(N$_2$,O$_2$)]-collisions.

For ion-atom collisions, at sufficiently low velocities where (at least for some collision pairs) the polarization force dominates, the momentum-transfer cross-section is based on the polarization potential (r^{-4}). Thus, a procedure, which seems to be on a relatively firm basis, is available for computing momentum-transfer cross-sections for (O$^+$+O)-collisions.

However, for (U$^+$+O)-collisions, we deduce evidence that the polarization potential appears to be inappropriate, owing to its smallness relative to the (r^{-6})-potential at the "orbiting radius." Perhaps the polarization potential should be replaced, in principle, by the (12,6,4)-potential or, in practice, by the (12,6)-potential (fitted to a ground-state UO$^+$ potential). As for atom-atom collisions, such a cross section can be extended to lower relative velocities by using the mentioned asymptotic results.

To proceed with [U$^+$+(O,N$_2$,O$_2$)]-collisions, in the middle of our U-release studies, we radically shifted our approach by detouring to study Ba$^+$ collisions with atmospheric species, hoping for useful insights. Indeed, that study, documented in Appendices A, B, C, and D, revealed the following very important facts (better appreciated after reading Appendix C) which were basic to the writer's subsequent U-release studies.

a.   The experimental mobility of Ba^+ in N_2 (at room conditions) agrees well with the theoretical value based on the polarization (r^{-4})-potential.

b.   The (r^{-6})-contribution dominates the (r^{-4})-contribution in the (12,6,4)-potential for (Ba^++O)-collisions (analogous to the situation for [(U,U^+)+O]-collisions).

c.   An effective value of the parameter $(r_m^6 \epsilon_o)^{1/3}$ – which appears in the asymptotic, low-energy momentum-transfer cross-section based on the (r^{-6})-potential – is postulated to be determined by requiring the equality of mobilities (at STP conditions) based on an effective (r^{-6})-potential and on the (r^{-4})-potential. (At non-STP conditions, the two mobilities will differ.)

d.   Values of the ambipolar diffusion coefficient $\left[D_{\|, \text{ Eff } (r^{-6})\text{-pot}} \right]$ computed from an effective (r^{-6})-potential are – for ionospheric ion temperatures ranging from 1135 K to 750 K – about 79% to 85% of the ambipolar diffusion coefficient $\left[D_{\|, \text{ pol. pot.}} \right]$ based on the polarization potential. An overall comparison of $D_{\|, \text{ Eff } (r^{-4})\text{-pot.}}$ with (sometimes ambiguous or uncertain) experimental values $\left[D_{\|, \text{ exp}} \right]$ derived from 12 Ba-releases is about the same as for $D_{\|, \text{ pol. pot.}}$, so that a strong preference cannot be established on this basis.

Not having the experimental mobility of U^+ in N_2 (or any gas), we qualitatively extrapolate from (Ba^++N_2)-collisions to [U^++(O,N_2,O_2)]-collisions and postulate that (a) the mobilities of U^+ in atmospheric species at STP conditions can be predicted by using the (r^{-4})-potential and (b) the effective values of the collision parameter $(r_m^6 \epsilon_o)^{1/3}$ can be determined by requiring equality of the mobilities (at STP conditions) based on an effective (r^{-6})-potential and on the (r^{-4})-potential. These postulates allow us to use all the general formulas developed in the Appendices for Ba^+ (and Ba) collisions and apply them to U^+ (and U) collisions. Those applications are documented in the remaining portions of Section 2.

In Section 3 the overall goal is to obtain simple range-energy relations for low-energy uranium species traversing the ambient atmosphere. Such relations are obtained by integrating an appropriate stopping-power formula involving mean values of the momentum-transfer cross-sections developed in Section 2.

To obtain a stopping-power formula for a single particle traversing a Maxwellian gas, we adapt ideas from Banks [Ref. 6] who was interested in the related problem of elastic collisions and energy transfer between gases which have separate Maxwellian velocity distributions. Banks [Ref. 6] shows that the

3

exact equation, derived by Deslogue [Ref. 17], for the energy transfer rate between gases of arbitrary temperature and particle mass, can be separated into three fundamental factors, each of which depends on a different aspect of the collision process and gas composition, i.e., (1) a ratio of particle masses, (2) the difference in the gas thermal energies, and (3) a nonequilibrium collision frequency for energy transfer which entails a mean nonequilibrium momentum-transfer cross-section.

Banks [Ref. 6] acknowledges that his decomposition of Deslogue's formula [Ref. 17] is not rigorous since he did not use the proper averaging techniques of kinetic theory needed to arrive at an exact expression. Whatever shortcoming that fact imposes probably is not very important relative to (a) our additional approximations and (b) the uncertainty in the basic cross sections used in our applications. To provide insights concerning the numerous approximations required to obtain simple analytical expressions, we first sketch Banks' development in general terms, followed by more details with equations and our adapted formulas, as given in Section 3.

In Section 4 we present (a) formulas (developed in Appendices A and D) for the ordinary and ambipolar diffusion coefficients, based on both the polarization potential and the effective (r^{-6})-potential discussed in Section 2 and (b) evaluation of the diffusion coefficients at four altitudes [200(25)275 km] in a quiet MSIS-83 atmosphere.

In Section 5 we compare some of our momentum-transfer cross-sections developed in Section 2 with cross sections for certain uranium-oxide reactions, specially atom-transfer reactions. (This writer expects momentum-transfer cross-sections should exceed atom-transfer cross-sections.) As a by-product of these considerations, rate coefficients are derived for selected uranium oxide reactions for which velocity-dependent cross-sections are either known or assumed, based on extrapolations and/or averaged values of measurements.

As previously mentioned, the work presented in Appendices A, B, C, and D was developed during the auxiliary study of Ba^+ collisions. Early in that study the writer found that the (ordinary) ion diffusion coefficient was written differently by various authors. Thus, a first step was to reconcile those different expressions, as is done in Appendix A. We also specialize the formulas for several parameters [(a) the mean momentum-transfer cross-section, (b) the collision time, (c) the mobility, and (d) the diffusion coefficient] for three interaction potentials [(a) polarization (r^{-4}), (b) (r^{-6}), and (c) (hybrid) effective (r^{-6})]. These formulas are written explicitly for a binary gas, except that for the diffusion coefficient which is valid for a multicomponent gas.

In Appendix B we elaborate on ion-neutral collisions in a multicomponent gas by (a) commenting on literature formulas for collision time, (b) presenting explicit formulas based on both the polarization potential and effective (r^{-6})-potential, valid in a multicomponent gas, for mobility, collision time, and diffusion coefficient, and (c) comparing the Ba^+ collision times computed from various formulas for a number of altitudes in a selected atmosphere.

In Appendix C we discuss Ba and Ba^+ collisions with atmospheric species. (It is these considerations which influenced our treatment of uranium collisions.) For (Ba^++O)-collisions, we have two simple methods for estimating momentum-transfer cross-sections. The first, based on a polarization-potential interaction, would probably be the natural choice. However, estimates indicate that the r^{-6} term is much more important than the r^{-4} term. Thus, we are led to seek a compromise between these two conflicting approaches. Several observations obtain:

(a)   The experimental mobility of Ba^+ in N_2 [Powell and Brata, unpublished [Ref. 58]] can be predicted to within about four percent by use of the polarization potential, as shown in detail.

(b)   A similar situation is postulated to hold for (Ba^++O)-collisions.

(c)   There are reservations about the applicability of the polarization potential at the higher velocities.

(d)   There is concern about the (r^{-6})-potential giving a larger momentum-transfer cross-section for $(Ba+O)$-collisions than that given by the polarization potential for (Ba^++O)-collisions at (room) thermal energies.

In view of these considerations we suggest a compromise by introducing what we will call an effective (r^{-6})-potential, determined by requiring an equality of mobilities (at STP conditions) based on (a) an effective (r^{-6})-potential and on (b) the polarization potential. This requirement is equivalent to an equality of mean momentum-transfer cross-sections (at STP conditions) based on the same two potentials, since the mobility is (inversely) proportional to the mean momentum-transfer cross-section. The effective (r^{-6})-potential is also applied to $[Ba^++(N_2,O_2)]$-collisions.

In Appendix D we introduce the ambipolar diffusion coefficient, $D_a \approx D_i (1 + T_e / T_i)$ (where D_i is the ordinary diffusion coefficient, and T_e and T_i are the electron and ion temperatures), and present limited comparisons of (a) theoretical results for the coefficient of ambipolar diffusion of Ba^+ along the direction of the geomagnetic field, $D_{||}$ (taken to be equal to D_a), with (b) experimental results for some barium release experiments. The motivation is to see whether such experiments can provide a basis for preferring either the polarization potential or the effective (r^{-6})-potential in computing the ambipolar diffusion coefficient. Such comparisons have many uncertainties, including those

5

for selection of a model (neutral-particle) atmosphere and the assignment of the ratio of the electron- and ion-temperatures. An overall comparison of $D_{\|, \text{Eff } (r^{-6})\text{-pot}}$ with $D_{\|, \text{exp}}$ (derived from 12 Ba-releases) is about the same as for $D_{\|, \text{pol pot}}$, so that a strong preference cannot be established on this basis, unless one should have reasons (unknown to the writer) to select or exclude certain experimental data.

In Appendix E we present the relative speed for a monoenergetic beam traversing a Maxwellian gas, based on two approximate formulas and the exact formula; one of the approximate expressions is used in Section 3. Appendix F presents the differential and integral Maxwellian energy distributions.

SECTION 2

MOMENTUM-TRANSFER CROSS-SECTIONS

A very useful and convenient survey of momentum-transfer cross-sections is given by Stoeckly, Stagat, and Kilb [Ref. 65], but values directly applicable to U-release species and conditions are not given. Hence, our approach will be (a) to present some general formulas for atom-atom and ion-atom collisions, (b) to apply and extend those formulas to [(O,O$^+$)+(O,N$_2$,O$_2$)]-collisions, and (c) to consider procedures for uranium-species collisions.

2.1 ATOM-ATOM AND ION-ATOM COLLISIONS: GENERAL.

2.1.1 Atom-Atom Collisions.

2.1.1.1 <u>Lennard-Jones (12,6)-Potential.</u> For the Lennard-Jones (12,6)-potential, which is written in alternative forms,

$$\Phi(r) = 4\varepsilon_o\left[\left(\frac{D}{r}\right)^{12} - \left(\frac{D}{r}\right)^6\right] = \varepsilon_o\left[\left(\frac{r_m}{r}\right)^{12} - 2\left(\frac{r_m}{r}\right)^6\right] \qquad (1a,b)$$

$$D = r_m / 2^{1/6} = 0.8909\, r_m \ , \qquad (1c)$$

Hirschfelder, Bird, and Spatz [Ref. 31] tabulate the reduced momentum-transfer cross-section $S^{(1)}(\kappa)$ (in units of πD^2) for the reduced-energy range $0.1 \le \kappa \le 100$ (from which selected values will be presented later). Here, ε_o is the depth of the potential at its minimum, r_m is the radius at which the minimum energy $(-\varepsilon_o)$ occurs, and D is the radius at which the potential is zero. The cross section πD^2 is interpreted as that for rigid spherical particles of collision diameter D. Hence, for such spheres, $S^{(1)}(\kappa)$ would be unity. The reduced energy κ is defined as

$$\kappa = E_{CM} / \varepsilon_o \qquad (2a)$$
$$E_{CM} = \tfrac{1}{2}\mu g^2 \qquad (2b1)$$
$$E_{CM}(eV) = 5.188\times10^{-3}\,\mu(A)\; g^2_{km/sec} \qquad (2b2)$$

where μ is the reduced mass for the colliding particles,

$$\mu = \frac{M_1 M_2}{M_1 + M_2} = M_o\,\mu(A) \qquad (3a)$$

7

$$\mu(A) = \frac{A_1 A_2}{A_1 + A_2}, \qquad M_o = 1.66 \times 10^{-24} \text{ g},$$

(3b,c)

and g is the relative velocity. To relate g to κ we write

$$g = \left[\frac{2\varepsilon_o \kappa}{\mu}\right]^{1/2} = 1.388 \times 10^6 \left[\frac{\varepsilon_o \kappa}{\mu(A)}\right]^{1/2}.$$

(4a,b)

The momentum-transfer cross-section $\sigma(g)$, based on the Lennard-Jones (12,6)-potential, is

$$\sigma(g) = \pi D^2 S^{(1)}(\kappa).$$

(5)

2.1.1.2 <u>Asymptotic Extension to Low Energies.</u> To extend these cross sections to lower velocities, we use asymptotic values derived by Monchick and Mason [Ref. 59] who state that the reduced cross-section (in units of πD^2),

$$S^{(\lambda)} \equiv 2\left[1 - \frac{1}{2}\frac{1+(-1)^\lambda}{1+\lambda}\right]^{-1} \int_0^\infty (1-\cos^\lambda \chi)\, b\, db,$$

(6)

takes the asymptotic form

$$S^{(\lambda)} \equiv 2\left[1 - \frac{1}{2}\frac{1+(-1)^\lambda}{1+\lambda}\right]^{-1} \left[\frac{nd}{\frac{1}{2}\mu g^2}\right]^{2/n} A_{\pm}^{(\lambda)}(n)$$

(7)

at low energy for which the potential becomes, in general,

$$\phi(r) = \pm |d| \left[\frac{D}{r}\right]^n.$$

(8)

In Eq. (7), $A_{\pm}^{(\lambda)}(n)$ is a pure number whose value depends only on the power n of the potential and on whether the potential is repulsive (subscript +) or attractive (subscript -). Reference 59 gives the values of $A_{\pm}^{(\lambda)}(n)$ in its Table I, taken from Kihara, Taylor, and Hirschfelder [Ref. 38].

For the Lennard-Jones (12,6)-potential, at low energy we have

$$\phi(r) \Rightarrow -4\varepsilon_o \left[\frac{D}{r}\right]^6.$$

(9)

Thus,

$$n = 6, \qquad d = 4\varepsilon_o$$

(10a,b)

and we need $A_-^{(1)}(6)$, given in Table I of Ref. 59 as

$$A_-^{(1)}(6) = 0.4342$$

(11)

8

Thus, from Eqs. (7), (3), (10), and (11), we have

$$S^{(1)} = 3.117 \times 10^4 \left[\frac{\varepsilon_o}{\mu(A)\, g^2} \right]^{1/3} . \qquad (12a)$$

By combining Eqs. (5), (1c), and (12a) (cf. Appendix A.3.1.2), we have

$$\sigma(g)\big|_{(r^{-6})\text{-pot.}} = C \left(\frac{r_m^6 \varepsilon_o(eV)}{\mu\, g^2} \right)^{1/3} = C' \left(\frac{r_m^6 \varepsilon_o(eV)}{\mu(A)g^2} \right)^{1/3} \qquad (12b,c)$$

$$= C'' \left(\frac{r_m^6 \varepsilon_o(eV)}{\mu(A)\, g_{km/sec}^2} \right)^{1/3} \qquad (12d)$$

$$C = 9.204 \times 10^{-4}, \qquad C' = 7.773 \times 10^4 \qquad (12e,f)$$

$$C'' = 36.08. \qquad (12g)$$

2.1.2 Ion-Atom Collisions.

2.1.2.1 Polarization Potential. At sufficiently low velocities where the polarization force between an ion and neutral dominates, the velocity-dependent momentum-transfer cross-section for singly-charged ions [Ref. 7, Pt. A, p. 218] is

$$\sigma_D = 2.21\pi\, [\alpha e^2 / \mu\, g^2]^{1/2} = 2.59 \times 10^{-9} [\alpha' / \mu(A)]^{1/2}\, g^{-1}, \qquad (13a,b)$$

where α is the polarizability of the neutral particle (with α' in units of 10^{-24} cm^3), e is the electronic charge, and μ and g are as defined in Section 2.1.1.

This cross section is only a little larger than that for "orbiting collisions" [Ref. 55, p. 72],

$$q_o = \pi\, b_o^2 = 2\pi\, [\alpha e^2 / \mu\, g^2]^{1/2} = \pi [2\alpha e^2 / E_{CM}]^{1/2} \qquad (13c1)$$

$$b_o(10^{-8}\, cm) = 8.635\, [\alpha' / \mu(A)]^{1/4}\, g_{km/sec}^{-1/2} \qquad (13c2)$$

For an impact parameter equal to b_o, the ion spirals into a circular orbit of radius

$$r_o = b_o / \sqrt{2} . \qquad (13d)$$

From Ref. 55, p. 72: "Orbits for which $b < b_o$ pass through the origin if no repulsive core is present, whereas those orbits for which $b \geq b_o$ come no closer than $r_o = b_o / \sqrt{2}$ "

2.1.2.2 <u>(12,6,4)-Potential.</u> The (12,6,4)-potential [cf. Ref. 65] is

$$\Phi(r) = \frac{\varepsilon_o}{2}\left[(1+\gamma)\left(\frac{r_m}{r}\right)^{12} - 4\gamma\left(\frac{r_m}{r}\right)^{6} - 3(1-\gamma)\left(\frac{r_m}{r}\right)^{4}\right] \qquad (14a1)$$

$$= \frac{\varepsilon_o}{2}[T_{12} + T_6 + T_4], \qquad (14a2)$$

where the dimensionless parameter γ is a measure of the relative contributions of the T_6 and T_4 terms. For $\gamma = 1$ we recover the Lennard-Jones (12,6)-potential given by Eq. (1) and for $\gamma = 0$ we have the (12,4)-potential. To determine γ, as was done in Ref. 65, we require the T_4 term to match the polarization potential,

$$\Phi(r)\big|_{polarization} = -\frac{e^2 \alpha}{2r^4}, \qquad (14b)$$

whereupon

$$\gamma = 1 - \frac{e^2 \alpha}{3\varepsilon_o r_m^4}$$

$$= 1 - 4.806\frac{\alpha'}{\varepsilon_o (eV)(r_m')^4}, \qquad (14c)$$

with r_m' in units of 10^{-8} cm.

We will be interested in the momentum-transfer cross-sections corresponding to the full (12,6,4)-potential. Such cross sections (in units of πr_m^2) have been computed for γ-values of 0, 0.25, and 0.50 by Mason and Schamp [Ref. 51, Table 2; Ref. 52; Ref. 56, Table 1-3]. Similar cross sections (in units of πD^2) have been computed for the (12,6)-potential – which implies $\gamma = 1$ for the (12,6,4)-potential – by Hirschfelder et al. [Ref. 31]. The calculations [Ref. 31] for $\gamma = 1$ were for a different set of κ-values than were those by Ref. 51; hence, the first step in using these results was to interpolate Ref. 31 results to obtain results for the same set of κs as in Ref. 51. Next, for later use, we interpolated between the results for $\gamma = 0.5$ and $\gamma = 1$ to obtain results for $\gamma = 0.75$. Finally, we interpolated again to obtain results at γ-values of interest for $(O^+ + O)$– and $(U^+ + O)$–collisions, i.e., at respective γ-values of 0.6869 and 0.960. The results from Ref. 51 and Ref. 31 (the latter multiplied by $(2^{1/6})^{-2}$) and the interpolated results are given in Table 1.

10

Table 1. Reduced momentum-transfer cross-sections for (12,6,4)-potential (in units of πr_m^2).

$\tan^{-1}\kappa$	κ	$\sigma/\pi r_m^2$						
		$\gamma=0$	0.25	0.50	0.6896[d]	0.75	0.960[e]	$\gamma=1$
	0.0		2.7072					
	0.1							4.322[b]
	0.2							3.553[b]
0.2[a]	0.20271[a]	5.501[a]	4.918[a]	4.306[a]	3.95[c]	3.84[c]	3.57[c]	3.52[c]
	0.4							2.673[b]
0.4[a]	0.42279[a]	3.719[a]	3.432[a]	3.137[a]	2.93[c]	2.87[c]	2.64[c]	2.60[c]
	0.6							2.309[b]
0.6[a]	0.68414[a]	2.892[a]	2.730[a]	2.506[a]	2.39[c]	2.35[c]	2.22[c]	2.19[c]
	0.8							2.002[b]
0.7[a]	0.84229[a]	2.394[a]	2.333[a]	2.258[a]	2.15[c]	2.12[c]	2.01[c]	1.99[c]
	0.9							1.988[b]
	0.95							1.958[b]
	1.0							1.906[b]
0.8[a]	1.0296[a]	1.974[a]	1.950[a]	1.926[a]	1.91[c]	1.91[c]	1.89[c]	1.89[c]

[a] Ref. 56, Table I-3.
[b] Ref. 31, Table VIII, multiplied by $(2^{1/6})^{-2} = 0.79370$.
[c] Interpolated.
[d] For $O^+ + O$; see Fig. 5.
[e] For $U^+ + O$; see Fig. 9

2.2 $[(O,O^+)+(O,N_2,O_2)]$-COLLISIONS.

2.2.1 (O+O)-Collisions.

Values of $S^{(1)}(\kappa)$ for the range $0.1 \le \kappa \le 2$ [HB-48] are reproduced in Table 2. To relate these data with results in Ref. 65, we apply the data to (O+O)-collisions. The potential energy parameters [Ref. 65, p. 40] are

$$\varepsilon_0 = 5.22\,\text{eV}, \qquad r_m = 1.22 \times 10^{-8}\,\text{cm}, \qquad (15a,b)$$

so that with use of Eq. (1c) we have

$$D = 1.09 \times 10^{-8}\,\text{cm}. \qquad (15c)$$

From Eq. (4) the relative velocity g is related to κ by

$$g = 1.121 \times 10^6\,\kappa^{-1/2}. \qquad (16)$$

The momentum-transfer cross-section $\sigma(g)$, Eq. (5), is given in units of 10^{-16} cm^2 in Table 2 and plotted in Fig. 1. These values for (O+O)-collisions agree well with those plotted in Fig. 4-3 of Ref. 65.

Table 2. Velocity-dependent momentum-transfer cross-sections from Ref. 31 for Lennard-Jones (12,6)-potential and application to (O+O)- and (U+O)-collisions.

κ	$[S^{(1)}(\kappa)]^a$	O + O		U + O	
		g,cm/sec	σ^b	g,cm/sec	σ^b
0.1	5.445	3.54 E+05	20.2	3.16 E+05	45.9
0.2	4.476	5.01 E+05	16.6	4.47 E+05	37.8
0.4	3.368	7.09 E+05	12.5	6.32 E+05	28.4
0.6	2.909	8.68 E+05	10.8	7.74 E+05	24.6
0.8	2.523	1.00 E+06	9.36	8.93 E+05	21.3
0.9	2.505	1.06 E+06	9.30	9.47 E+05	21.1
0.95	2.467	1.09 E+06	9.16	9.73 E+05	20.8
1.0	2.401	1.12 E+06	8.91	9.99 E+05	20.3
1.2	2.1007	1.23 E+06	7.80	1.09 E+06	17.7
1.4	1.8714	1.33 E+06	6.95	1.18 E+06	15.8
1.6	1.6974	1.42 E+06	6.30	1.26 E+06	14.3
1.8	1.5656	1.50 E+06	5.81	1.34 E+06	13.2
2.0	1.4801	1.59 E+06	5.49	1.41 E+06	12.5
		Fig. 1		Fig. 6	

[a] Reduced cross-sections $[S^{(1)}(\kappa)]$, in units of πD^2, from Ref. 31, Table VIII Potential parameters are given by Eq. (15) for (O+O) and by Eq. (22) for (U+O).

[b] Cross sections are in units of 10^{-16} cm^2.

To extend these cross sections to lower velocities, we use Eqs. (5) and (12) to give us

$$\sigma(O+O)\big|_{(r-6)-pot} = 1.00 \times 10^{-11}\, g^{-2/3}\ \mathrm{cm}^2 \tag{17a}$$

$$= 4.64 \times 10^{-15}\, g_{km/sec}^{-2/3}\ \mathrm{cm}^2. \tag{17b}$$

For $g = 3.54 \times 10^5$ cm/sec, Eq. (17) gives 20×10^{-16} cm^2, in excellent agreement with the lowest-energy value in Table 2. We will adopt Eq. (17) as the appropriate relative-velocity momentum-transfer cross-section for (O+O)-collisions for the

12

relative velocity range less than about 5×10^5 cm/sec, shown as the dashed line ($\leq 3 \times 10^5$ cm/sec) in Fig. 1
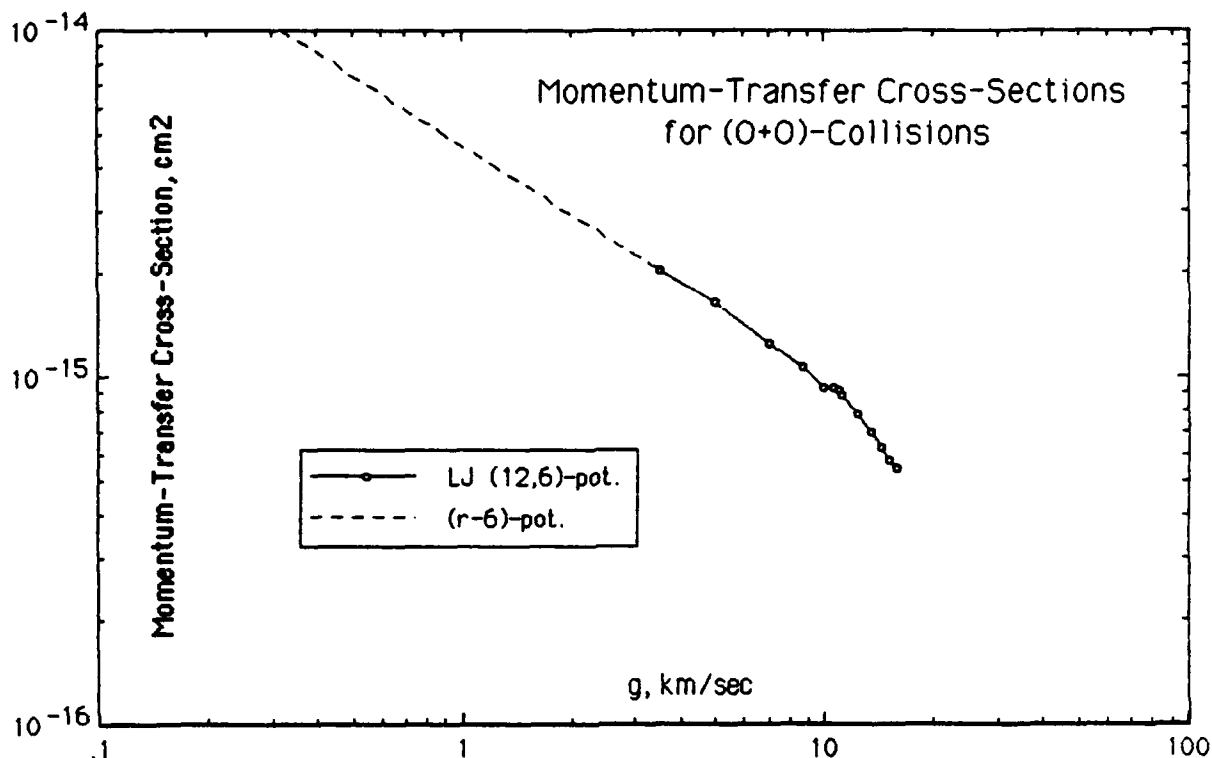
Figure 1. Velocity-dependent momentum-transfer cross-sections for (O+O)-collisions, based on Lennard-Jones (12,6)-potential and asymptotic (r^{-6})-potential.

2.2.2 [O+(N_2,O_2)]-Collisions.

To eventually obtain cross sections for [U+(N_2,O_2)]-collisions, we will appeal to collision-integral results for [O+(O,N_2,O_2)]-collisions, from which we infer an approximate scaling factor to relate [O+(N_2,O_2)]-collisions to (O+O)-collisions. That same scaling factor will then be applied to (U+O)-collisions.

We would prefer to see momentum-transfer *cross-sections* for [O+(O,N_2,O_2)]-collisions, but what we find to be available (without an exhaustive search) are *collision integrals*, i.e., momentum-transfer cross-sections averaged over the relative velocity distribution in a Maxwellian gas at temperature T. Such a cross section (or collision integral for diffusion) is defined by Eq. (A8c) in Appendix A. Yun and Mason [Ref. 69] have computed and tabulated such integrals

13

(called $\langle \bar{\sigma}^{(1,1)} \rangle$ in their notation and expressed in units of 10^{-16} cm^2 but without a necessary factor of π to make them a conventional cross section) for the various species in dissociating air for the temperature range $1000 \leq T(K) \leq 15000$. (It appears, notwithstanding an otherwise description, that Ref. 69 accounts for a large number of excited states in computing averages for atom-atom collisions, whereas we have limited our considerations to ground-state interactions.) We will regard these collision integrals as pseudo velocity-dependent momentum-transfer cross-sections by expressing them as a function of the average relative velocity between the two members of each of the three pairs of particles of interest, i.e., $O+O$, $O+N_2$, and $O+O_2$. In such a gas the average relative velocity [Eq. (A8b)] is

$$\bar{g}_{ik} = \left[\frac{8kT}{\pi \mu_{ik}} \right]^{1/2} = 1.45 \times 10^4 \left[\frac{T}{\mu(A_{ik})} \right]^{1/2}, \qquad (18)$$

where the reduced mass number $\mu(A_{ik})$ is 8, 10.18, and 10.67 for the three stated pairs. Values of $\bar{g}_{ik}$ are given in Cols. 2, 3, and 4 of Table 3. Collision integrals presented as a function of temperature in Ref. 69 (Tables III, VII, and VI) are given here (but multiplied by π) in Cols. 5, 6, and 7 of Table 3 as a function of the temperature and in Fig. 2 as a function of the average relative velocity.
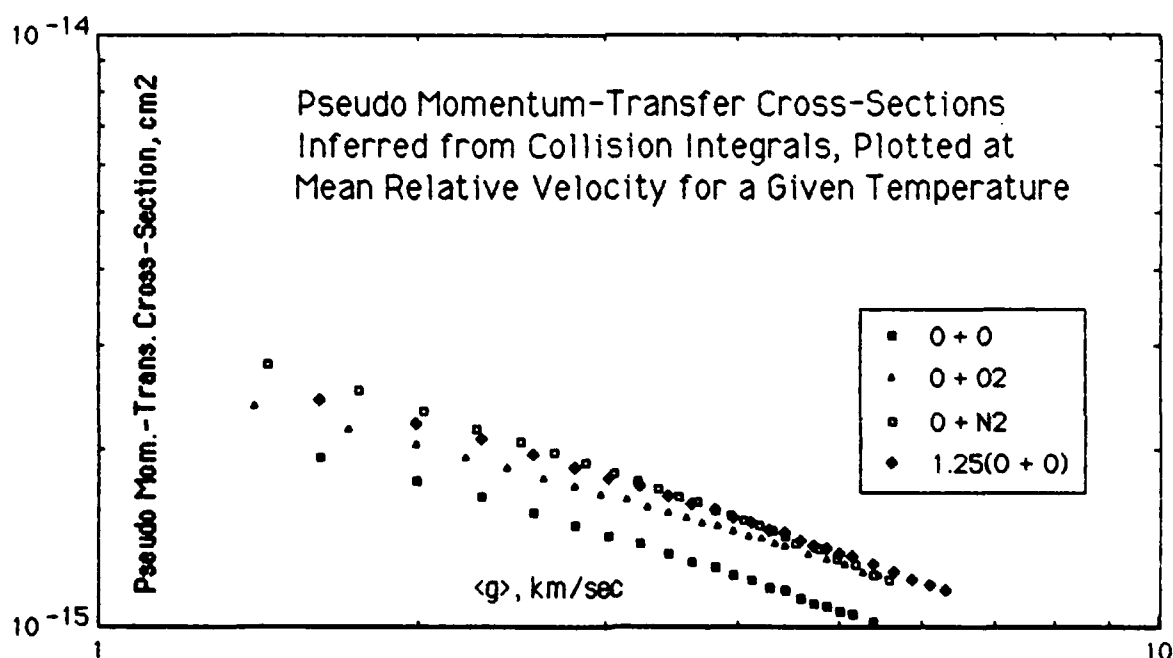
Figure 2. Pseudo momentum-transfer cross-sections versus mean relative velocity $\langle g \rangle = [8kT / \pi \mu]^{1/2}$, inferred from temperature-dependent collision integrals [Ref. 69] for $[O+(O,N_2,O_2)]$-collisions at gas temperatures in the range $1000 \leq T(K) \leq 15000$

Table 3. Pseudo momentum-transfer cross-sections versus mean relative velocity, inferred from collision integrals [Ref 69] for [O+(O,N$_2$,O$_2$)]-collisions for gas temperatures in the range $1000 \le T(K) \le 15000$

T	$\bar{g}_{ik}$, km/sec			$\pi\langle\bar{\Omega}^{(1,1)}\rangle$, 10^{-16} cm^2		
1000 K	O+O	O+N$_2$	O+O$_2$	O+O	O+N$_2$	O+O$_2$
1.0	1.62	1.44	1.40	19.4	27.9	23.6
1.5	1.99	1.76	1.72	17.7	25.1	21.6
2.0	2.29	2.03	1.99	16.6	23.2	20.3
2.5	2.56	2.27	2.22	15.6	21.7	19.3
3.0	2.81	2.49	2.43	14.9	20.6	18.5
3.5	3.03	2.69	2.63	14.3	19.7	17.8
4.0	3.24	2.87	2.81	13.8	18.9	17.3
4.5	3.44	3.05	2.98	13.3	18.2	16.8
5.0	3.62	3.21	3.14	12.9	17.6	16.4
5.5	3.80	3.37	3.29	12.6	17.1	16.0
6.0	3.97	3.52	3.44	12.3	16.6	15.6
6.5	4.13	3.66	3.58	12.0	16.2	15.3
7.0	4.29	3.80	3.71	11.7	15.8	15.0
7.5	4.44	3.94	3.84	11.5	15.4	14.8
8.0	4.59	4.06	3.97	11.2	15.1	14.5
8.5	4.73	4.19	4.09	11.0	14.8	14.3
9.0	4.86	4.31	4.21	10.8	14.5	14.1
9.5	5.00	4.43	4.33	10.6	14.2	13.9
10.0	5.13	4.54	4.44	10.5	13.9	13.7
11.0	5.38	4.77	4.66	10.2	13.5	13.3
12.0	5.62	4.98	4.86	9.89	13.0	13.0
13.0	5.84	5.18	5.06	9.64	12.7	12.7
14.0	6.07	5.38	5.25	9.41	12.3	12.4
15.0	6.28	5.57	5.44	9.21	12.0	12.2
(1)	(2)	(3)	(4)	(5)	(6)	(7)
				Fig. 2	Fig. 2	Fig. 2

It is of interest to relate the (O+O)-values in Fig. 2 to the asymptotic values given by Eq. (17). Firstly, in Fig. 2 the slope is closely -2/3 at the higher velocities, as in Eq. (17), but it decreases at the lower velocities. Secondly, substitution of Eq. (17) into Eq. (A8c) yields

$$Q_D(O+O) = 2.74 \times 10^{-15} (T/1000)^{-1/3}. \tag{19}$$

At 1000 K, Eq. (19) gives a value larger than the 1000-K value for (O+O)-collisions in Table 3 by the ratio 2.74/1.94 = 1.41 (a ratio which would be about 1.21 if the slope in Fig. 2 did not decrease). The lack of complete consistency between Eq. (17) and Fig. 2 may be due partly to the pseudo nature of the cross sections in Table 3 and Fig. 2 and partly to the aforementioned inclusion in Ref. 69 of excited states with their concomitant variety of potential curves.

We emphasize that we are less concerned with the absolute values in Fig. 2 than the values for (O+N$_2$)- and (O+O$_2$)-collisions relative to those for (O+O)-collisions. We see that, viewed very simply, 5/4 is a factor by which we can convert from (O+O)-cross-sections to approximate mean values for (O+N$_2$)- and (O+O$_2$)-collisions.

2.2.3 (O$^+$+O)-Collisions.

Since we will later describe some reservations about applying the polarization potential for UO$_n^+$-collisions with atmospheric species, we will consider, first, (O$^+$+O)-collisions for which we feel there is a relatively firm basis.

We now apply Eq. (14) for the (12,6,4)-potential. For O, $\alpha' = 0.79$ (cf. Table A-1); for O$_2^+$, $r_m \approx 1.164 \times 10^{-8}$ cm and $\varepsilon_o \approx 6.663$ eV [Ref. 34, p. 504]. Thus, from Eq. (14c) we find

$$\gamma(O^+ + O) = 0.6896. \tag{20}$$

In Fig. 3a we plot $-\varphi(r)$ from Eq. (14a) and in Fig. 3b, the ratio (R) of the T_4 term to the sum of the T_4 and T_6 terms:

$$R = \frac{T_4}{T_4 + T_6}. \tag{21}$$

In Fig. 4 we plot b_o from Eq. (13c), r_o from Eq. (13d), and the center-of-mass energy E_{CM} from Eq. (2b). Figures 3 and 4 enable one to consider the relative magnitudes of the T_4 and T_6 terms, for various velocities, as given in Table 4. We see that for velocities below 3 km/sec, the T_4 term is at least half of the total of the two attractive terms even at the orbit-radius $r_o = b_o/\sqrt{2}$. For such velocities, use of the T_4 term alone would probably be satisfactory in computing the momentum-transfer cross-section, shown in Fig. 5 as the solid line computed from Eq. (13d),

16

Figure 3a. Radial dependence of the (12,6,4)-potential for (O++O)-collisions.

Figure 3b. Radial dependence of the ratio of the (r^{-4})-term to the sum of the (r^{-4})- and (r^{-6})-terms in the (12,6,4)-potential for (O++O)-collisions.

17

Figure 4. Relative velocity dependence of the "orbiting impact parameter" b_o, "orbiting radius" r_o, and center-of-mass energy E_{CM} for (O⁺+O)-collisions.

Table 4. Comparison of the T_4 and T_6 terms in the (12,6,4)-potential for (O⁺+O)-collisions.

g	10^{-8} cm		E_{CM}	Eq.(21)	
km/sec	b_o	$b_o/\sqrt{2}$	eV	$R(b_o)$	$R(b_o/\sqrt{2})$
0.3	8.83	6.25	3.74 E-03	≈ 0.96	0.91
1	4.84	3.42	4.15 E-02	0.85	0.74
3	2.79	1.98	3.74 E-01	0.66	0.50
5	2.16	1.53	1.04 E+00	0.54	0.37

$$\sigma(O^+ + O)\big|_{pol.pot.} = 8.14 \times 10^{-10}\ g^{-1} = 8.14 \times 10^{-15}\ g_{km/sec}^{-1} \qquad (13d1,d2)$$

The cross sections corresponding to the reduced cross-sections in Table 1 (for the column corresponding to Eq. (20)) are plotted as the circled points in Fig. 5 for the relative velocity range $5.7 \leq g(\text{km/sec}) \leq 12.86$. The dashed line in Fig. 5 extrapolates these values to about 3 km/sec where the line intercepts the cross section [Eq. (13d)] for the pure polarization potential.

Figure 5. Velocity-dependent momentum-transfer cross-sections for $(O^+ + O)$- collisions, based on (12,6,4)-potential, its extrapolation, and polarization potential.

2.3 $[(U, U^+, UO^+) + (O, N_2, O_2)]$-COLLISIONS.

2.3.1 Introduction.

In midcourse of our U-release studies, we paused to study Ba^+ collisions with atmospheric species, hoping that useful insights would be obtained. That study, documented in Appendices A, B, C, and D, revealed the following important facts:

a. The experimental mobility of Ba^+ in N_2 (at room conditions) agrees well with the theoretical value based on the polarization (r^{-4})-potential.

b. The (r^{-6})-contribution dominates the (r^{-4})-contribution in the (12,6,4)-potential for $(Ba^+ + O)$-collisions (analogous to the situation for $[(U, U^+) + O]$-collisions, as will be shown later).

c. An effective value of the parameter $(r_m^6 \varepsilon_o)^{1/3}$ – which appears in the asymptotic, low-energy momentum-transfer cross-section based on the (r^{-6})-potential – is postulated to be determined by requiring the equality of mobilities (at STP conditions) based on an effective (r^{-6})-potential and on the (r^{-4})-potential. (At non-STP conditions, the two mobilities will differ.)

19

d. Values of the ambipolar diffusion coefficient $\left[D_{\parallel, \text{Eff } (r^{-6})\text{-pot}}\right]$ computed from an effective (r^{-6})-potential are — for ionospheric ion temperatures ranging from 1135 K to 750 K — about 79% to 85% of the ambipolar diffusion coefficient $\left[D_{\parallel, \text{pol pot}}\right]$ based on the polarization potential. An overall comparison of $D_{\parallel, \text{Eff } (r^{-6})\text{-pot}}$ with (sometimes ambiguous or uncertain) experimental values $\left[D_{\parallel, \text{exp}}\right]$ derived from 12 Ba-releases is about the same as for $D_{\parallel, \text{pol pot}}$, so that a strong preference cannot be established on this basis

It would be desirable to have an experimental mobility for U^+ in N_2 (or any gas). Not having that information, we will make the qualitative extrapolation from $(Ba^+ + N_2)$-collisions to $[U^+ + (O, N_2, O_2)]$-collisions and assume that the mobilities of U^+ in atmospheric species at STP conditions can be predicted by use of the (r^{-4})-potential. We will also assume that effective values of the parameter $(r_m^6 \varepsilon_o)^{1/3}$ can be determined by requiring equality of the mobilities (at STP conditions) based on an effective (r^{-6})-potential and on the (r^{-4})-potential. These assumptions allow us to use all the general formulas we developed in the Appendixes for Ba^+ collisions, and we will refer to them when convenient. For completeness, we will also include the work performed prior to our consideration of Ba^+ collisions. Table 5 collates numerous parameters needed in the subsequent discussion

Table 5. Parameters for UO_n^{m+} collisions with neutral atmospheric species

k	α'_k	$\mu(A_{i,k})$ $i = U, U^+$	UO^+	UO_2^+	$[\alpha'_k / \mu(A_{i,k})]^{1/2}$ $i = U, U^+$	UO^+
0	0.79	14.99	15.05	15.10	0.230	0.229
N_2	1.76	25.05	25.22	25.37	0.265	0.264
O_2	1.59	28.21	28.42	28.61	0.237	0.236

k	$[\alpha'_k]^{1/2}[\mu(A_{i,k})]^{-1/3}$ $i = U, U^+$	UO^+	$[\alpha'_k \mu(A_{i,k})]^{1/2}$ $i = U, U^+$	UO^+	UO_2^+
0	0.360	0.360	3.44	3.45	3.45
N_2	0.453	0.452	6.64	6.66	6.68
O_2	0.414	0.413	6.70	6.72	6.74

2.3.2 [U+(O,N$_2$,O$_2$)]-Collisions.

2.3.2.1 (U+O)-Collisions. To obtain the momentum-transfer cross-section for (U+O)-collisions based on the (r^{-6})-potential, we adopt values of the potential parameters available at the beginning of this study, i.e., those given by Michels [Ref. 57, p. 185].

$$\varepsilon_o \approx 7.76\,eV, \qquad r_m \approx r_e = 1.84 \times 10^{-8}\ cm \qquad (22a,b)$$
$$D = 0.8909\,r_m = 1.64 \times 10^{-8}\ cm. \qquad (22c)$$

To relate the relative velocity to κ, we use Eq. (3b) to get
$$\mu(A) = 14.99, \qquad (23a)$$

which, with Eqs. (22) and (4b), gives

$$g = 9.987 \times 10^5\,\kappa^{1/2}. \qquad (23b)$$

The momentum-transfer cross-section from Eq. (5), based on the Lennard-Jones (12,6)-potential,
$$\sigma(g) = 8.44 \times 10^{-16}\,S^{(1)}(\kappa), \qquad (24)$$

is given in units of 10^{-16} cm^2 in Table 2 and plotted in Fig. 6.

To obtain cross sections at velocities below about 3×10^5 cm/sec, we use Eq. (12a), with Eqs. (22a), (22c), and (23), to get

$$\sigma(U+O)\big|_{(r^{-6})-pot} = 2.11 \times 10^{-11}\,g^{-2/3} = 9.79 \times 10^{-15}\,g_{km/sec}^{-2/3}\ cm^2. \qquad (25a,b)$$

For $g = 3.16 \times 10^5$ cm/sec, Eq. (25) gives 45.5×10^{-16} cm^2, in excellent agreement with the lowest-energy value in Table 2. We will adopt Eq. (25) as the appropriate relative-velocity momentum-transfer cross-section for (U+O)-collisions, based on the (r^{-6})-potential, for the relative velocity range less than about 5×10^5 cm/sec, as shown as the dashed line ($\leq 3 \times 10^5$ cm/sec) in Fig. 6.

To obtain the cross section for the effective (r^{-6})-potential, we use Eq. (A20) and the parameters in Table 5 to get

$$\sigma(U+O)\big|_{Eff.(r^{-6})-pot.} = 1.38 \times 10^{-11}\,g^{-2/3} = 6.41 \times 10^{-15}\,g_{km/sec}^{-2/3}\ cm^2. \qquad (26a,b)$$

Equation (26) is also plotted in Fig. 6.
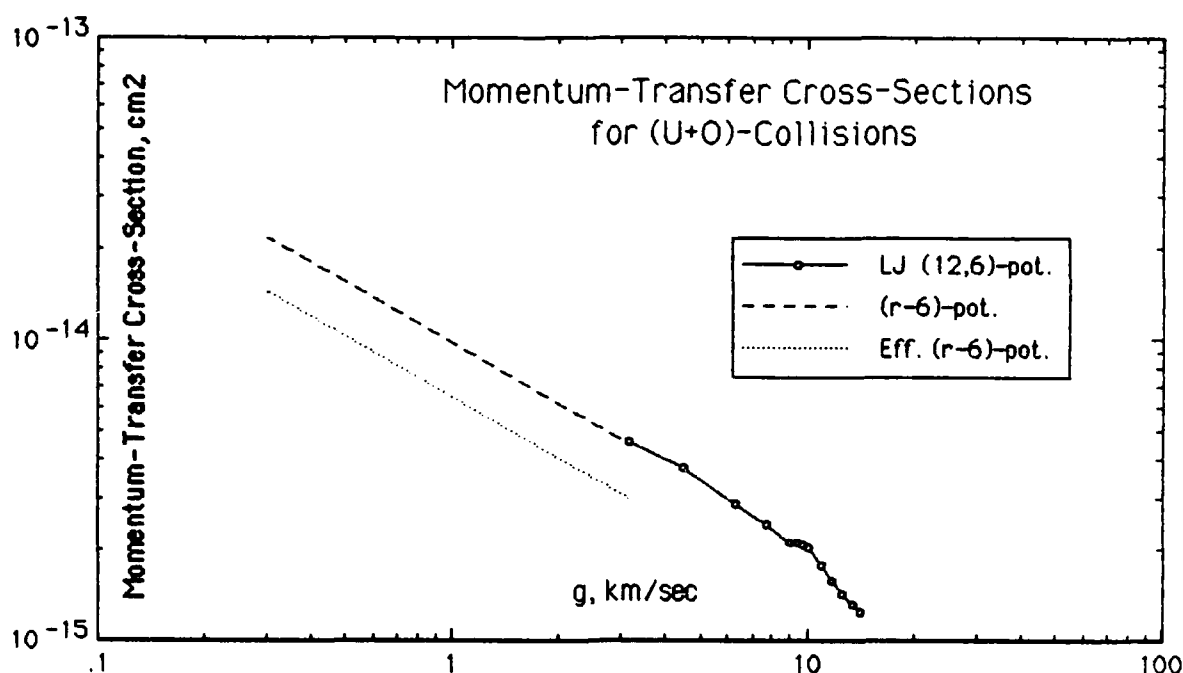
Figure 6. Velocity-dependent momentum-transfer cross-sections for (U+O)-collisions, based on Lennard-Jones (12,6)-potential, asymptotic (r^{-6})-potential, and effective (r^{-6})-potential.

2.3.2.2 [U+(N$_2$,O$_2$)]-Collisions. For an interaction we will label $\approx$(r^{-6})-potential (even though it is straining the concept), we appeal to results for [O+(O,N$_2$,O$_2$)]-collisions and apply the approximate scaling factor inferred in Section 2.2.2 to relate [O+(N$_2$,O$_2$)]-collisions to (O+O)-collisions, i.e., 5/4. By applying this factor to Eq. (25) we have

$$\sigma[U+(N_2,O_2)]\big|_{\approx(r^{-6})\text{-pot.}} = \tfrac{5}{4}\,\sigma(U+O)\big|_{(r^{-6})\text{-pot.}} \tag{27a1}$$

$$= 2.64\times10^{-11}\,g^{-2/3}\ \text{cm}^2 \tag{27a2}$$

$$= 1.24\times10^{-14}\,g_{km/sec}^{-2/3}\ \text{cm}^2. \tag{27a3}$$

For the effective (r^{-6})-potential, we use Eq. (A20) and parameters in Table 5 to get

$$\sigma(U+N_2)\big|_{\text{Eff.}(r^{-6})\text{-pot.}} = 1.74\times10^{-11}\,g^{-2/3}\ \text{cm}^2 \tag{27b1}$$

$$= 8.08\times10^{-15}\,g_{km/sec}^{-2/3}\ \text{cm}^2 \tag{27b2}$$

$$\sigma(U+O_2)\big|_{\text{Eff.}(r^{-6})\text{-pot.}} = 1.59\times10^{-11}\,g^{-2/3}\ \text{cm}^2 \tag{27c1}$$

$$= 7.38\times10^{-15}\,g_{km/sec}^{-2/3}\ \text{cm}^2. \tag{27c2}$$

22

2.3.3 [U^{++}(O,N$_2$,O$_2$)]-Collisions.

2.3.3.1 (U$^+$+O)-Collisions. For (U^{++}O)-collisions characterized by the (12,6,4)-potential given in Eq. (14a), we use the UO$^+$ parameters [Ref. 57, p. 196]

$$\varepsilon_o \approx 8.15\,eV, \qquad r_m \approx 1.843 \times 10^{-8}\,cm \qquad\qquad (28a,b)$$

and find from Eq. (14c) that

$$\gamma(U^+ + O) = 0.960. \qquad\qquad (28c)$$

We interpret the closeness of γ to 1 as a strong hint that the polarization potential by itself is unsatisfactory for (U^{++}O)-collisions in the velocity range of current interest.

In Fig. 7a we plot $-\Phi(r)$ from Eq. (14a), evaluated for the parameters given in Eq. (28), and in Fig. 7b, the ratio (R) given by Eq. (21). In Fig. 8 we plot b_o from Eq. (13c), r_o from Eq. (13a), and the center-of-mass energy E_{CM} from Eq. (2b). In Table 6 we collate the comparison of the T_4 and T_6 terms for (U^{++}O)-collisions. The smallness of the T_4 term relative to the total of the two attractive terms, even at the lowest velocity of interest here (0.3 km/sec), seems to be another strong hint that the polarization potential by itself is unsatisfactory for (U^{++}O)-collisions. In Fig. 9 the momentum-transfer cross-section for the polarization potential is shown as the short-dash line, computed from Eq. (13b) and

$$\sigma(U^+ + O)\big|_{pol.pot.} = 5.96 \times 10^{-10}\,g^{-1} \quad cm^2 \qquad\qquad (29a)$$

$$= 5.96 \times 10^{-15}\,g^{-1}_{km/sec} \quad cm^2. \qquad\qquad (29b)$$

Table 6. Comparison of the T_4 and T_6 terms in the (12,6,4)-potential for (U^{++}O)-collisions.

g	10^{-8} cm		E_{CM}	Eq.(21)	
km/sec	b_o	$b_o/\sqrt{2}$	eV	$R(b_o)$	$R(b_o/\sqrt{2})$
0.3	7.55	5.34	7.00 E-03	0.35	0.21
1	4.14	2.93	7.78 E-02	0.14	0.073
5	1.85	1.31	1.94 E+00	0.031	0.016

Again, we are interested in using the full (12,6,4)-potential to obtain the momentum-transfer cross-section. (Owing to the closeness of $\gamma(U^+ + O)$ to unity per Eq. (28), we expect little difference from using just the (12,6)-potential.) The interpolated values of the reduced cross-section are given in Table 1 for $\gamma = 0.960$ and the actual cross-sections are given in Table 7 and plotted in Fig. 9 as the
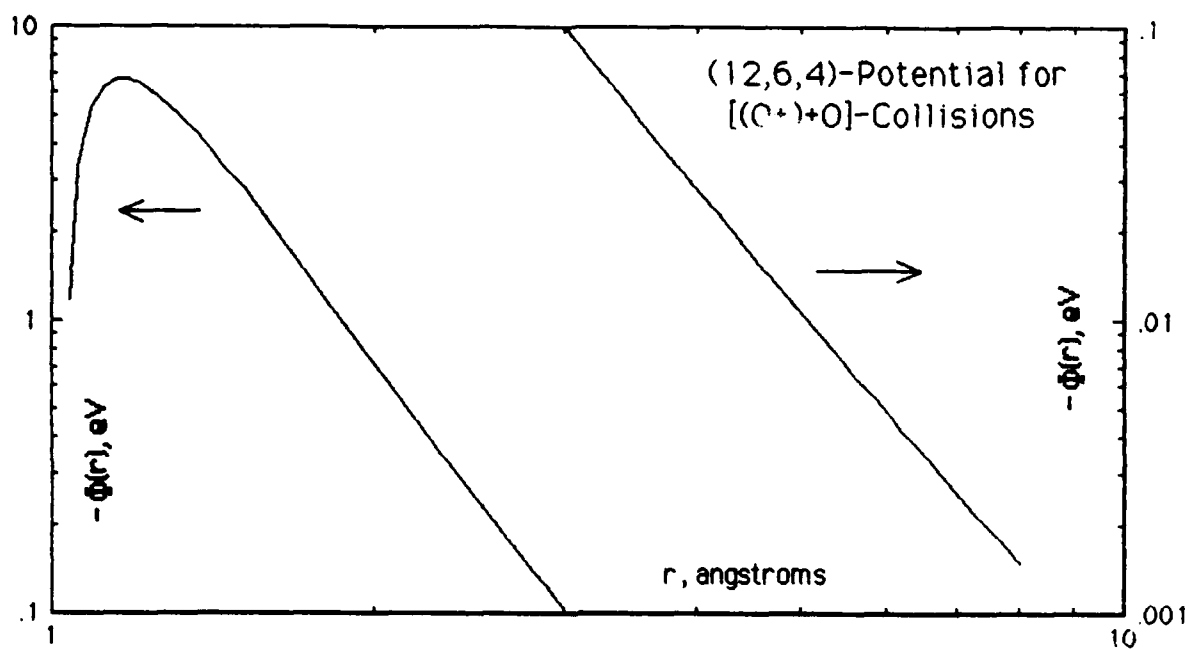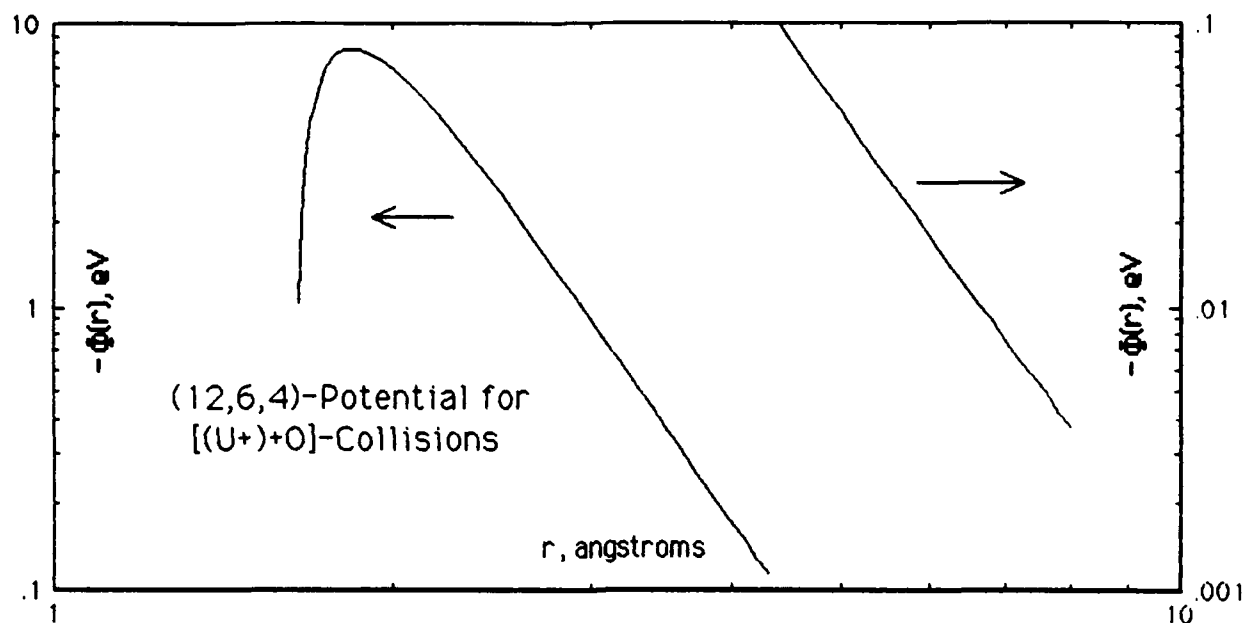
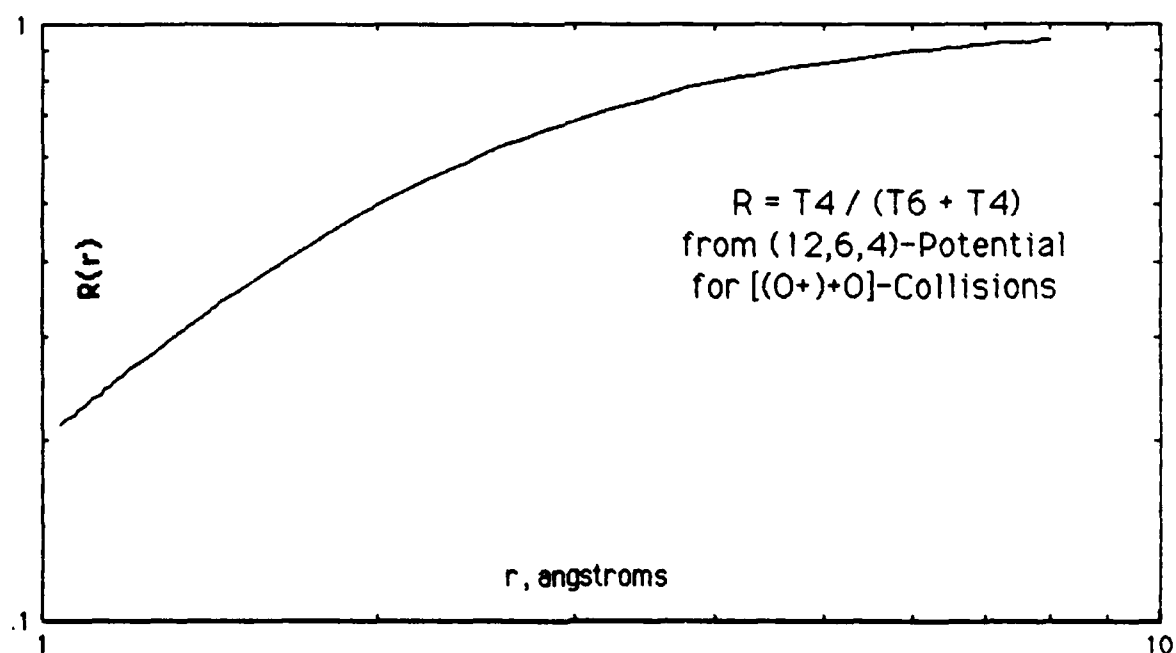Figure 7a. Radial dependence of the (12,6,4)-potential for (U$^+$+O)-collisions.
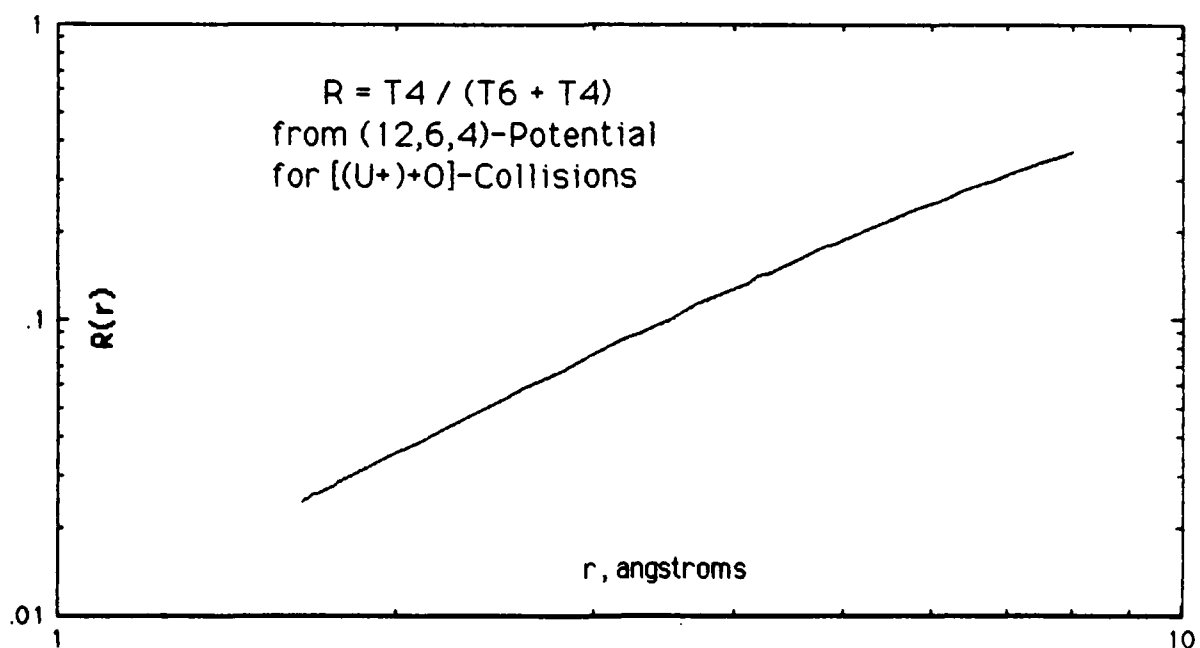
Figure 7b. Radial dependence of the ratio of the (r^{-4})-term to the sum of the (r^{-4})- and (r^{-6})-terms in the (12,6,4)-potential for (U$^+$+O)-collisions
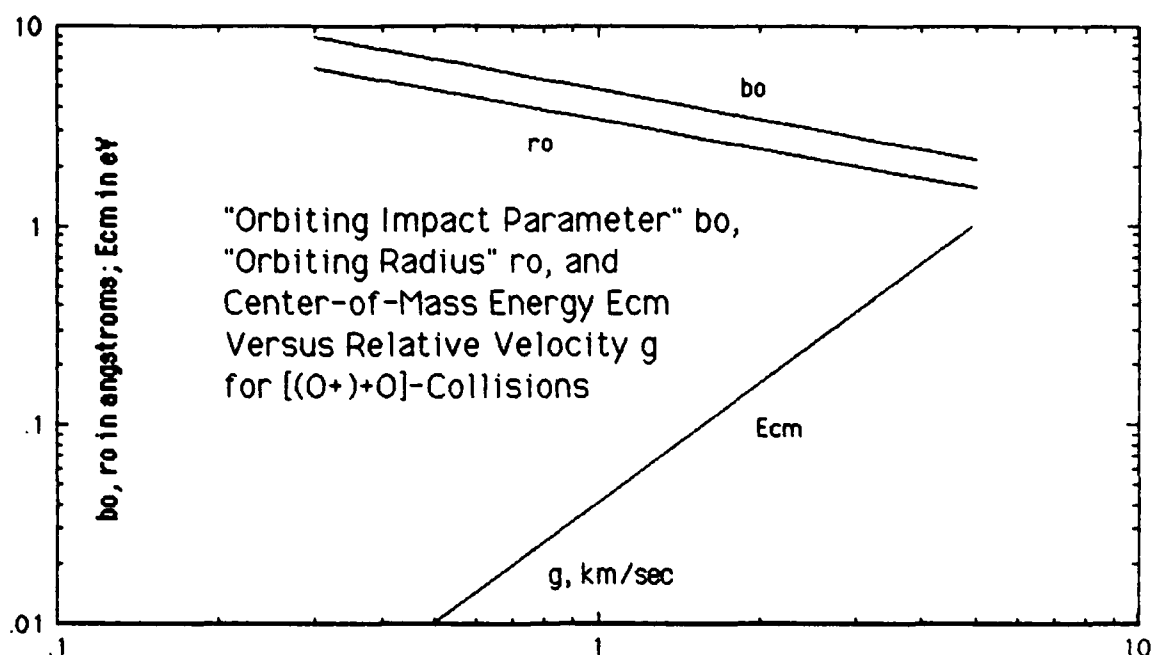
24
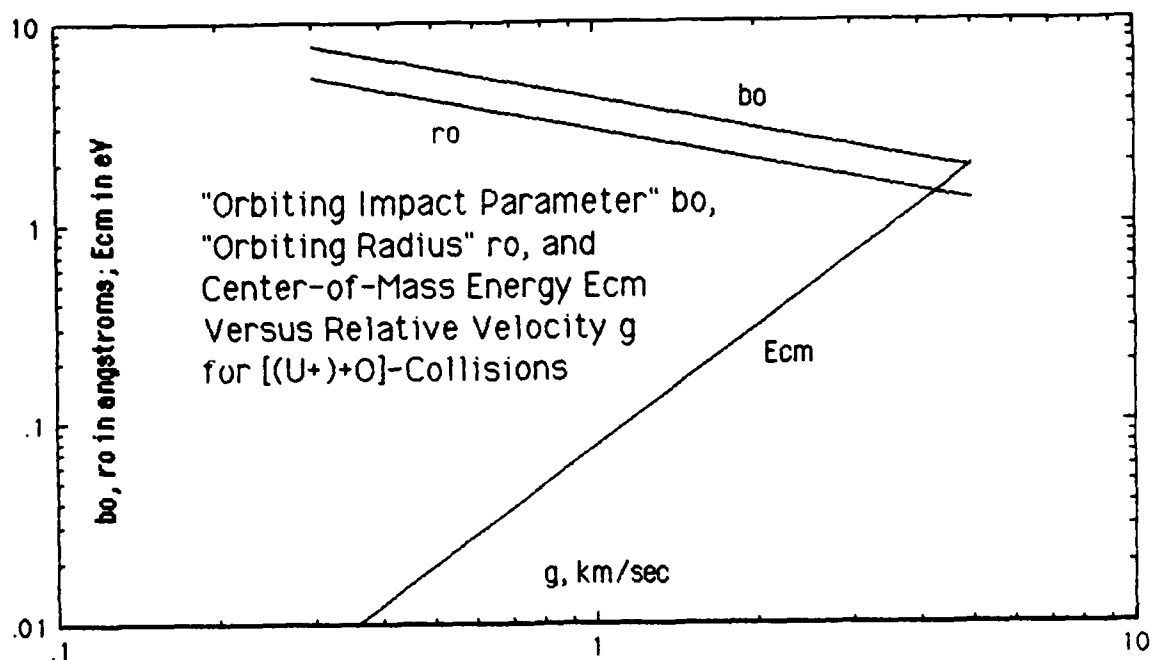
Figure 8. Relative velocity dependence of the "orbiting impact parameter" b_o, "orbiting radius" r_o, and center-of-mass energy E_{CM} for $(U^+ + O)$-collisions.
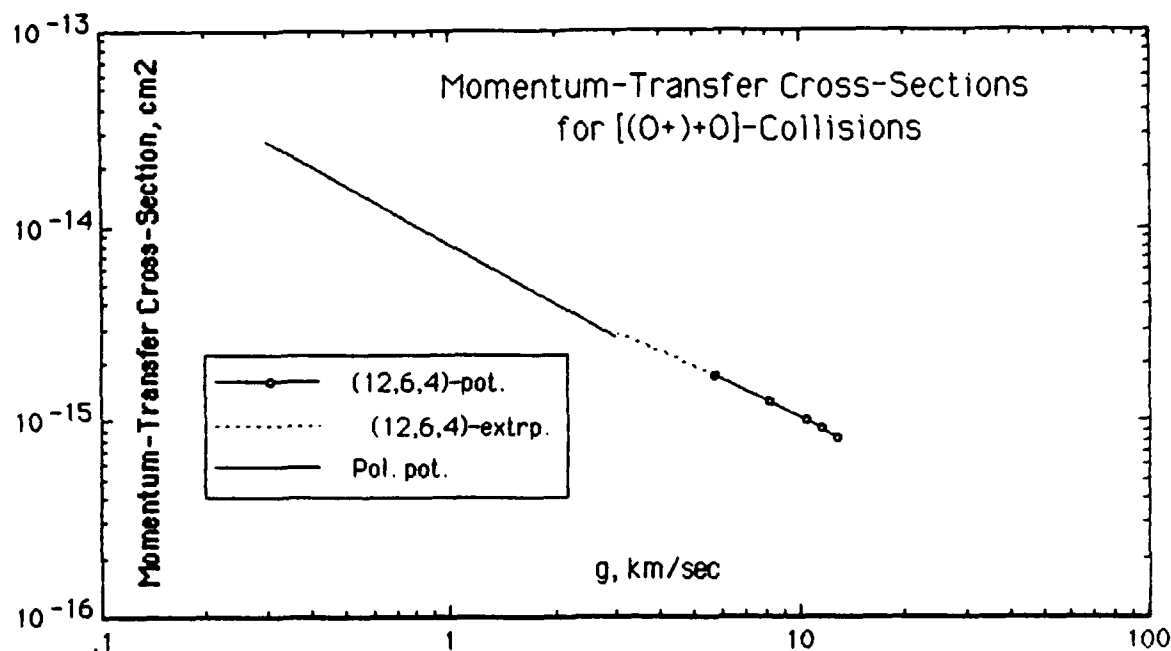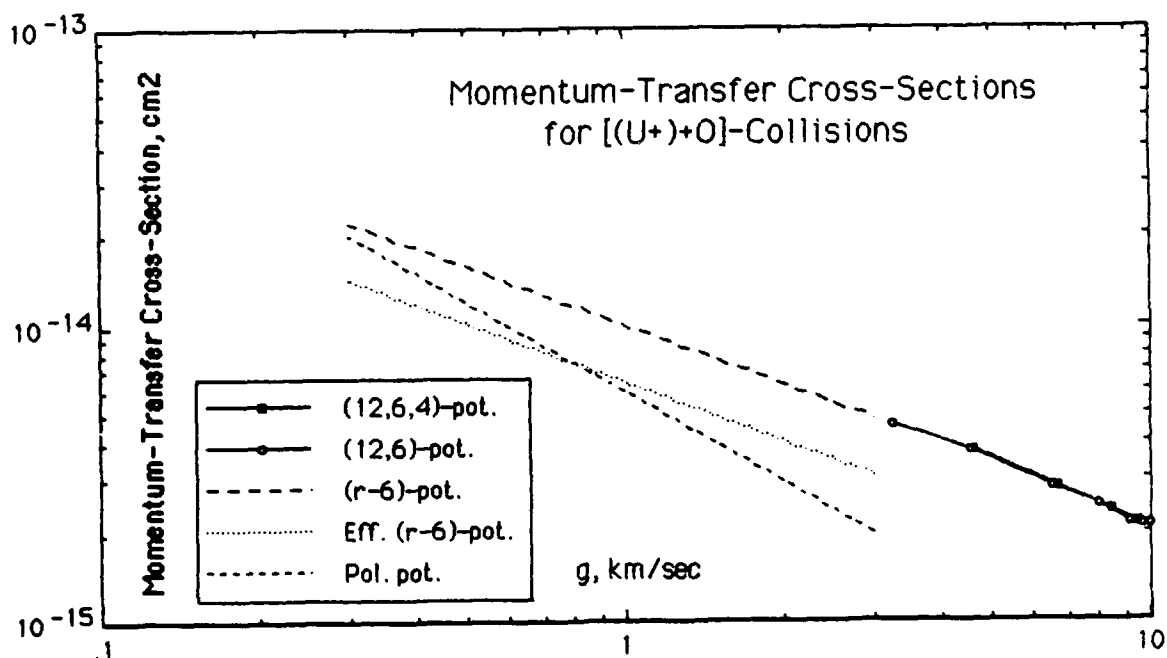

Figure 9. Velocity-dependent momentum-transfer cross-sections for $(U^+ + O)$-collisions, based on (12,6,4)-potential, Lennard-Jones (12,6)-potential, asymptotic (r^{-6})-potential, effective (r^{-6})-potential, and polarization potential.

solid-square points. The velocities in Table 7 are computed from Eq. (4b), with ξ_0 given by Eq. (28a) and $\mu(A) = 14.99$ from Table 5, giving

$$g\text{(km/sec)} = 10.24\sqrt{\kappa}. \tag{30}$$

Table 7. Momentum-transfer cross-sections based on the (12,6,4)-potential with $\gamma = 0.960$ for (U$^+$+O)-collisions.

κ	g, km/sec	$\sigma/(\pi\, r_m^2)$	σ, 10^{-15} cm^2
0.20271	4.61	3.57	3.80
0.42279	6.66	2.64	2.82
0.68414	8.47	2.22	2.37
0.84229	9.40	2.01	2.14
1.0296	10.39	1.89	2.02
Table 1	Eq. (30)	Table 1	Col.3 & Eq. (28b) Fig. 9

For completeness we also use the (12,6)-potential to obtain the momentum-transfer cross-section for (U$^+$+O)-collisions. The reduced energies and cross sections (in units of πD^2) from Ref. 31, with the velocity from Eq. (30), are given in Table 8; the actual cross-sections are plotted as the open-circle points in Fig. 9.

Table 8. Momentum-transfer cross-sections based on the (12,6)-potential for (U$^+$+O)-collisions.

κ	g, km/sec	$\sigma/(\pi D^2)$	σ, 10^{-15} cm^2
0.1	3.24	5.445	4.61
0.2	4.58	4.476	3.79
0.4	6.48	3.368	2.85
0.6	7.93	2.909	2.46
0.8	9.16	2.523	2.14
0.9	9.71	2.505	2.12
0.95	9.98	2.467	2.09
1.0	10.24	2.401	2.03
Table 1	Eq. (30)	Table 1 Eq. (1c)	Col. 3 & Eqs. (1c), (28b) Fig. 9

The long-dash line in Fig. 9 is computed from the asymptotic expression in Eq. (12c), with parameters from Eq. (28a,b), giving

$$\sigma(U^+ + O)\big|_{(r^{-6})-pot} = 2.15 \times 10^{-11} \ g^{-2/3} = 9.98 \times 10^{-15} \ g_{km/sec}^{-2/3} \ cm^2 \quad (31a,b)$$

We will adopt Eq. (31) as the relative-velocity momentum-transfer cross-section for $(U^+ + O)$-collisions, based on the (r^{-6})-potential, for the velocity range less than about 5×10^5 cm/sec. Note that this expression hardly differs from Eq. (25) for $(U+O)$-collisions; the uncertainty in the calculation does not warrant distinguishing the two formulas.

To obtain the cross section for the effective (r^{-6})-potential, we use Eq. (A20) and the parameters in Table 5 to get

$$\sigma(U^+ + O)\big|_{Eff.\,(r^{-6})-pot} = 1.38 \times 10^{-11} \ g^{-2/3} = 6.41 \times 10^{-15} \ g_{km/sec}^{-2/3} \ cm^2 \quad (32a,b)$$

Equation (32), which is the same as Eq. (26) for $(U+O)$-collisions, is also plotted as the dotted line in Fig. 9.

2.3.3.2 <u>$[U^+ + (N_2, O_2)]$-Collisions.</u> By using Eq. (13b) for the polarization potential and the polarizabilities and reduced mass numbers from Table 5, we have

$$\sigma(U^+ + N_2)\big|_{pol.pot.} = 6.86 \times 10^{-10} \ g^{-1} = 6.86 \times 10^{-15} \ g_{km/sec}^{-1} \ cm^2 \quad (33a1,a2)$$

$$\sigma(U^+ + O_2)\big|_{pol.pot.} = 6.14 \times 10^{-10} \ g^{-1} = 6.14 \times 10^{-15} \ g_{km/sec}^{-1} \ cm^2 . \quad (33b1,b2)$$

For the (r^{-6})-potential in Eq. (27a) we used a factor of 5/4 for a larger target size. Similarly, we apply a factor of 5/4 to Eq. (31) and thereby suggest the expression

$$\sigma[U^+ + (N_2, O_2)]\big|_{=(r^{-6})-pot} = \tfrac{5}{4} \ \sigma(U^+ + O)\big|_{(r^{-6})-pot} \quad (34a)$$

$$= 2.69 \times 10^{-11} \ g^{-2/3} \ cm^2 \quad (34b)$$

$$= 1.25 \times 10^{-14} \ g_{km/sec}^{-2/3} \ cm^2 . \quad (34c)$$

Note that this expression hardly differs from Eq. (27a) for $[U+(N_2, O_2)]$-collisions, the uncertainty in the calculation does not warrant distinguishing the two formulas.

To obtain the cross sections for the effective (r^{-6})-potential, we use Eq. (A20) and the parameters in Table 5 to get

$$\sigma(U^+ + N_2)\big|_{\text{Eff }(r^{-6})\text{-pot}} = 1.74 \times 10^{-11} \, g^{-2/3} = 8.08 \times 10^{-15} \, g_{\text{km/sec}}^{-2/3} \quad \text{cm}^2 \, (35a1,a2)$$

$$\sigma(U^+ + O_2)\big|_{\text{Eff.}(r^{-6})\text{-pot.}} = 1.59 \times 10^{-11} \, g^{-2/3} = 7.38 \times 10^{-15} \, g_{\text{km/sec}}^{-2/3} \quad \text{cm}^2 \, (35b1,b2)$$

These two expressions are the same as Eq. (27b) for $[U+(N_2,O_2)]$-collisions.

2.3.3.3 Summary Formula for Polarization and Effective (r^{-6})-Potential. The following expression, with the parameters in Table 5, combines all the formulas for $[U^+ + (O,N_2,O_2)]$-collisions based on the polarization and effective (r^{-6})-potentials:

$$\sigma_{i,k}(g)\big|_\beta = 2.59 \times 10^{-9} \left[\frac{\alpha_k'}{\mu(A_{i,k})}\right]^{1/2} \frac{1}{g} \left[1.06 \times 10^{-11} \, \mu(A_{i,k}) \, g^2\right]^\beta \quad \text{cm}^2 \quad (36a1)$$

$$= 2.59 \times 10^{-15} \left[\frac{\alpha_k'}{\mu(A_{i,k})}\right]^{1/2} \frac{1}{g_{\text{km/sec}}} \left[0.106 \, \mu(A_{i,k}) \, g_{\text{km/sec}}^2\right]^\beta \quad (36a2)$$

$$\Rightarrow 3.84 \times 10^{-11} \, [\alpha_k']^{1/2} \, [\mu(A_{i,k}) \, g^2]^{-1/3}, \quad \beta = 1/6 \quad\quad (36b1)$$

$$= 1.78 \times 10^{-14} \, [\alpha_k']^{1/2} \, [\mu(A_{i,k}) \, g_{\text{km/sec}}^2]^{-1/3}, \quad \beta = 1/6 \quad\quad (36b2)$$

$$\beta = \begin{cases} 0, & \text{polarization potential} \\ 1/6, & \text{effective}\,(r^{-6})\text{-potential} \end{cases}$$

Equation (36b1) is the same as Eq. (A20a2).

2.3.4 $[UO^+ + (O,N_2,O_2)]$-Collisions.

For $[UO^+ + (O,N_2,O_2)]$-collisions, we are unaware of any simplified procedure we might use to estimate the cross sections. We are inclined to discount possible use of the polarization potential – despite our presenting formulas based on it – for qualitative reasons similar to those to which we appealed in discounting it for $(U^+ + O)$-collisions, even though we cannot provide numerical estimates.

For the polarization potential, we have from Eq. (13b) and parameters in Table 5, formulas for UO^+ collisions which are virtually the same as those for U^+ collisions owing to little difference in the reduced mass numbers:

$$\sigma(UO^+ + O)\big|_{pol.pot.} \approx \sigma(U^+ + O)\big|_{pol.pot.} \tag{37a}$$
$$\Rightarrow Eq.(29)$$

$$\sigma(UO^+ + N_2)\big|_{pol.pot.} \approx \sigma(U^+ + N_2)\big|_{pol.pot.} \tag{37b}$$
$$\Rightarrow Eq.(33a)$$

$$\sigma(UO^+ + O_2)\big|_{pol.pot.} \approx \sigma(U^+ + O_2)\big|_{pol.pot.} \tag{37c}$$
$$\Rightarrow Eq.(33b)$$

For the (r^{-6})-potential, to account for the larger size of UO^+ compared with U^+, we will make the ad hoc assumption that the cross sections for $[U^+ + (O, N_2, O_2)]$-collisions should be multiplied by $5/4$ to obtain the cross sections for $[UO^+ + (O, N_2, O_2)]$-collisions:

$$\sigma(UO^+ + O)\big|_{\approx(r^{-6})-pot.} \approx \tfrac{5}{4}\sigma(U^+ + O)\big|_{(r^{-6})-pot.} \tag{38a}$$
$$\Rightarrow \tfrac{5}{4} \times Eq.(31)$$

$$\sigma[UO^+ + (N_2, O_2)]\big|_{\approx(r^{-6})-pot.} \approx \tfrac{5}{4}\sigma[U^+ + (N_2, O_2)]\big|_{\approx(r^{-6})-pot.} \tag{38b}$$
$$\Rightarrow \tfrac{5}{4} \times Eq.(34)$$

For the effective (r^{-6})-potential, we use Eq. (A19) for the parameter $(r_m^5 \varepsilon_o)^{1/3}$ – since it depends only on the target species – with Eqs. (12c) and (12e). The results for the $[UO^+ + (O, N_2, O_2)]$-collisions will differ from those for $[U^+ + (O, N_2, O_2)]$-collisions only by a very slightly different reduced mass number, certainly too little to matter. Hence, we write

$$\sigma(UO^+ + O)\big|_{Eff.(r^{-6})-pot.} = \sigma(U^+ + O)\big|_{Eff.(r^{-6})-pot.} \tag{39a}$$
$$\Rightarrow Eq.(32)$$

$$\sigma(UO^+ + N_2)\big|_{Eff.(r^{-6})-pot.} = \sigma(U^+ + N_2)\big|_{Eff.(r^{-6})-pot.} \tag{39b}$$
$$\Rightarrow Eq.(35a)$$

$$\sigma(UO^+ + O_2)\big|_{Eff.(r^{-6})-pot.} = \sigma(U^+ + O_2)\big|_{Eff.(r^{-6})-pot.} \tag{39c}$$
$$\Rightarrow Eq.(35b)$$

2.3.5 Summary Form for [(U,U⁺,UO⁺)+(O,N₂,O₂)]-Collisions.

For later use it is convenient to write the summary formula

$$
\sigma_{i,k}(g) = \sigma_{ik}^{0,P} \, [g_1 / g_{km/sec}]^{2p} \; cm^2
$$
$$
g_1 = 1 \; km/sec
$$
$$
p = \begin{cases} 1/2, & \text{polarization potential} \\ 1/3, & (r^{-6})\text{- and eff.}(r^{-6})\text{-pot.} \end{cases}
$$

(40)

with the coefficients $\sigma_{ik}^{0,P}$ given in Table 9.

Table 9. Summary-equation parameters for [(U,U⁺,UO⁺)+(O,N₂,O₂)]-collisions.

k	$\sigma_{ik}^{0,P}$, 10^{-15} cm²			Potential	p
	$i=U$	$i=U^+$	$i=UO^+$		
O		5.96	5.96	pol.	1/2
	9.79	9.98	12.5	r^{-6}	1/3
	6.41	6.41	6.41	eff. (r^{-6})	1/3
N₂		6.86	6.86	pol.	1/2
	12.4	12.5	15.6	$\approx r^{-6}$	1/3
	8.08	8.08	8.08	eff. (r^{-6})	1/3
O₂		6.14	6.14	pol.	1/2
	12.4	12.5	15.6	$\approx r^{-6}$	1/3
	7.38	7.38	7.38	eff. (r^{-6})	1/3

SECTION 3

STOPPING POWER, MEAN MOMENTUM-TRANSFER CROSS-SECTIONS, AND RANGE-ENERGY RELATIONS

3.1 INTRODUCTION.

The goal of this Section is to obtain simple range-energy relations for low-energy uranium species traversing the ambient atmosphere. Such relations are obtained by integrating an appropriate stopping-power formula involving mean values of the momentum-transfer cross-sections developed in Section 2.

To obtain a stopping-power formula for a single particle traversing a Maxwellian gas, we will adapt ideas from Banks [Ref. 6] who was interested in the related problem of elastic collisions and energy transfer between gases which have separate Maxwellian velocity distributions. Banks [Ref. 6] shows that the exact equation, derived by Deslogue [Ref. 17] and presented below as Eq. (41), for the energy transfer rate between gases of arbitrary temperature and particle mass, can be separated into three fundamental factors, each of which depends on a different aspect of the collision process and gas composition, i.e., (1) a ratio of particle masses, (2) the difference in the gas thermal energies, and (3) a nonequilibrium collision frequency for energy transfer which entails a mean nonequilibrium momentum-transfer cross-section.

Banks [Ref. 6] acknowledges that his decomposition of Desloque's formula [Ref. 17] is not rigorous since he did not use the proper averaging techniques of kinetic theory needed to arrive at an exact expression. Whatever shortcoming that fact imposes probably is not very important relative to (a) our additional approximations and (b) the uncertainty in the basic cross sections used in our applications. To provide insights concerning the numerous approximations required to obtain simple analytical expressions, we will first sketch Banks' development in general terms, followed by more details with equations and our adapted formulas.

3.2 ENERGY EXCHANGE BETWEEN MAXWELLIAN GASES.

3.2.1 Desloge's Exact Formula.

Desloge's [Ref. 17] result for the average rate of change of the total kinetic energy of one gas is

$$\frac{dU_1}{dt} = -4\pi\, n_1 n_2 \frac{(m_1 m_2)^{7/2}(T_1 - T_2)}{(m_1 + m_2)^2 (2\pi k)^{3/2}(m_2 T_1 + m_1 T_2)^{5/2}} \int_0^\infty g^5 q_D(g) \exp(-Kg^2)\, dg \qquad (41a)$$

where

$$U_1 = \int \tfrac{1}{2} m_1 v_1^2 f_1 \, d^3\vec{v}_1$$ (41b)

$$K = \left[\frac{2kT_1}{m_1} + \frac{2kT_2}{m_2} \right]^{-1}$$ (41c)

$$q_D(g) = 2\pi \int \sigma(g,\theta)(1-\cos\theta)\sin\theta \, d\theta$$ (41d)

and

U – gas total kinetic energy

n – particle number density

m – particle mass

T – Maxwellian temperature

k – Boltzmann's constant

g – relative velocity between particles

$q_D(g)$ – velocity-dependent momentum-transfer cross-section

v – particle velocity in laboratory system

$d^3\vec{v}$ – velocity-space volume element

θ – center-of-mass scattering angle

$\sigma(g,\theta)$ – differential scattering cross-section

f – velocity distribution function.

3.2.2 Banks' Heuristic Formula.

Banks' development is based initially on a simple model of energy transfer for a *single particle moving in a gas* (exactly our case of interest!), but that particle soon becomes a member of a Maxwellian gas interacting with the original gas. By defining an appropriate collision frequency for energy transfer and a momentum-transfer cross-section, Banks derives a general functional form for the energy exchange rate between two gases. By comparing that form with Eq. (41a), Banks obtains specific equations for the collision frequency and momentum-transfer cross-section which are applicable to the problem of energy transfer.

The average loss of kinetic energy per collision, $\Delta\varepsilon_1$, of a single particle of mass m_1 and kinetic energy ε_1 traveling through a gas composed of particles of mass m_2 and average energy $\bar{\varepsilon}_2$ is, as shown (for isotropic scattering in the center-of-mass system) by Huxley and Crompton [Ref. 35],

$$\Delta\varepsilon_1 = -\frac{2 m_1 m_2}{(m_1 + m_2)^2} (\varepsilon_1 - \bar{\varepsilon}_2).$$ (42)

To describe the rate at which the single particle loses energy, Banks introduces the concept of the single-particle collision frequency, given by

$$v_{12} = n_2 \, g \, Q_D , \qquad (43)$$

with n_2 the ambient gas number density. To obtain the average rate at which the single particle loses energy, Banks combines Eqs. (42) and (43):

$$\overline{\frac{\Delta \varepsilon_1}{\Delta t}} = -\frac{2 m_1 m_2}{(m_1 + m_2)^2} (\varepsilon_1 - \bar{\varepsilon}_2) v_{12} . \qquad (44)$$

Next, instead of a single particle, Banks considers a large number of particles forming a Maxwellian gas mixed with the original gas, and approximates the total average energy exchange rate by the expression

$$\frac{dU_1}{dt} = -\frac{2 m_1 m_2}{(m_1 + m_2)^2} n_1 (\bar{\varepsilon}_1 - \bar{\varepsilon}_2) \bar{v}_{12} \qquad (45)$$

with

$$U_1 = n_1 \tfrac{1}{2} m_1 \overline{v_1^2} = n_1 \bar{\varepsilon}_1 , \qquad (46)$$

where $\bar{\varepsilon}_1$ is now an average energy which corresponds to the Maxwellian distribution of single particles permitted to become the mixed gas. Similarly, $\bar{v}_{12}$ is now an average collision frequency which, unlike Eq. (43), must be suitably defined to account for the many different relative velocities between the various gas particles.

Banks states that Eq. (45), while not rigorous, provides a functional form which can be used to decompose Eq. (41) into three factors: (1) a ratio of masses, (2) a difference in average particle energies, and (3) an energy-transfer collision frequency. Only the third factor involves the interparticle forces.

Banks argues that, in order that the correct form may be synthesized by comparing Eqs. (41a) and (45), the functional form of the average collision frequency must be

$$\bar{v}_{12} \propto n_2 \, \bar{g} \, Q_D \qquad (47)$$

which allows for an arbitrary numerical factor in the final result for $\bar{v}_{12}$. The quantity $\bar{g}$ is the average relative velocity between the particles of the two Maxwellian gases,

$$\bar{g} = \int\int f_1 f_2 |\vec{v}_1 - \vec{v}_2| \, d^3\vec{v}_1 \, d^3\vec{v}_2 \qquad (48a)$$

$$= \left[\frac{8k}{\pi}\right]^{1/2} \left[\frac{T_1}{m_1} + \frac{T_2}{m_2}\right]^{1/2} , \qquad (48b)$$

while Q_D is the average momentum-transfer cross-section appropriate for thermal nonequilibrium,

33

$$Q_D = K^3 \int_0^\infty g^5 \, q_D(g) \, \exp(-Kg^2) \, dg \qquad (49)$$

with K given by Eq. (41c). By comparing Eqs. (41a), (45), (47), and (49), Banks recognizes the average momentum-transfer collision frequency,

$$\bar{\nu}_{12} = \tfrac{4}{3} \, n_2 \, \bar{g} \, Q_D , \qquad (50a)$$

with $\bar{g}$ given by Eq. (48b), and Q_D by Eq. (49), as the generalization to conditions of different Maxwellian velocity distributions of two gases. In a later reference [Ref. 7, Pt. A, pp. 190, 191], Banks observes that this collision frequency is in the center-of-mass system and related to that in the laboratory system by

$$\bar{\nu}_{L12} = [m_2 / (m_1 + m_2)] \bar{\nu}_{12} . \qquad (50b)$$

Finally, as the goal of his derivation, Banks expresses Eq. (41a) in terms of his decomposition factors as

$$\frac{dU_1}{dt} = -3 n_1 \frac{m_1 m_2}{(m_1 + m_2)^2} \, K (T_1 - T_2) \bar{\nu}_{12} , \qquad (51a)$$

or, alternatively, as given in Ref. 7, Pt. A, p. 191, as

$$\frac{dU_1}{dt} = -3 n_1 \frac{m_1}{m_1 + m_2} \, K (T_1 - T_2) \bar{\nu}_{L12} . \qquad (51b)$$

3.3 PARTICLE TRAVERSING A MAXWELLIAN GAS.

3.3.1 Energy Loss Rate.

For our applications, we want to retain the identity of a single particle traversing the ambient Maxwellian gas. Our equation corresponding to Eq. (42) will be written as

$$\overline{\delta E_{ik}(E_i)} = \Delta_{ik} (E_i - E_a) \qquad (42*)$$

where the ambient energy per particle and temperature are related by

$$E_a = E_{ambient} = \tfrac{3}{2} k T_a = \tfrac{1}{2} M_k V_k^2 \qquad (42a*)$$

and the mean fractional loss in laboratory energy is

$$\Delta_{ik} = \frac{2 M_i M_k}{(M_i + M_k)^2} = \frac{2 \mu(A_{ik})}{A_i + A_k} \qquad (42b*)$$

with the reduced mass number

$$\mu(A_{ik}) = \frac{A_i A_k}{A_i + A_k} . \qquad (42c*)$$

Our expressions corresponding to Eqs. (43) and (44) are

$$\nu_{ik} = n_k \, g \, q_{Dik} \qquad (43*)$$

and

$$\frac{dE_i}{dt} = -\overline{\delta E_{ik}(E_i)} \nu_{ik} . \qquad (44*)$$

For our use we will replace v_{ik} in Eq. (44*) by $\bar{v}_{ik}$ with a functional form corresponding to Banks' expression, Eq. (50), for the mean collision frequency,

$$\bar{v}_{ik} = \tfrac{4}{3} n_k \, \bar{g}_{ik} \, Q_{Dik} \tag{50a*}$$

$$\bar{v}_{Lik} = [(M_2/(M_1+M_2))]\bar{v}_{ik}\,, \tag{50b*}$$

but we will associate a fictitious temperature T_i^{fict} with the incident particle by the expression

$$E_i = \tfrac{1}{2} M_i V_i^2 = \tfrac{3}{2} k T_i^{\text{fict}} \tag{52}$$

so that our mean relative velocity corresponding to Eq. (48b) is

$$\bar{g}_{ik} = \left[\frac{8k}{\pi}\right]^{1/2} \left[\frac{V_i^2}{3k} + \frac{T_a}{M_k}\right]^{1/2} \tag{48b1*}$$

$$= \left[\frac{8}{3\pi}\right]^{1/2} \left[V_i^2 + V_k^2\right]^{1/2} \tag{48b2*}$$

$$= \left[\frac{8}{3\pi}\right]^{1/2} \left[\frac{2E_i}{M_i} + \frac{2E_a}{M_k}\right]^{1/2} . \tag{48b3*}$$

In Appendix E we show that, for our applications, Eq. (48b*) for the mean relative velocity compares very well with an expression based on the exact relative velocity distribution for a particle traversing a Maxwellian gas.

Our mean momentum-transfer cross-section corresponding to Eq. (49) is

$$Q_{Dik} = K^3 \int_0^\infty g^5 q_{Dik}(g) \exp(-K g^2)\,\mathrm{d}g \tag{49*}$$

with the parameter K corresponding to Eq. (41c) now given by

$$K = \left[\tfrac{2}{3} V_i^2 + \frac{2k T_a}{M_k}\right]^{-1} \tag{41c1*}$$

$$= \frac{3}{2} \frac{1}{(V_i^2 + V_k^2)} . \tag{41c2*}$$

Thus, our expression corresponding to Banks' Eq. (51a), except that it pertains to a single incident particle instead of an entire gas, is

$$\frac{\mathrm{d}E_i}{\mathrm{d}t} = -\overline{\delta E_{ik}(E_i)}\,\bar{v}_{ik} \tag{51a*}$$

with the auxiliary Eqs. (50a*), (48b*), (49*), and (41c*).

3.3.2 Mean Momentum-Transfer Cross-Sections.

Before introducing the stopping power, we specialize Eq. (49*) to the momentum-transfer cross-sections in Section 2 for $[(U, U^+, UO^+) + (O, N_2, O_2)]$-collisions. Use of $\sigma_{ik}(g)$, given by Eq. (40), for $q_{Dik}(g)$ in Eq. (49*), gives

$$Q_{Dik} = \sigma_{ik}^{0,p} \tfrac{1}{2}(10^5)^{2p} K^p J_p\,, \tag{53}$$

where $\mathcal{J}_p$ is defined in terms of Euler's integral for the gamma function [Ref. 1, p. 255],

$$\mathcal{J}_p = \int_0^\infty x^{3-p-1} e^{-x} \, dx \tag{54a}$$

$$= \Gamma(3-p) \tag{54b}$$

$$= \begin{cases} \Gamma(8/3) = [(2\times 5)/3^2]\, \Gamma(2/3) = 1.5046, & p = 1/3 \\ \Gamma(5/2) = [(1\times 3)/2^2]\, \Gamma(1/2) = 1.3293, & p = 1/2 \end{cases} \tag{54c}$$

and from Eqs. (41c*) and (42a*),

$$(10^{10}\, K)^p = \left[\frac{3}{2}\right]^p \left[\frac{10^{10}}{V_i^2 + V_k^2}\right]^p \tag{55a}$$

$$= \left[\frac{3}{2}\right]^p \left[\frac{E_i^0}{E_i + E_{ik}}\right]^p \tag{55b}$$

with

$$E_i^0 = \tfrac{1}{2} M_i (10^5)^2 \tag{56a}$$

$$= 5.18 \times 10^{-3} A_i, \quad eV \tag{56b}$$

$$E_{ik} = E_a (M_i / M_k) = E_a (A_i / A_k). \tag{57}$$

3.3.3 Stopping Power.

To obtain a stopping-power formula we divide dE_i / dt by the incident (laboratory) velocity V_i to obtain the energy transfer per unit path length (the stopping power) and sum the stopping-power terms for the several species in the ambient atmosphere:

$$\frac{dE_i}{dR_i} = \frac{1}{V_i}\frac{dE_i}{dt} = -\frac{1}{V_i} \sum_{k=0,\,N_2,\,O_2} n_k\, \overline{\delta E_{ik}(E_i)}\, \tfrac{4}{3}\, \bar{g}_{ik}\, Q_{0ik}. \tag{58}$$

Use of Eqs. (48b2*), (54), and (56b) in Eq. (58) gives

$$\frac{dE_i}{dR_i} = -F_p \frac{1}{V_i} \sum_k n_k\, \overline{\delta E_{ik}(E_i)}\, [V_i^2 + V_k^2]^{1/2}\, \sigma_{ik}^{0,\,p} \left[\frac{E_i^0}{E_i + E_{ik}}\right]^p \tag{59a}$$

or, with use of Eqs. (42*), (52), (48b3*), and (57),

$$\frac{dE_i}{dR_i} = -F_p \frac{E_i - E_a}{E_i^{1/2}} (E_i^0)^p \sum_k \left[\lambda_{ik}^{0,\,p}\right]^{-1} A_{ik} [E_i + E_{ik}]^{\frac{1}{2}-p} \tag{59b}$$

with

$$\lambda_{ik}^{0,\,p} = \left[n_k\, \sigma_{ik}^{0,\,p}\right]^{-1} \tag{59c}$$

and where the numerical factor is

36

$$F_p \equiv \left[\frac{8}{3\pi}\right]^{1/2}\left[\frac{2}{3}\right]^{1-p} \mathcal{J}_p \qquad (59d1)$$

$$= \begin{cases} 1.0579 & p = 1/3 \\ 0.99997 & p = 1/2 . \end{cases} \qquad (59d2)$$

We now make two related approximations in the factor

$$F(E_i, E_{ik}) \equiv [E_i + E_{ik}]^{\frac{1}{2}-p} \qquad (59e)$$

appearing in the stopping-power expression in Eq. (59b). First, owing to (1) the weak dependence (for p = 1/3) (there is no dependence for p = 1/2) of the stopping power on the factor $F(E_i, E_{ik})$ and (2) our desire to get a relatively simple range-energy formula, we will eliminate the dependence on A_k in the factor by using an average value of A_k, $\overline{A_k}$, with plausible but nonunique weighting factors, defined as

$$\overline{A_k} = A_i^{o,p} \sum_k \Delta_{ik} \left[\lambda_{ik}^{o,p}\right]^{-1} A_k \qquad (60)$$

with

$$[A_i^{o,p}]^{-1} = \sum_k \Delta_{ik} \left[\lambda_{ik}^{o,p}\right]^{-1} \qquad (61)$$

Then, from Eq. (57), we can write

$$\overline{E}_{ik} = E_a (A_i / \overline{A_k}) \qquad (62)$$

and our stopping-power formula as

$$\frac{dE_i}{dR_i} = -F_p [E_i^o]^p [A_i^{o,p}]^{-1} \frac{E_i - E_a}{E_i^{1/2}} [E_i + \overline{E}_{ik}]^{\frac{1}{2}-p} . \qquad (63)$$

Before assessing the consequence of using the first approximation expressed in Eqs. (60) and (62) for p = 1/3, we introduce some necessary parameters for current and later use. Table 10 contains selected properties (provided by I. L. Kofsky) at four altitudes in a MSIS-83 atmosphere [Ref. 29] for low-latitude (33 deg), low solar 10.7-cm flux (78), and magnetically-quiet conditions (A_p = 3). Table 11 provides mass parameters for [(U, U+, UO+) + (O, N₂, O₂)]-collisions. Table 12 provides the rms thermal velocities of U, U+, and UO+ for the temperatures in Table 10. For the collision pairs in Table 11, stopping-power and range-energy parameters are given in Tables 13a and 13b for the polarization potential, in Tables 14a, 14b, and 14c for the (r^{-6})-potential, and in Tables 15a and 15b for the effective (r^{-6})-potential, corresponding to the momentum-transfer cross-sections summarized in Table 9.

Table 10. Selected properties for a quiet MSIS-83 atmosphere [Ref 29].

| h, km | T, K | E_a, eV | cm^{-3} | | |
			[O]	[N$_2$]	[O$_2$]
200	752.6	0.0973	2.30 E+09	2.36 E+09	1.22 E+08
225	778.7	0.1007	1.23 E+09	8.33 E+08	3.74 E+07
250	792.7	0.1025	6.82 E+08	3.09 E+08	1.20 E+07
275	800.3	0.1035	3.89 E+08	1.18 E+08	4.00 E+06

h, km	cm^{-3} n(total)	f[O]	f[N$_2$]	f[O$_2$]
200	4.78 E+09	0.481	0.494	0.025
225	2.10 E+09	0.586	0.397	0.017
250	1.00 E+09	0.680	0.308	0.012
275	5.11 E+08	0.761	0.231	0.008

Table 11. Mass parameters for [(U,U$^+$,UO$^+$)+(O,N$_2$,O$_2$)]-collisions.

i	k	A	$\mu(A_{ik})$	Δ_{ik}
U, U$^+$		238		
	O	16	14.99	0.118
	N$_2$	28	25.05	0.188
	O$_2$	32	28.21	0.209
UO$^+$		254		
	O	16	15.05	0.111
	N$_2$	28	25.22	0.179
	O$_2$	32	28.42	0.199

Table 12. Root-mean-square thermal velocities of U, U$^+$, and UO$^+$ in the Table-10 atmosphere.

| i | $V_{i,a}$, km/sec | | | |
	h = 200	h = 225	h = 250	h = 275
U, U$^+$	0.2809	0.2858	0.2883	0.2897
UO$^+$	0.2719	0.2766	0.2791	0.2804

Table 13a. Stopping-power and range-energy parameters for polarization potential in $[U^+ + (O, N_2, O_2)]$-collisions.

		200 km		225 km	
		$\lambda_{ik}^{o,P}$	$\Delta_{ik} [\lambda_{ik}^{o,P}]^{-1}$	$\lambda_{ik}^{o,P}$	$\Delta_{ik} [\lambda_{ik}^{o,P}]^{-1}$
i	k	10^5 cm	10^{-6} cm^{-1}	10^5 cm	10^{-6} cm^{-1}
U^+	O	0.730	1.62	1.36	0.87
	N$_2$	0.618	3.04	1.75	1.07
	O$_2$	13.3	0.16	43.5	0.05
		$[\Delta_i^{o,P}]^{-1} =$	4.82	$[\Delta_i^{o,P}]^{-1} =$	1.99
		$\Delta_i^{o,P} =$	2.07 km	$\Delta_i^{o,P} =$	5.03 km
		$\varepsilon^o =$	12.7	$\varepsilon^o =$	12.2

		250 km		275 km	
		$\lambda_{ik}^{o,P}$	$\Delta_{ik} [\lambda_{ik}^{o,P}]^{-1}$	$\lambda_{ik}^{o,P}$	$\Delta_{ik} [\lambda_{ik}^{o,P}]^{-1}$
i	k	10^5 cm	10^{-7} cm^{-1}	10^5 cm	10^{-7} cm^{-1}
U^+	O	2.46	4.80	4.31	2.74
	N$_2$	4.72	3.98	12.4	1.52
	O$_2$	136	0.15	407	0.05
		$[\Delta_i^{o,P}]^{-1} =$	8.93	$[\Delta_i^{o,P}]^{-1} =$	4.31
		$\Delta_i^{o,P} =$	11.2 km	$\Delta_i^{o,P} =$	23.2 km
		$\varepsilon^o =$	12.0	$\varepsilon^o =$	11.9

Table 13b. Stopping-power and range-energy parameters for polarization potential in $[UO^+ + (O, N_2, O_2)]$-collisions.

		200 km		225 km	
		$\lambda_{ik}^{o,P}$	$\Delta_{ik} [\lambda_{ik}^{o,P}]^{-1}$	$\lambda_{ik}^{o,P}$	$\Delta_{ik} [\lambda_{ik}^{o,P}]^{-1}$
i	k	10^5 cm	10^{-6} cm^{-1}	10^5 cm	10^{-6} cm^{-1}
UO^+	O	0.730	1.52	1.36	0.82
	N$_2$	0.618	2.90	1.75	1.02
	O$_2$	13.3	0.15	43.5	0.05
		$[\Delta_i^{o,P}]^{-1} =$	4.57	$[\Delta_i^{o,P}]^{-1} =$	1.89
		$\Delta_i^{o,P} =$	2.19 km	$\Delta_i^{o,P} =$	5.29 km
		$\varepsilon^o =$	13.5	$\varepsilon^o =$	13.1

Table 13b. Stopping-power and range-energy parameters. (Cont'd)

		250 km		275 km	
		$\lambda_{ik}^{o,P}$	$\Delta_{ik}\,[\lambda_{ik}^{o,P}]^{-1}$	$\lambda_{ik}^{o,P}$	$\Delta_{ik}\,[\lambda_{ik}^{o,P}]^{-1}$
i	k	10^5 cm	10^{-7} cm^{-1}	10^5 cm	10^{-7} cm^{-1}
UO$^+$	O	2.46	4.51	4.31	2.58
	N$_2$	4.72	3.79	12.4	1.44
	O$_2$	136	0.15	407	0.05
		$[\Delta_i^{o,P}]^{-1} =$	8.45	$[\Delta_i^{o,P}]^{-1} =$	4.07
		$\Delta_i^{o,P} =$	11.8 km	$\Delta_i^{o,P} =$	24.6 km
		$\varepsilon^o =$	12.8	$\varepsilon^o =$	12.7

Table 14a. Stopping-power and range-energy parameters for
(r^{-6})- potential in [U+(O,N$_2$,O$_2$)]-collisions.

		200 km		225 km	
		$\lambda_{ik}^{o,P}$	$\Delta_{ik}\,[\lambda_{ik}^{o,P}]^{-1}$	$\lambda_{ik}^{o,P}$	$\Delta_{ik}\,[\lambda_{ik}^{o,P}]^{-1}$
i	k	10^5 cm	10^{-6} cm^{-1}	10^5 cm	10^{-6} cm^{-1}
U	O	0.444	2.66	0.830	1.42
	N$_2$	0.342	5.50	0.968	1.94
	O$_2$	6.61	0.32	21.6	0.10
		$[\Delta_i^{o,P}]^{-1} =$	8.48	$[\Delta_i^{o,P}]^{-1} =$	3.46
		$\Delta_i^{o,P} =$	1.18 km	$\Delta_i^{o,P} =$	2.89 km
		$A_i\,/\,\overline{A}_k =$	9.76	$A_i\,/\,\overline{A}_k =$	10.3

		250 km		275 km	
		$\lambda_{ik}^{o,P}$	$\Delta_{ik}\,[\lambda_{ik}^{o,P}]^{-1}$	$\lambda_{ik}^{o,P}$	$\Delta_{ik}\,[\lambda_{ik}^{o,P}]^{-1}$
i	k	10^5 cm	10^{-7} cm^{-1}	10^5 cm	10^{-7} cm^{-1}
U	O	1.50	7.87	2.63	4.49
	N$_2$	2.61	7.20	6.83	2.75
	O$_2$	67.2	0.31	202	0.10
		$[\Delta_i^{o,P}]^{-1} =$	15.38	$[\Delta_i^{o,P}]^{-1} =$	7.34
		$\Delta_i^{o,P} =$	6.50 km	$\Delta_i^{o,P} =$	13.6 km
		$A_i\,/\,\overline{A}_k =$	10.8	$A_i\,/\,\overline{A}_k =$	11.5

Table 14b. Stopping-power and range-energy parameters for
(r^{-6})- potential in $[U^+ + (O, N_2, O_2)]$-collisions.

		200 km		225 km	
		$\lambda_{ik}^{o,P}$	$\Delta_{ik}[\lambda_{ik}^{o,P}]^{-1}$	$\lambda_{ik}^{o,P}$	$\Delta_{ik}[\lambda_{ik}^{o,P}]^{-1}$
i	k	10^5 cm	10^{-6} cm^{-1}	10^5 cm	10^{-6} cm^{-1}
U^+	O	0.436	2.71	0.815	1.45
	N$_2$	0.339	5.55	0.960	1.96
	O$_2$	6.56	0.32	21.4	0.10
	$[\Delta_i^{o,P}]^{-1} =$	8.58		$[\Delta_i^{o,P}]^{-1} =$	3.51
	$\Delta_i^{o,P} =$	1.17 km		$\Delta_i^{o,P} =$	2.85 km
	$A_i / \overline{A}_k =$	9.77		$A_i / \overline{A}_k =$	10.3

		250 km		275 km	
		$\lambda_{ik}^{o,P}$	$\Delta_{ik}[\lambda_{ik}^{o,P}]^{-1}$	$\lambda_{ik}^{o,P}$	$\Delta_{ik}[\lambda_{ik}^{o,P}]^{-1}$
i	k	10^5 cm	10^{-7} cm^{-1}	10^5 cm	10^{-7} cm^{-1}
U^+	O	1.47	8.03	2.58	4.57
	N$_2$	2.59	7.26	6.78	2.77
	O$_2$	66.7	0.31	200	0.10
	$[\Delta_i^{o,P}]^{-1} =$	15.60		$[\Delta_i^{o,P}]^{-1} =$	7.44
	$\Delta_i^{o,P} =$	6.41 km		$\Delta_i^{o,P} =$	13.4 km
	$A_i / \overline{A}_k =$	10.9		$A_i / \overline{A}_k =$	11.5

Table 14c. Stopping-power and range-energy parameters for
(r^{-6})- potential in $[UO^+ + (O, N_2, O_2)]$-collisions.

		200 km		225 km	
		$\lambda_{ik}^{o,P}$	$\Delta_{ik}[\lambda_{ik}^{o,P}]^{-1}$	$\lambda_{ik}^{o,P}$	$\Delta_{ik}[\lambda_{ik}^{o,P}]^{-1}$
i	k	10^5 cm	10^{-6} cm^{-1}	10^5 cm	10^{-6} cm^{-1}
UO^+	O	0.348	3.19	0.650	1.71
	N$_2$	0.272	6.58	0.770	2.32
	O$_2$	5.25	0.38	17.1	0.12
	$[\Delta_i^{o,P}]^{-1} =$	10.15		$[\Delta_i^{o,P}]^{-1} =$	4.15
	$\Delta_i^{o,P} =$	0.985 km		$\Delta_i^{o,P} =$	2.41 km
	$A_i / \overline{A}_k =$	10.4		$A_i / \overline{A}_k =$	11.0

Table 14c. Stopping-power and range-energy parameters. (Cont'd)

		250 km		275 km	
		$\lambda_{ik}^{o,P}$	$\Delta_{ik}[\lambda_{ik}^{o,P}]^{-1}$	$\lambda_{ik}^{o,P}$	$\Delta_{ik}[\lambda_{ik}^{o,P}]^{-1}$
i	k	10^5 cm	10^{-7} cm^{-1}	10^5 cm	10^{-7} cm^{-1}
UO$^+$	O	1.17	9.49	2.06	5.39
	N$_2$	2.07	8.65	5.43	3.30
	O$_2$	53.4	0.37	160	0.12
		$[\Delta_i^{o,P}]^{-1} =$	18.51	$[\Delta_i^{o,P}]^{-1} =$	8.81
		$\Delta_i^{o,P} =$	5.40 km	$\Delta_i^{o,P} =$	11.4 km
		$A_i/\overline{A}_k =$	11.6	$A_i/\overline{A}_k =$	12.3

Table 15a. Stopping-power and range-energy parameters for effective (r^{-6})- potential in $[(U,U^+)+(O,N_2,O_2)]$-collisions.

		200 km		225 km	
		$\lambda_{ik}^{o,P}$	$\Delta_{ik}[\lambda_{ik}^{o,P}]^{-1}$	$\lambda_{ik}^{o,P}$	$\Delta_{ik}[\lambda_{ik}^{o,P}]^{-1}$
i	k	10^5 cm	10^{-6} cm^{-1}	10^5 cm	10^{-6} cm^{-1}
U, U$^+$	O	0.678	1.74	1.27	0.93
	N$_2$	0.524	3.59	1.49	1.26
	O$_2$	11.1	0.19	36.2	0.06
		$[\Delta_i^{o,P}]^{-1} =$	5.52	$[\Delta_i^{o,P}]^{-1} =$	2.25
		$\Delta_i^{o,P} =$	1.81 km	$\Delta_i^{o,P} =$	4.44 km
		$A_i/\overline{A}_k =$	9.77	$A_i/\overline{A}_k =$	10.3

		250 km		275 km	
		$\lambda_{ik}^{o,P}$	$\Delta_{ik}[\lambda_{ik}^{o,P}]^{-1}$	$\lambda_{ik}^{o,P}$	$\Delta_{ik}[\lambda_{ik}^{o,P}]^{-1}$
i	k	10^5 cm	10^{-7} cm^{-1}	10^5 cm	10^{-7} cm^{-1}
U, U$^+$	O	2.29	5.15	4.01	2.94
	N$_2$	4.01	4.69	10.5	1.79
	O$_2$	113	0.18	339	0.06
		$[\Delta_i^{o,P}]^{-1} =$	10.02	$[\Delta_i^{o,P}]^{-1} =$	4.79
		$\Delta_i^{o,P} =$	9.98 km	$\Delta_i^{o,P} =$	20.9 km
		$A_i/\overline{A}_k =$	10.9	$A_i/\overline{A}_k =$	11.5

Table 15b. Stopping-power and range-energy parameters for effective (r^{-6})- potential in $[UO^{+}+(O,N_2,O_2)]$-collisions.

i	k	200 km		225 km	
		$\lambda_{ik}^{0,P}$	$\Delta_{ik}[\lambda_{ik}^{0,P}]^{-1}$	$\lambda_{ik}^{0,P}$	$\Delta_{ik}[\lambda_{ik}^{0,P}]^{-1}$
		10^5 cm	10^{-6} cm^{-1}	10^5 cm	10^{-6} cm^{-1}
UO^+	O	0.678	1.64	1.27	0.88
	N_2	0.524	3.42	1.49	1.20
	O_2	11.1	0.18	36.2	0.05
	$[A_i^{0,P}]^{-1} =$		5.24		2.13
	$A_i^{0,P} =$		1.91 km		4.69 km
	$A_i/\overline{A}_k =$		10.4		11.0

i	k	250 km		275 km	
		$\lambda_{ik}^{0,P}$	$\Delta_{ik}[\lambda_{ik}^{0,P}]^{-1}$	$\lambda_{ik}^{0,P}$	$\Delta_{ik}[\lambda_{ik}^{0,P}]^{-1}$
		10^5 cm	10^{-7} cm^{-1}	10^5 cm	10^{-7} cm^{-1}
UO^+	O	2.29	4.85	4.01	2.27
	N_2	4.01	4.46	10.5	1.70
	O_2	113	0.18	339	0.06
	$[A_i^{0,P}]^{-1} =$		9.49		4.53
	$A_i^{0,P} =$		10.5 km		22.1 km
	$A_i/\overline{A}_k =$		11.6		12.3

To proceed now with the assessment of the first approximation, we use the information in Table 15a to evaluate the following two expressions for $[(U, U^+) + (O, N_2, O_2)]$-collisions, based on the effective (r^{-6})-potential, at 250-km altitude in the atmosphere given in Table 10.

$$\text{(exact)} \sum_k \Delta_{ik}\left[\lambda_{ik}^{0,P}\right]^{-1}\left[\varepsilon + A_i/A_k\right]^{1/6} = 1.599\times10^{-6} \qquad (64a)$$

$$\text{(approx.)}\left[\varepsilon + A_i/\overline{A}_k\right]^{1/6} \sum_k \Delta_{ik}\left[\lambda_{ik}^{0,P}\right]^{-1} = 1.588\times10^{-6} \qquad (64b)$$

with the reduced energy

$$\varepsilon = E_i/E_a. \qquad (64c)$$

For $\varepsilon = 5$, the error is only 0.69%, which is certainly acceptable.

The second approximation is to replace the slowly-varying factor $F(E_i, \bar{E}_{i,k})$ by a constant factor, $F(\bar{E}_i, \bar{E}_{i,k})$, where the average energy $\bar{E}_i$ is defined somewhat arbitrarily as

$$\bar{E}_i = \tfrac{1}{2}[E_i^{(s)} + E_i^{(f)}] \qquad (65a)$$

with

$$E_i^{(s)} = \text{starting energy} \qquad (65b)$$

$$E_i^{(f)} = \text{finishing energy.} \qquad (65c)$$

In support of the second approximation, note that the variation of the factor $F(E_i, \bar{E}_{i,k})$ is less than about 10 percent over the energy range of principal interest, as seen in Table 16 where we use a nominal value of 10 for the ratio $A_i / \bar{A}_k$.

Table 16. Illustration of a slowly-varying factor in the stopping-power formula for p = 1/3.

$\varepsilon =$	1	3	5	10
$\left[\dfrac{1+10}{\varepsilon+10}\right]^{1/6} =$	1	0.973	0.950	0.905

With this second approximation, our stopping-power formula in Eq. (63) becomes

$$\boxed{\frac{dE_i}{dR_i} \approx -C_{E,i,p}^{-1} \frac{E_i - E_0}{E_i^{1/2}} \quad \text{eV/km}} \qquad (66a)$$

with

$$C_{E,i,p} = \frac{A_i^{0,P}}{F_p \, [E_i^{\circ}]^P \, [\bar{E}_i + \bar{E}_{i,k}]^{\frac{1}{2}-P}} \qquad (66b1)$$

$$= \frac{A_i^{0,P} \, E_0^{-1/2}}{F_p \, [\varepsilon^{\circ}]^P \, [\bar{\varepsilon} + A_i / \bar{A}_k]^{\frac{1}{2}-P}} \quad \text{km eV}^{-1/2} \qquad (66b2)$$

$$\bar{\varepsilon} = \bar{E}_i / E_0 \qquad (66c1)$$

$$= \tfrac{1}{2}(\varepsilon_s + \varepsilon_f) \qquad (66c2)$$

$$\varepsilon^{\circ} = E_i^{\circ} / E_0 \qquad (66d1)$$

$$= 5.18 \times 10^{-3} \, A_i / E_0 (\text{eV}) \qquad (66d2)$$

$$\varepsilon_s = \varepsilon^{\circ} \, [V_i(\text{km/sec})]_s^2 . \qquad (66e)$$

Values of ε° are given in Tables 13a and 13b.

44

3.3.4 Range-Energy Relation.

If we integrate Eq. (66a) from start (s) to finish (f) (and remember that R_i is the distance traversed, not the residual range), we have

$$R_i = C_{E,i,p} \int_{E_f^{(n)}}^{E_i^{(s)}} \frac{E_i^{1/2}}{[E_i - E_a]} \, dE_i \tag{67a}$$

$$\boxed{R_i = C_{\epsilon,i,p} \, \mathcal{E}(\epsilon_f, \epsilon_s) \quad \text{km}} \tag{67b}$$

with the reduced energy given by Eq. (64c) and the coefficient $C_{\epsilon,i,p}$ by

$$C_{\epsilon,i,p} = E_a^{1/2} \, C_{E,i,p} \quad \text{km,} \tag{67c}$$

collated in Table 17 for U, U$^+$, and UO$^+$ at the altitudes and atmosphere in Table 10.

The integral in Eq. (67) may be expressed and evaluated [Ref. 13, p. 63, No. 92] as

$$\mathcal{E}(\epsilon_f, \epsilon_s) \equiv \int_{\epsilon_f}^{\epsilon_s} \frac{\epsilon^{1/2}}{\epsilon - 1} \, d\epsilon \tag{67d1}$$

$$= T_1 + T_2 \tag{67d2}$$

$$T_1 \equiv 2 \left[\epsilon_s^{1/2} - \epsilon_f^{1/2} \right] \tag{67d3}$$

$$T_2 \equiv \ln \left[\frac{\epsilon_s^{1/2} - 1}{\epsilon_s^{1/2} + 1} \frac{\epsilon_f^{1/2} + 1}{\epsilon_f^{1/2} - 1} \right] \quad \text{for } \epsilon_f > 1. \tag{67d4}$$

If one ignored the ambient energy in the denominator of the integrand, the integrand would be $\epsilon^{-1/2}$ and only the term T_1 would obtain. But with retention of the ambient energy in the denominator, we have a logarithmically-divergent integral for $\epsilon_f = 1$. This means, of course, that our formulation of the energy-loss process is inappropriate for obtaining a range-energy relation if one insists on slowing the particle all the way to ambient energy. We shall not so insist! We recognize that nature knows how to thermalize an energetic particle. We expect that as the particle slows to the point where it is a viable candidate for inclusion as a member of the thermal distribution, one should probably be concerned with some sort of a random walk or diffusion problem (for which projected-motion questions could be investigated) instead of a (linear) range-energy problem. But investigating that aspect of the problem is beyond the scope of the current considerations.

Table 17. Range-energy coefficients $C_{e,i,p}$ for U, U$^+$, and UO$^+$ at several altitudes in a quiet MSIS-83 atmosphere.

Potential	i	$h = 200$	$h = 225$	$h = 250$	$h = 275$
			$C_{e,i,p}$, km		
Polariz.	U$^+$	0.581	1.44	3.23	6.73
	UO$^+$	0.596	1.46	3.30	6.90
	(U$^+$, UO$^+$)	0.589	1.45	3.27	6.82
(r^{-6})	U, U$^+$	0.315	0.776	1.74	3.63
	UO$^+$	0.255	0.625	1.40	2.95
Eff. (r^{-6})	U, U$^+$	0.482	1.19	2.68	5.58
	UO$^+$	0.492	1.22	2.73	5.71
	(U, U$^+$, UO$^+$)	0.487	1.21	2.71	5.65

Notes:

1. For the polarization potential, the difference between the U$^+$ and UO$^+$ parameters here (and in Tables 13a and 13b) is due to slightly different reduced masses, maintenance of which is not justified since it was ignored in the summary cross-section parameters in Table 9 in Section 2

2. To obtain numerical values for the (r^{-6})- and effective (r^{-6})-potentials, we have evaluated the weakly energy-dependent factor involving $\bar{\varepsilon}$ [Eq. (66c2)] by using a value of 0.57 km/sec (the rms velocity for a 3100-K U source) for V_i in Eq. (66e) for ε_s and a value of 1.0 for ε_f in Eq. (66c2). Some applications may require re-setting these values.

3. For the (r^{-6})-potential,
   (a) the formal distinction between U and U$^+$ parameters in Tables 14a and 14b is ignored here by using only the U parameters from Table 14a, and
   (b) the difference between the UO$^+$ and U$^+$ results is due almost entirely to the ad hoc factor of 5/4 introduced in Eq. (38) and only slightly to the reduced-mass difference.

4. For the effective (r^{-6})-potential, the difference between the (U, U$^+$) and UO$^+$ parameters here (and in Tables 15a and 15b) is due to slightly different reduced masses, maintenance of which is not justified since it was ignored in the summary cross-section parameters in Table 9 in Section 2.

To gain some insight into the behavior of the integral in Eq. (67d1), we have recorded in Table 18 the results of evaluating the terms T_1, T_2, the sum T_1+T_2, and the ratio $(T_1+T_2)/T_1$ for starting reduced-energies ε_s of 3, 5, and 10. For some applications where a very simple expression for the integral is desired — and one can accept the corresponding approximation — one may choose to use only the term T_1 with $\varepsilon_f = 1$. In this regard it is of interest to note from Table 18 that

$$T_1[\varepsilon_f = 1] \approx (T_1+T_2)[\varepsilon_f = 2]. \tag{68}$$

The significance of ε_f equalling 2 (i.e., that it corresponds approximately to the 89th percentile of the integral Maxwellian energy distribution) can be seen from Table 19 which provides a selected set of fractional values of the integral Maxwellian energy distribution, $F(\varepsilon_f)$, with energies not exceeding ε_f, as derived from Appendix F giving equations and graphs for the differential and integral distribution functions. Table 19 may also aid one in determining where the cutoff might be set for the integral in Eq. (67).

Table 18. Comparison of approximate reduced range-energy integrals.

ε_f	$\varepsilon_s = 3$				$\varepsilon_s = 5$				$\varepsilon_s = 10$			
	T_1	T_2	T_1+T_2	$\frac{T_1+T_2}{T_1}$	T_1	T_2	T_1+T_2	$\frac{T_1+T_2}{T_1}$	T_1	T_2	T_1+T_2	$\frac{T_1+T_2}{T_1}$
1.0	1.46				2.47				4.32			
1.1	1.37	2.42	3.79	2.77	2.37	2.77	5.15	2.17	4.23	3.08	7.31	1.73
1.2	1.27	1.77	3.05	2.39	2.28	2.13	4.41	1.93	4.13	2.43	6.57	1.59
1.3	1.18	1.41	2.59	2.19	2.19	1.76	3.96	1.80	4.04	2.07	6.12	1.51
1.4	1.10	1.16	2.26	2.06	2.11	1.52	3.62	1.72	3.96	1.82	5.78	1.46
1.5	1.01	0.98	1.99	1.96	2.02	1.33	3.35	1.66	3.88	1.64	5.51	1.42
1.6	0.93	0.83	1.76	1.89	1.94	1.18	3.13	1.61	3.79	1.49	5.29	1.39
1.7	0.86	0.71	1.57	1.83	1.86	1.06	2.93	1.57	3.72	1.37	5.09	1.37
1.8	0.78	0.61	1.39	1.78	1.79	0.96	2.75	1.54	3.64	1.27	4.91	1.35
1.9	0.71	0.52	1.23	1.74	1.72	0.88	2.59	1.51	3.57	1.18	4.75	1.33
2.0	0.64	0.45	1.08	1.70	1.64	0.80	2.44	1.49	3.50	1.11	4.60	1.32
2.1	0.57	0.38	0.95	1.67	1.57	0.73	2.31	1.47	3.43	1.04	4.47	1.30
2.2	0.50	0.32	0.82	1.64	1.51	0.67	2.18	1.45	3.36	0.98	4.34	1.29
2.3	0.43	0.27	0.70	1.62	1.44	0.62	2.06	1.43	3.29	0.93	4.22	1.28
2.4	0.37	0.22	0.58	1.60	1.37	0.57	1.95	1.42	3.23	0.88	4.11	1.27
2.5	0.30	0.17	0.48	1.58	1.31	0.53	1.84	1.40	3.16	0.84	4.00	1.26
2.6	0.24	0.13	0.37	1.56	1.25	0.49	1.74	1.39	3.10	0.80	3.90	1.26
2.7	0.18	0.10	0.27	1.54	1.19	0.45	1.64	1.38	3.04	0.76	3.80	1.25

Table 18. Comparison of approximate reduced range-energy integrals. (Cont'd)

ε_f	$\varepsilon_s=3$				$\varepsilon_s=5$				$\varepsilon_s=10$			
	T_1	T_2	T_1+T_2	$\frac{T_1+T_2}{T_1}$	T_1	T_2	T_1+T_2	$\frac{T_1+T_2}{T_1}$	T_1	T_2	T_1+T_2	$\frac{T_1+T_2}{T_1}$
2.8	0.12	0.06	0.18	1.53	1.13	0.42	1.54	1.37	2.98	0.72	3.70	1.24
2.9	0.06	0.03	0.09	1.51	1.07	0.38	1.45	1.36	2.92	0.69	3.61	1.24
3.0	0.00	0.00	0.00		1.01	0.35	1.36	1.35	2.86	0.66	3.52	1.23
3.2					0.89	0.30	1.19	1.34	2.75	0.61	3.35	1.22
3.4					0.78	0.25	1.04	1.32	2.64	0.56	3.20	1.21
3.6					0.68	0.21	0.89	1.31	2.53	0.52	3.05	1.20
3.8					0.57	0.17	0.74	1.30	2.43	0.48	2.90	1.20
4.0					0.47	0.14	0.61	1.29	2.32	0.44	2.77	1.19
4.5					0.23	0.06	0.29	1.27	2.08	0.37	2.45	1.18
5.0					0.00	0.00	0.00		1.85	0.31	2.16	1.17
5.5									1.63	0.26	1.89	1.16
6.0									1.43	0.21	1.64	1.15
6.5									1.23	0.17	1.40	1.14
7.0									1.03	0.14	1.17	1.14
7.5									0.85	0.11	0.96	1.03
8.0									0.67	0.08	0.75	1.03
8.5									0.49	0.06	0.55	1.12
9.0									0.32	0.04	0.36	1.12
9.5									0.16	0.02	0.18	1.11
10.0									0.00	0.00	0.00	

Table 19. Integral fraction of Maxwellian energy distribution.

ε_f	$F(\varepsilon_f)$	ε_f	$F(\varepsilon_f)$	ε_f	$F(\varepsilon_f)$	ε_f	$F(\varepsilon_f)$
1.0	0.608	1.5	0.788	2.0	0.888	2.5	0.942
1.1	0.652	1.6	0.813	2.1	0.902	2.6	0.950
1.2	0.692	1.7	0.835	2.2	0.914	2.7	0.956
1.3	0.728	1.8	0.855	2.3	0.925	2.8	0.962
1.4	0.759	1.9	0.873	2.4	0.934	2.9	0.966
						3.0	0.971

3.3.5 Energy-Time Relation.

From the basic relationship between energy-loss rate and stopping power, Eq. (58), we can write

$$dt = \frac{dE_i}{V_i \; dE_i / dR_i} \tag{69a}$$

$$= \sqrt{\frac{M_i}{2E_i}} \; \frac{dE_i}{dE_i / dR_i} \tag{69b}$$

By using Eq. (66a) for the stopping power, we have

$$dt = - t^o \frac{dE_i}{E_i - E_a} \tag{69c}$$

$$= - t^o \frac{d\varepsilon}{\varepsilon - 1} \tag{69d}$$

with the scale time

$$t^o = C_{E,i,p} \sqrt{M_i / 2} \quad \text{sec} \tag{69e1}$$

$$= C_{e,i,p} \sqrt{M_i / (2E_a)} \tag{69e2}$$

$$= C_{e,i,p} \left\{ \overline{V_{i,a}^2} \right\}^{-1/2} \tag{69e3}$$

Values of $\left\{ \overline{V_{i,a}^2} \right\}^{1/2}$, the rms thermal velocity of U, U^+, and UO^+, are given in Table 12 for the temperatures and altitudes in Table 10. Values of the scale time t^o, corresponding to the conditions in Table 17, are given in Table 20.

Table 20. Scale time t^o for U, U^+, and UO^+ in energy-time and range-time relations at several altitudes in a quiet MSIS-83 atmosphere.

Potential	i	$h = 200$	$h = 225$	$h = 250$	$h = 275$
			t^o, sec		
Polariz.	U^+	2.07	5.04	11.2	23.2
	UO^+	2.19	5.28	11.8	24.6
	(U^+, UO^+)	2.13	5.16	11.5	23.9
(r^{-6})	U, U^+	1.12	2.72	6.04	12.5
	UO^+	0.938	2.26	5.02	10.5
Eff. (r^{-6})	U, U^+	1.72	4.16	9.30	19.3
	UO^+	1.81	4.41	9.78	20.4
	(U, U^+, UO^+)	1.77	4.29	9.54	19.9

Integrating Eq. (69d), we have

$$t_f = \int_0^{t_f} dt' = t^0 \int_{\varepsilon_f}^{\varepsilon_s} \frac{d\varepsilon}{\varepsilon - 1} \tag{70a}$$

$$= t^0 \ln\left[\frac{\varepsilon_s - 1}{\varepsilon_f - 1}\right], \quad \varepsilon_f > 1 \tag{70b}$$

or

$$\boxed{\varepsilon_f - 1 = (\varepsilon_s - 1)\exp(-t_f/t^0).} \tag{71}$$

Equation (71), which is exact relative to the simplified stopping power expressed by Eq. (66a), has been used to provide in Table 21, for several values of the reduced starting energy (ε_s), values of the reduced finishing energy (ε_f) as a function of the reduced time (t_f/t^0). The fact that infinite time is required for ε_f to be reduced to 1.0 corresponds to the divergent integrand in Eq. (67d1).

If one ignored the ambient energy in the denominator of the integrand of Eq. (70a), the integrand would be ε^{-1} and the integral would be

$$t_f \approx t^0 \ln\left[\frac{\varepsilon_s}{\varepsilon_f}\right], \quad \varepsilon_f \geq 1 \tag{72a}$$

or

$$\varepsilon_f \approx \varepsilon_s \exp(-t_f/t^0), \quad \varepsilon_f \geq 1. \tag{72b}$$

Equation (72b) has been used to provide in Table 22, for several values of the reduced starting energy (ε_s), values of the reduced finishing energy ($\varepsilon_f \geq 1$) as a function of the reduced time (t_f/t^0).

3.3.6 Range-Time Relation.

Three range-time relations will be presented.

First, to obtain range-time information, one can use the energy-time relation given by Eq. (71) with the range-energy relation, Eq. (67), with a reasonable value for the cutoff. To gain further insight into the behavior of the integral in Eq. (67d1) when it is used for range-time relations instead of range-energy relations, we have recorded in Table 23 the results of evaluating the terms T_1, T_2, the sum T_1+T_2, and the ratio $(T_1+T_2)/T_1$ as a function of the reduced time (t_f/t^0), for starting reduced-energies ε_s of 3, 5, and 10. (In this implementation, the result of evaluating ε_f from Eq. (71) was used in Eqs. (67d3) and (67d4).)

50

Table 21. Reduced finishing energy versus reduced time for several values of reduced starting energy, per Eq. (71).

t_f / t^o	ε_f		
	$\varepsilon_s = 3$	$\varepsilon_s = 5$	$\varepsilon_s = 10$
0.0	3.00	5.00	10.00
0.1	2.81	4.62	9.14
0.2	2.64	4.27	8.37
0.3	2.48	3.96	7.67
0.4	2.34	3.68	7.03
0.5	2.21	3.42	6.46
0.6	2.10	3.20	5.94
0.7	1.99	2.99	5.47
0.8	1.90	2.80	5.04
0.9	1.31	2.63	4.66
1.0	1.74	2.47	4.31
1.1	1.67	2.33	4.00
1.2	1.60	2.20	3.71
1.3	1.55	2.09	3.45
1.4	1.49	1.99	3.22
1.5	1.45	1.89	3.01
1.6	1.40	1.81	2.82
1.7	1.37	1.73	2.64
1.8	1.33	1.66	2.49
1.9	1.30	1.60	2.35
2.0	1.27	1.54	2.22
2.1	1.24	1.49	2.10
2.2	1.22	1.44	2.00
2.3	1.20	1.40	1.90
2.4	1.18	1.36	1.82
2.5	1.16	1.33	1.74
2.6	1.15	1.30	1.67
2.7	1.13	1.27	1.60
2.8	1.12	1.24	1.55
2.9	1.11	1.22	1.50
3.0	1.10	1.20	1.45
∞	1.00	1.00	1.00

Table 22. Reduced finishing energy versus reduced time for several values of reduced starting energy, per Eq. (72b).

t_f/t^o	ε_f		
	$\varepsilon_s = 3$	$\varepsilon_s = 5$	$\varepsilon_s = 10$
0.0	3.00	5.00	10.00
0.1	2.71	4.52	9.05
0.2	2.46	4.09	8.19
0.3	2.22	3.70	7.41
0.4	2.01	3.35	6.70
0.5	1.82	3.03	6.07
0.6	1.65	2.74	5.49
0.7	1.49	2.48	4.97
0.8	1.35	2.25	4.49
0.9	1.22	2.03	4.07
1.0	1.10	1.84	3.68
1.1	1.00	1.66	3.33
1.2		1.51	3.01
1.3		1.36	2.73
1.4		1.23	2.47
1.5		1.12	2.23
1.6		1.01	2.02
1.7			1.83
1.8			1.65
1.9			1.50
2.0			1.35
2.1			1.22
2.2			1.11
2.3			1.00

Table 23: Comparison of approximate reduced range-time integrals.

$\frac{t_f}{t^\circ}$	$\varepsilon_s = 3$				$\varepsilon_s = 5$				$\varepsilon_s = 10$			
	T_1	T_2	T_1+T_2	$\frac{T_1+T_2}{T_1}$	T_1	T_2	T_1+T_2	$\frac{T_1+T_2}{T_1}$	T_1	T_2	T_1+T_2	$\frac{T_1+T_2}{T_1}$
0.0	0.00	0.00	0.00		0.00	0.00	0.00		0.00	0.00	0.00	
0.1	0.00	0.06	0.17	1.53	0.17	0.05	0.22	1.26	0.28	0.03	0.31	1.12
0.2	0.22	0.12	0.34	1.55	0.34	0.09	0.43	1.28	0.54	0.07	0.61	1.12
0.3	0.31	0.18	0.50	1.58	0.49	0.14	0.63	1.29	0.79	0.10	0.89	1.13
0.4	0.40	0.25	0.65	1.61	0.63	0.19	0.83	1.30	1.02	0.14	1.16	1.14
0.5	0.49	0.31	0.80	1.64	0.77	0.25	1.02	1.32	1.24	0.18	1.42	1.14
0.6	0.57	0.38	0.95	1.67	0.90	0.30	1.20	1.34	1.45	0.22	1.67	1.15
0.7	0.64	0.45	1.09	1.70	1.02	0.36	1.37	1.35	1.65	0.26	1.91	1.16
0.8	0.71	0.52	1.23	1.74	1.13	0.42	1.54	1.37	1.83	0.30	2.14	1.17
0.9	0.77	0.60	1.37	1.77	1.23	0.48	1.71	1.39	2.01	0.35	2.36	1.17
1.0	0.83	0.67	1.50	1.81	1.33	0.54	1.87	1.41	2.17	0.40	2.57	1.18
1.1	0.88	0.75	1.63	1.85	1.42	0.61	2.02	1.43	2.33	0.44	2.77	1.19
1.2	0.93	0.83	1.76	1.89	1.50	0.67	2.17	1.45	2.47	0.50	2.97	1.20
1.3	0.98	0.91	1.88	1.93	1.58	0.74	2.32	1.47	2.61	0.55	3.16	1.21
1.4	1.02	0.99	2.01	1.97	1.65	0.81	2.46	1.49	2.74	0.60	3.34	1.22
1.5	1.06	1.07	2.13	2.01	1.72	0.88	2.60	1.51	2.86	0.66	3.52	1.23
1.6	1.09	1.15	2.25	2.05	1.78	0.96	2.74	1.54	2.97	0.72	3.69	1.24
1.7	1.13	1.24	2.37	2.10	1.84	1.03	2.87	1.56	3.07	0.78	3.85	1.25
1.8	1.16	1.32	2.48	2.14	1.89	1.11	3.00	1.58	3.17	0.84	4.01	1.27
1.9	1.18	1.41	2.60	2.19	1.94	1.19	3.13	1.61	3.26	0.91	4.17	1.28
2.0	1.21	1.50	2.71	2.24	1.99	1.27	3.25	1.64	3.35	0.97	4.32	1.29
2.1	1.23	1.59	2.82	2.29	2.23	1.35	3.38	1.66	3.42	1.04	4.46	1.30
2.2	1.25	1.68	2.93	1.34	2.07	1.43	3.50	1.69	3.50	1.11	4.61	1.32
2.3	1.27	1.77	3.04	2.39	2.10	1.51	3.62	1.72	3.57	1.18	4.75	1.33
2.4	1.29	1.86	3.15	2.44	2.14	1.60	3.74	1.75	3.63	1.25	4.88	1.35
2.5	1.31	1.95	3.26	2.50	2.17	1.68	3.85	1.78	3.69	1.33	5.02	1.36
2.6	1.32	2.05	3.37	2.55	2.19	1.77	3.97	1.81	3.74	1.41	5.15	1.38
2.7	1.33	2.14	3.47	2.60	2.22	1.86	4.08	1.84	3.79	1.48	5.28	1.39
2.8	1.35	2.23	3.58	2.66	2.24	1.95	4.19	1.87	3.84	1.56	5.40	1.41
2.9	1.36	2.33	3.69	2.72	2.26	2.04	4.30	1.90	3.88	1.65	5.52	1.42
3.0	1.37	2.42	3.79	2.77	2.28	2.13	4.41	1.93	3.92	1.73	5.65	1.44
∞	1.46				2.47				4.32			

53

In those special cases where the ambient energy may be ignored in obtaining an approximate range-energy relation, such as is given by only term T_1 in Eq (67d2), two approximate range-time expressions can be obtained. Use of Eq (71) for ε_f gives the first of these two approximate expressions,

$$R_1 \approx 2C_{r,1,p}\left[\varepsilon_s^{1/2}-[1+(\varepsilon_s-1)\exp(-t_f/t^o)]^{1/2}\right]. \tag{73}$$

Equation (73) has a hybrid character because Eq. (71) for ε_f, as noted above, is an exact expression relative to the stopping power expressed by Eq. (66a) and includes the effect of the ambient energy.

The second of these two approximate expressions is obtained by use of Eq (72b) for ε_f,

$$R_1 \approx 2C_{r,1,p}\,\varepsilon_s^{1/2}\left[1-\exp(-t_f/2t^o)\right], \tag{74a}$$

provided

$$\varepsilon_s \geq \exp(t_f/t). \tag{74b}$$

SECTION 4

DIFFUSION COEFFICIENTS

4 1 ORDINARY DIFFUSION COEFFICIENT

In Appendix A, motivated in part by subsequent applications to Ba releases in Appendix D, we develop ordinary diffusion coefficients (D_i) based on the interaction potentials discussed in Section 2 for momentum-transfer cross-sections. Here, we present those formulas for application to uranium oxide ions Equation (A32), based on the polarization potential and effective (r^{-6})-potential is

$$D_i\Big|_\beta = \frac{3.21\times 10^6}{n_{tot}} \left(\frac{T_{STP}}{T}\right)^\beta \frac{T}{\sum_k f_k [\mu(A_{i,k})\alpha_k']^{1/2}} \quad \frac{km^2}{sec} \qquad (75)$$

$$\beta = \begin{cases} 0, & \text{polarization potential} \\ 1/6, & \text{effective } (r^{-6})\text{-potential} \end{cases}$$

Values of the collision parameters (involving the reduced mass and polarizabilities) are given in Table 5 in Section 2. Values of the atmospheric parameters are given in Table 10 in Section 3 for four altitudes in a quiet MSIS-83 atmosphere There is little difference between the reduced masses of U^+, UO^+, and UO_2^+ for collisions with atmospheric species Hence, we will evaluate Eq (75) specifically for UO^+, but apply the results to U^+, UO^+, and UO_2^+, as recorded in Table 24

Table 24 U^+, UO^+, and UO_2^+ diffusion coefficients at several altitudes in a quiet MSIS-83 atmosphere

h	$D_\perp$, km²/sec		$1+T_e/T_i$	$D_\parallel$, km²/sec	
km	Polariz	Eff.(r^{-6})		Polariz	Eff. (r^{-6})
200	0.099	0.083	2.5	0.25	0 21
225	0 25	0 21	2.5	0 62	0 5
250	0.57	0.48	2.5	1.4	1 2
275	1 2	1 0	2.5	3 0	2 5

4.2 AMBIPOLAR DIFFUSION COEFFICIENT.

The formula normally applied as the coefficient for ambipolar diffusion along the geomagnetic field ($D_\parallel$) is that given for the ambipolar diffusion coefficient by Eq. (D4b) In Appendix D,

$$D_\parallel \approx D_i [1 + T_e / T_i], \tag{76}$$

where D_i is the ordinary diffusion coefficient in Eq. (75) and T_e and T_i respectively are the electron and ion temperatures in the atmosphere. Such temperatures, not easily predicted for a given model atmosphere, are discussed in Appendix D with respect to applications to Ba releases. Here, we shall simply adopt a nominal value of 1.5 for the ratio T_e / T_i. Values of the ambipolar diffusion coefficient are given in Table 24 for four altitudes in a quiet MSIS-83 atmosphere.

SECTION 5

COMPARISONS OF MOMENTUM-TRANSFER CROSS-SECTIONS
WITH SELECTED URANIUM OXIDE REACTION CROSS-SECTIONS;
RATE COEFFICIENTS FOR SELECTED URANIUM OXIDE REACTIONS

5.1 INTRODUCTION.

It is interesting to compare some of our momentum-transfer cross-sections developed in Section 2 with cross sections for certain reactions, specially atom-transfer reactions. (The writer expects momentum-transfer cross-sections should not be less than atom-transfer cross-sections.) Also, as an auxiliary product of these considerations, rate coefficients are derived for selected uranium oxide reactions for which velocity-dependent cross-sections are either known or assumed, based on extrapolations and/or averaged values of measurements.

Before considering specific reactions, we develop a needed relation between a power-law reaction cross-section in the form

$$\sigma(g) = \sigma_o(g_o)\left[\frac{g_o}{g}\right]^n \tag{77}$$

and the corresponding rate coefficient, k. We start with the general relation between the rate coefficient and velocity-dependent cross-section for a Maxwellian distribution of velocities, given as, e.g., by Light, Ross, and Shuler [Ref. 42, Eq. (30)],

$$k = \left[\frac{\mu}{2\pi\kappa T}\right]^{3/2} 4\pi \int_0^\infty g^3\sigma(g)\exp\left[-\frac{\mu g^2}{2\kappa T}\right]dg . \tag{78}$$

By using Eq. (77) and letting g_o be the mean value of the relative velocity distribution, i.e.,

$$g_o = \bar{g} = \left[\frac{8\kappa T}{\pi\mu}\right]^{1/2}, \tag{79a}$$

we get

$$k(T) = \sigma_o(\bar{g})\,\bar{g}(T)\,G_n \tag{79b}$$

with G_n, proportional to Euler's integral for the gamma function [Ref. 1, p. 255],

$$G_n = \left[4/\pi\right]^{n/2} \Gamma(2 - n/2) \tag{79c}$$

$$\Gamma(2 - n/2) = \int_0^\infty x^{1-n/2}e^{-x}\,dx , \tag{79d}$$

tabulated in Table 25 for several values of n.

57

Table 25. Values of the parameter G_n relating rate coefficient and power-law reaction cross-section.

n	$\Gamma(2-n/2)$	$[4/\pi]^{n/2}$	$G_n =[4/\pi]^{n/2}\,\Gamma(2-n/2)$
0	$\Gamma(2)$ = 1.00000	1.0000	1.0000
1/2	$\Gamma(7/4)$ = 0.91906	1.0622	0.9763
1	$\Gamma(3/2)$ = 0.88623	1.1284	1.000
3/2	$\Gamma(5/4)$ = 0.90640	1.1986	1.086

5.2 $U^+ + O_2 \rightarrow UO^+ + O$.

5.2.1 Results of Armentrout and Beauchamp [Ref. 4].

The cross section measured by Armentrout and Beauchamp [Ref 4] for the reaction

$$U^+ + O_2 \rightarrow UO^+ + O \tag{80}$$

is well represented by the expression

$$\sigma[U^+(O_2,0)UO^+] = \begin{cases} \dfrac{50\times10^{-16}}{E_{CM}^{1/4}} & , \ 0.24 < E_{CM} \le 3.43\,eV \\[3mm] 21\times10^{-16}\,\dfrac{6}{E_{CM}} & , \ 3.43 \le E_{CM} \le 18\,eV \end{cases} \tag{81a}$$

The exponents of the energy dependence in Eq. (81a) are given in Ref. 4, but the coefficients are inferred by the writer from reading the small graphs in Ref 4. To express the lower-energy portion of the cross section in terms of the relative velocity, we first write

$$E_{CM} = \frac{1.66\times10^{-24}\,\mu(A_{i,k})g^2}{2\times1.6\times10^{-12}} = 1.46\times10^{-11}g^2 \tag{81b1}$$

$$= 0.146\,g^2_{km/sec} \tag{81b2}$$

so that substitution of Eq. (81b2) in Eq. (81a1) gives

$$\sigma[U^+(O_2,0)UO^+] = \frac{8.08\times10^{-15}}{g_{km/sec}^{1/2}}\,cm^2, \ 1.28 \le g_{km/sec} \le 4.84 \tag{81c}$$

The cross section in Eq. (81c) is shown in Fig. 10 as the solid line and extrapolated to lower velocities as the short-dash line.

Armentrout and Beauchamp [Ref. 4] also quote a rate coefficient at 300 K for Reaction (80),
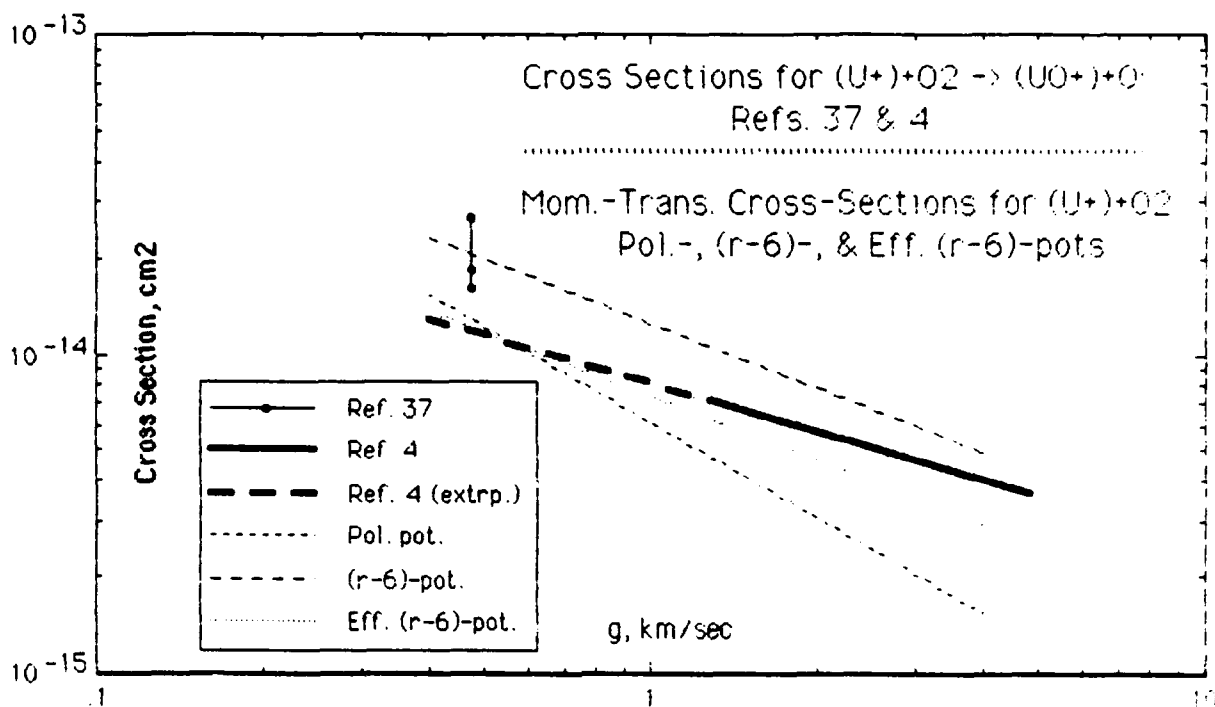
Figure 10. Comparison of momentum-transfer cross-sections, based on various
interaction potentials, for $(U^+ + O_2)$-collisions with the cross sections
for the atom-exchange reaction $U^+ + O_2 \rightarrow UO^+ + O$.

$$k[U^+(O_2,O)UO^+] = 5.6 \times 10^{-10} \frac{cm^3}{molecule\ sec}, \qquad (82)$$

obtained by extrapolating their data to lower velocities and averaging over a
Maxwellian distribution. We now show the essential consistency between Eq. (82)
and our formalism. First, we rewrite Eq. (81c) in the form of Eq. (77), i.e.,

$$\sigma[U^+(O_2,O)UO^+] = 1.18 \times 10^{-14} \left[\frac{4.74 \times 10^4}{g_{cm/sec}}\right]^{1/2}, \qquad (83a)$$

so that

$$\sigma_0 = 1.18 \times 10^{-14} \ cm^2, \quad g_0 = 4.74 \times 10^4 \ cm/sec, \quad n = 1/2. \qquad (83b,c,d)$$

Then, from Eq. (79b), we have

$$k[U^+(O_2,O)UO^+] = 5.44 \times 10^{-10} \frac{cm^3}{molecule\ sec}, \qquad (83e)$$

in essential agreement with the value quoted by Ref. 4, Eq. (82). The 2.9%
difference is probably due to our error in reading the small graph in Ref. 4

59

5.2.2 Results of Johnsen and Biondi [Ref. 37].

Johnsen and Biondi [Ref. 37] measured the rate coefficient for Reaction (80) at a temperature of 300 K and report

$$k[U^+(O_2,0)UO^+] = 8.5 \begin{bmatrix} -1 \\ +4 \end{bmatrix} \times 10^{-10} \frac{cm^3}{molecule\ sec} . \tag{84}$$

We now infer the constant $\sigma_0(g_0)$ [cf. Eq. (77)] implied by the rate coefficient in Eq. (84). If we assume the exponent n is the same as in the measurements reported by Ref. 4, namely, n = 1/2, then from Eq. (79b) we have

$$\sigma_0(\bar{g}) = \frac{k}{0.9763\,\bar{g}} \tag{85a}$$

$$\bar{g} = \left[\frac{8\kappa T}{\pi \mu} \right]^{1/2} = 4.74 \times 10^4\ cm/sec = 0.474\ km/sec \tag{85b}$$

$$\sigma_0(\bar{g}) = \frac{8.5 \begin{bmatrix} -1 \\ +4 \end{bmatrix} \times 10^{-10}}{0.9763 \times 4.74 \times 10^4} \tag{85c}$$

$$\boxed{\sigma_0(\bar{g}) = 1.84 \begin{bmatrix} -0.22 \\ +0.86 \end{bmatrix} \times 10^{-14}\ cm^2 .} \tag{85d}$$

In Fig. 10, the cross-section value in Eq. (85d) is plotted at the relative velocity in Eq. (85b) and labeled as Ref. 37. The central point of this inferred cross-section value is larger than the extrapolated cross-section of Ref. 4 by a factor of ≈ 1.6.

5.2.3 Momentum-Transfer Cross-Sections for $U^+ + O_2$.

From Eq. (40) and Table 9 in Section 2 (or equivalently, Eqs. (33b2), (34c), and (35b2)), we have three momentum-transfer cross-sections for the collision pair $U^+ + O_2$,

$$\sigma(U^+ + O_2)|_{pol.pot.} = 6.14 \times 10^{-15} g_{km/sec}^{-1}\ cm^2 \tag{86a}$$

$$\sigma[U^+ + O_2]_{\approx(r^{-6})-pot.} = 1.25 \times 10^{-14}\ g_{km/sec}^{-2/3}\ cm^2 \tag{86b}$$

$$\sigma(U^+ + O_2)|_{Eff.(r^{-6})-pot.} = 7.38 \times 10^{-15}\ g_{km/sec}^{-2/3}\ cm^2 . \tag{86c}$$

These cross sections are plotted and respectively labeled in Fig. 10 as "Pol. pot.", "$\approx(r^{-6})$-pot.", and "Eff. (r^{-6})-pot." The slope of the cross-section based on the polarization potential certainly disagrees with that measured by Ref. 4; the slope of the other two momentum-transfer cross-sections disagrees less strongly. At about 0.47 km/sec, Eq. (86b) is certainly consistent with the value inferred from the Ref. 37 measurement of rate coefficient; Eq. (86c) disagrees only mildly with the extrapolation of the Ref. 4 data.

5.2.4 Comments on Literature Rate Coefficients.

The following comments are peripheral to the main thrust of this section, but are relevant to the aspect of rate coefficient for Reaction (80). Gilmore's suggested rate coefficient [Ref. 24], 7×10^{-10} cm³/(molecule sec), for Reaction (80) is the average of the value determined (by extrapolation) in Ref. 4 and the Ref. 37 value. Since an energy-dependent cross-section was assumed in the Ref. 4 extrapolation, we suggest that a temperature dependence should appear in such an averaged rate coefficient. To express the Ref. 4 results in a temperature-dependent rate-coefficient form, we first use Eq. (81b) to write

$$\sigma_o(\bar{g}) = \frac{2.56 \times 10^{-12}}{\left[\bar{g}_{cm/sec} \right]^{1/2}} \qquad (87a)$$

so that we have the product

$$\sigma_o(\bar{g}) \, \bar{g}(T) = 2.56 \times 10^{-12} \left[\bar{g}(T) \right]^{1/2} \qquad (87b)$$

or, with Eq. (79a),

$$\sigma_o(\bar{g}) \, \bar{g}(T) = 2.56 \times 10^{-12} \left[\frac{8 \kappa T}{\pi \mu} \right]^{1/4} \qquad (87c)$$

$$= 5.58 \times 10^{-10} \left[\frac{T}{300} \right]^{1/4} . \qquad (87d)$$

Substitution of Eq. (87d), and the value of $G_{1/2}$ from Table 25, in Eq. (79b) gives

$$k[U^+(O_2,0)UO^+] = 5.44 \times 10^{-10} \left[\frac{T}{300} \right]^{1/4} \frac{cm^3}{molecule \ sec} \qquad (87e)$$

Thus, the temperature-dependent factor is $[T/300]^{1/4}$. Hence, we suggest modifying the Ref. 24 rate coefficient to become

$$k[U^+(O_2,0)UO^+] = 7 \times 10^{-10} \left[\frac{T}{300} \right]^{1/4} \frac{cm^3}{molecule \ sec} . \qquad (88)$$

The essence of the above comment on temperature dependence also applies to the rate coefficient for Reaction (80) given in Table I of Ref. 5, where the extrapolation-based value from Ref. 4 is given, i.e., 5.6×10^{-10}. We suggest that, in generalizing that value, one should write

$$k[U^+(O_2,0)UO^+] = 7 \times 10^{-10} \left[\frac{T}{300} \right]^{1/4} \frac{cm^3}{molecule \ sec} . \qquad (89)$$

5.3 $UO^+ + O_2 \rightarrow UO_2^+ + O$.

5.3.1 Results of Armentrout and Beauchamp [Ref. 4].

The cross section measured by Armentrout and Beauchamp [Ref. 4] for the reaction

$$UO^+ + O_2 \rightarrow UO_2^+ + O \qquad (90)$$

is well represented by the expression

$$\sigma[UO^+(O_2,O)UO_2^+] = \begin{cases} 40 \times 10^{-16} \left[\dfrac{0.6}{E_{CM}} \right]^{0.55} & , \ 0.42 \leq E_{CM} \leq 6.07 \, eV \\ 7.4 \times 10^{-16} \left[\dfrac{8}{E_{CM}} \right]^{1.5} & , \ 6.07 \leq E_{CM} \leq 22 \, eV \end{cases} \qquad (91a)$$

The exponents of the energy dependence in Eq. (91a) are given in Ref. 4, but the coefficients are inferred by the writer from reading the small graphs in Ref. 4. To express the lower-energy portion of the cross section in terms of the relative velocity, we first write

$$E_{CM} = \frac{1.66 \times 10^{-24} \mu(A_{i,k}) g^2}{2 \times 1.6 \times 10^{-12}} = 1.47 \times 10^{-11} g^2 \qquad (92a)$$

$$= 0.147 \, g^2_{km/sec} \qquad (92b)$$

so that substitution of Eq. (92b) in Eq. (91a1) gives

$$\boxed{\sigma[UO^+(O_2,O)UO_2^+] = \frac{8.67 \times 10^{-15}}{g^{1.1}_{km/sec}} \, cm^2, \quad 1.75 \leq g_{km/sec} \leq 6.42} \qquad (91b)$$

The cross section in Eq. (91b) is shown in Fig. 11 as the solid line and extrapolated to lower velocities as the short-dash line.

To develop the rate coefficient at temperature T corresponding to the (downward extrapolated, where necessary) cross section in Eq. (91b), we first rewrite Eq. (91b) in the form of Eq. (77), i.e.,

$$\sigma[UO^+(O_2,O)UO_2^+] = \frac{2.74 \times 10^{-9}}{[\bar{g}(T)]^{1.1}} \left[\frac{\bar{g}(T)}{g_{cm/sec}} \right]^{1.1} \qquad (93a)$$

so that

$$\sigma_o = \frac{2.74 \times 10^{-9}}{[\bar{g}(T)]^{1.1}}, \quad g_o = \bar{g}(T), \quad n = 1.1. \qquad (93b,c,d)$$

Then, from Eq. (79b), we have

$$k[UO^+(O_2,O)UO_2^+] = \frac{2.74 \times 10^{-9}}{[\bar{g}(T)]^{1.1}} \, \bar{g}(T) G_{1.1} \qquad (93e)$$

62
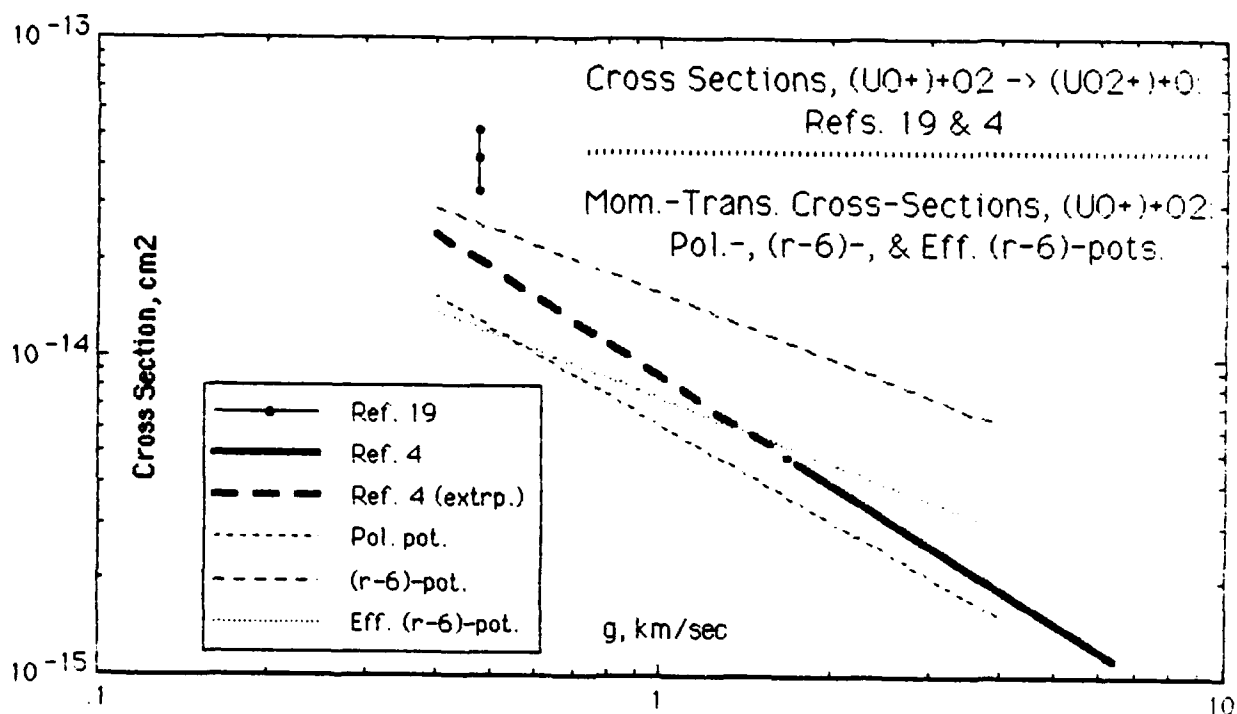
Figure 11. Comparison of momentum-transfer cross-sections, based on various
interaction potentials, for $(UO^+ + O_2)$-collisions with the cross
sections for the atom-exchange reaction $UO^+ + O_2 \rightarrow UO_2^* + O$.

$$k[UO^+(O_2,O)UO_2^*] = 2.74 \times 10^{-9} [\bar{g}(T)]^{-0.10} G_{11} \qquad (93f)$$

$$= 2.74 \times 10^{-9} \left[\frac{8kT}{\pi\mu}\right]^{-0.05} 1.011 \qquad (93g)$$

$$= 9.44 \times 10^{-10} \left[\frac{T}{300}\right]^{-0.05} \frac{cm^3}{molecule\,sec} \qquad (93h)$$

5.3.2 Results of Fite and Lo [Ref. 19].

Fite and Lo [Ref. 19] measured the rate coefficient for Reaction (90) at
thermal energies and reported

$$k[UO^+(O_2,O)UO_2^*] = (2.03 \pm 0.44) \times 10^{-9} \frac{cm^3}{molecule\,sec} \qquad (94)$$

The term "thermal energies" is not further defined. This rate coefficient is
typically quoted and used as being implicitly temperature independent [e.g., Ref. 3,

p. 48; Ref. 5, Table I; Ref. 24]. Such usage implies an assumed g^{-1}-dependence for the cross section, which is certainly close to that found by Ref. 4 at higher energies.

Similar to our treatment of the Ref. 37 rate coefficient in Eq. (84), we infer the constant σ_0 [cf. Eq. (77)] implied by the rate coefficient in Eq. (94). If we assume the exponent n is the same as in the measurements reported by Ref. 4, namely, n = 1.1 (although use of n = 1.0 would not make a significant difference), then from Eq. (79b), for T = 300 K, we have

$$\sigma_0 = \frac{k}{\bar{g}\,G_n} = \frac{(2.03\pm0.44)\times10^{-9}}{4.73\times10^4\times1.011} = (4.24\pm0.92)\times10^{-14}\,cm^2. \qquad (95)$$

In Fig. 11 this cross section is plotted at a relative velocity of 0.473 km/sec and labeled as Ref. 19. The central point of this inferred cross-section is larger than the extrapolated cross-section of Ref. 4 by a factor of $\approx$2.2.

Before leaving the rate coefficient reported in Ref. 19, it is worth noting that Eq. (10) in Ref. 19 used to evaluate k for Reaction (90) is proportional to the ratio of two rate coefficients, each of which is corrected upward by the factor 2.39 reported by Halle, Lo, and Fite [Ref. 27]. Thus, the rate coefficient given by Eq. (94) is unaffected by the correction factor from Ref. 27.

5.3.3 Momentum-Transfer Cross-Sections for $UO^+ + O_2$.

From Eq. (40) and Table 9 in Section 2 (or equivalently, Eqs. (37c, (38b), and (39c)), we have three momentum-transfer cross-sections for the collision pair $UO^+ + O_2$,

$$\sigma(UO^+ + O_2)\big|_{pol.pot.} \approx 6.14\times10^{-15}\,g^{-1}_{km/sec}\,cm^2 \qquad (96a)$$

$$\sigma[UO^+ + O_2]\big|_{\approx(r^{-6})-pot.} \approx 1.56\times10^{-14}\,g^{-2/3}_{km/sec}\,cm^2 \qquad (96b)$$

$$\sigma(UO^+ + O_2)\big|_{Eff.(r^{-6})-pot.} = 7.38\times10^{-15}\,g^{-2/3}_{km/sec}\,cm^2. \qquad (96c)$$

These cross sections are plotted and respectively labeled in Fig. 11 as "Pol. pot.", "$\approx(r^{-6})$-pot.", and "Eff. (r^{-6})-pot." The slope of the polarization-potential based cross-section closely agrees with that measured by Ref. 4; the slope of the other two momentum-transfer cross-sections disagrees more strongly. At about 0.47 km/sec, Eq. (96b) lies between the value inferred from the Ref. 19 measurement of rate coefficient and the extrapolation of the Ref. 4 data.

5.4 $U+O_2 \rightarrow UO_2^+ + e$.

5.4.1 Results of Fite, Lo, and Irving [Ref. 20] and of Halle, Lo, and Fite [Ref. 27].

The effective cross-section for the associative-ionization reaction
$$U+O_2 \rightarrow UO_2^+ + e \tag{97}$$
measured by Fite, Lo, and Irving [Ref. 20] is

$$\sigma[U(O_2,e)UO_2^+]^{eff} = (1.68 \pm 0.27) \times 10^{-17} \text{ cm}^2 \tag{98a}$$

at a relative velocity, e.g., of 6.30×10^4 cm/sec [Ref. 20]. Fite et al. [Ref. 20] also explain that the "true" cross-section – instead of the "effective" cross-section given above – is smaller by the factor $1/1.42$ under the experimentally-based assumption that the cross section is independent of velocity [but the velocity range is not given]. Thus,

$$\sigma[U(O_2,e)UO_2^+]^{true} = (1.42)^{-1} \times \sigma[U(O_2,e)UO_2^+]^{eff}$$
$$= (1.18 \pm 0.19) \times 10^{-17} \text{ cm}^2. \tag{98b}$$

This correction factor apparently takes account of the finite thermal velocities of the O_2 targets, as explained in detail in Ref. 20, Appendix A.

These cross sections were revised upward by Halle, Lo, and Fite [Ref. 27] who state the revised effective cross-section is
$$\sigma[U(O_2,e)UO_2^+]^{eff}_{revised} = (4.01 \pm 0.55) \times 10^{-17} \text{ cm}^2, \tag{99a}$$
larger by a factor of 2.39 than the value determined in Ref. 20. Correspondingly, we have
$$\sigma[U(O_2,e)UO_2^+]^{true}_{revised} = (1.42)^{-1} \times \sigma[U(O_2,e)UO_2^+]^{eff}_{revised}$$
$$\boxed{\sigma[U(O_2,e)UO_2^+]^{true}_{revised} = (2.83 \pm 0.39) \times 10^{-17} \text{ cm}^2.} \tag{99b}$$

The rate coefficient corresponding to Eq. (99b), from Eq. (79b) and for n = 0, is

$$k[U(O_2,e)UO_2^+]^{true}_{revised} = \sigma[U(O_2,e)UO_2^+]^{true}_{revised} \, \bar{g}(T) \, G_0$$
$$= 2.82 \times 10^{-17} \left[\frac{8kT}{\pi \mu} \right]^{1/2} \times 1$$
$$= 1.34 \times 10^{-12} \left[\frac{T}{300} \right]^{1/2} \frac{\text{cm}^3}{\text{molecule sec}} \tag{100}$$

This rate coefficient differs from that in Table I of Ref. 5 in that we have (a) used $\sigma^{true}_{revised}$ instead of $\sigma^{eff}_{revised}$ and (b) explicitly written the temperature dependence.

65

5.4.2 Results of Young, Dehmer, Cohen, Pobo, and Wexler [Ref. 68]

Reaction (97) was measured by Young et al. [Ref. 68] who report results which can be expressed as

$$\sigma[U(O_2,e)UO_2^+] = 1.58 \times 10^{-17} \left[\frac{0.63}{g_{km/sec}} \right]^{0.99} cm^2, \quad 1.2 \le g_{km/sec} \le 6.5 \tag{101}$$

Young et al. [Ref. 68] state that

"... extrapolation of the deconvoluted UO_2^+ cross section to
$v_r \simeq 6.3 \times 10^4$ cm/sec (E_{rel} = 0.058 eV) with the use of the functional form derived in Sec. III [our Eq. (101)] leads to a value of 1.58×10^{-17} cm2, which is to be compared with the "Q-true" of 1.19×10^{-17} cm2 reported by the authors of Ref. 20 at the same average relative velocity in their Maxwellian beam-gas experiment."

"While this level of agreement is encouraging, it is to be emphasized that the conditions of the present experiment were not optimized for the measurement of absolute cross sections, ..."
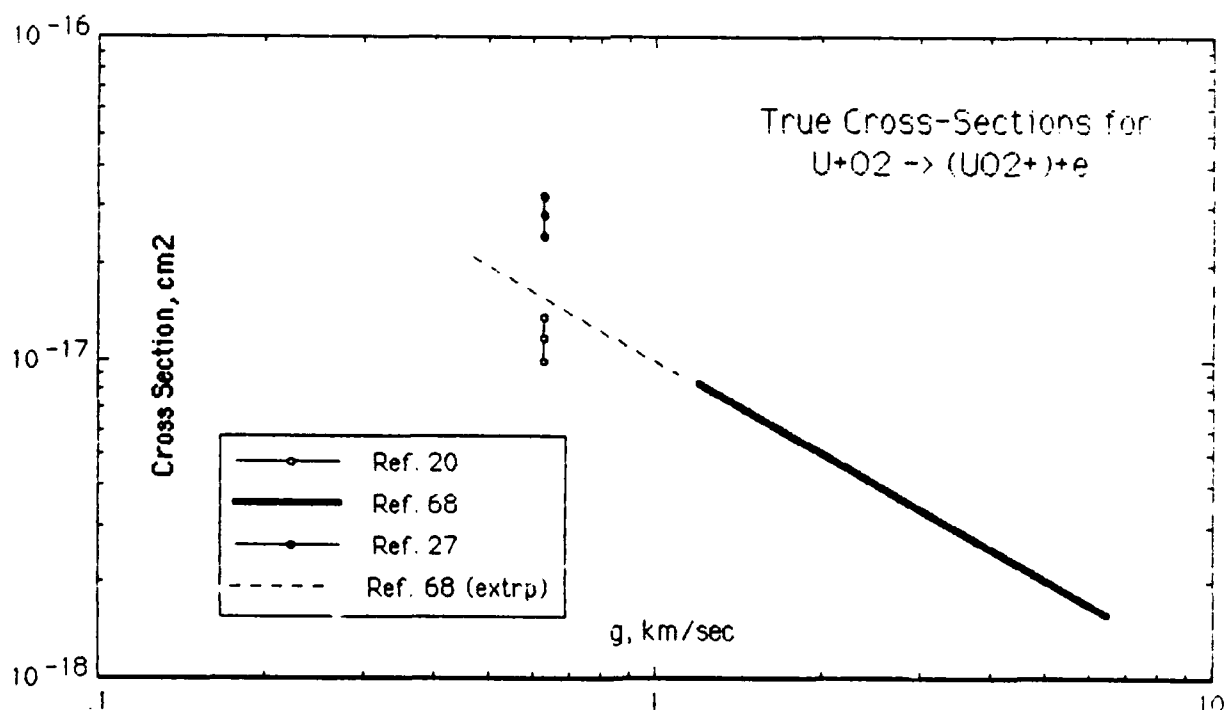
Figure 12. Cross sections for the associative ionization reaction $U+O_2 \rightarrow UO_2^+ + e$.

In Fig. 12 we show the results from Young et al. [Ref. 68], from Fite et al. [Ref. 20], and from Halle et al. [Ref. 27]. It is unfortunate that the work of Young et al. [Ref. 68] was done before Halle et al. [Ref. 27] reported the upward correction factor to their earlier work in Ref. 20 to which Ref. 68 refers. How would Young et al. have regarded the comparison of their results with that in Ref. 27? To this writer, the level of agreement is certainly far less encouraging than earlier

5.4.3 Momentum-Transfer Cross-Sections for $U+O_2$.

For completeness we present momentum-transfer cross-sections for the collision pair $U+O_2$, but we do not expect such cross sections should be comparable to the cross-section for Reaction (97). From Eq. (40) and Table 9 in Section 2 (or equivalently, Eqs. (27a3) and (27c2)), we have two momentum-transfer cross-sections for the collision pair $U+O_2$,

$$\sigma[U+O_2]\big|_{*(r^{-6})-pot.} = 1.24 \times 10^{-14} \, g_{km/sec}^{-2/3} \text{ cm}^2 \qquad (102a)$$

$$\sigma(U+O_2)\big|_{Eff.(r^{-6})-pot.} = 7.38 \times 10^{-15} \, g_{km/sec}^{-2/3} \text{ cm}^2. \qquad (102b)$$

These two momentum-transfer cross-sections are several orders-of-magnitude larger than the cross section for Reaction (97). If we consider a value of 0.63 km/sec for the relative velocity, then the average reaction cross-section – derived from (1) the extrapolated value (1.58×10^{-17} cm^2) from Ref. 68 and (2) the value (true, revised: ($1.68/1.42$) $\times 10^{-17} \times 2.39 = 2.83 \times 10^{-17}$ cm^2) from Ref. 27 – is $0.5(1.58 + 2.83) \times 10^{-17} = 2.21 \times 10^{-17}$ cm^2, smaller than the two momentum-transfer cross-sections by respective factors of 763 and 454.

5.5 $U+O_2 \rightarrow UO+O$.

5.5.1 Results of Fite, Lo, and Irving [Ref. 20] and of Halle, Lo, and Fite [Ref. 27].

It appears that the reaction of $U+O_2$, at low energy, has two principal branches, one described by Reaction (97) for associative ionization and the other with neutral products – with a much smaller cross-section – by

$$U+O_2 \rightarrow UO+O \qquad (103)$$

The total effective cross-section for the $U+O_2$ reaction is [Ref. 20]

$$\sigma[U(O_2,X)Y]_{total}^{eff} = (1.78 \pm 0.45) \times 10^{-15} \text{ cm}^2. \qquad (104)$$

By subtracting the associative ionization cross-section from the total cross-section, we get that for the neutral products,

$$\sigma[U(O_2,O)UO]^{eff} = \sigma[U(O_2,X)Y]_{total}^{eff} - \sigma[U(O_2,e)UO_2^+]_{revised}^{eff} \qquad (105a)$$

$$= (1.78 \pm 0.45) \times 10^{-15} - (4.01 \pm 0.55) \times 10^{-17} \qquad (105b)$$

$$= (1.74 \pm 0.45) \times 10^{-15} \text{ cm}^2. \qquad (105c)$$

For the "true" cross-section, we have

$$\sigma[U(O_2,0)UO]^{true} = (1.42)^{-1} \times \sigma[U(O_2,0)UO]^{eff} \qquad (106a)$$

$$\boxed{\sigma[U(O_2,0)UO]^{true} = (1.22 \pm 0.32) \times 10^{-15} \ cm^2} \qquad (106b)$$

The rate coefficient corresponding to Eq. (106b), from Eq. (79b) and for $n = 0$, is

$$k[U(O_2,0)UO]^{true} = \sigma[U(O_2,0)UO]^{true} \ \bar{g}(T) \ G_0$$

$$= 1.22 \times 10^{-15} \left[\frac{8kT}{\pi \mu} \right]^{1/2} \times 1$$

$$\boxed{k[U(O_2,0)UO]^{true} = 5.79 \times 10^{-11} \left[\frac{T}{300} \right]^{1/2} \frac{cm^3}{molecule \ sec}} \qquad (107)$$

This rate coefficient differs from that in Table I of Ref. 5 principally in that we have (a) used σ^{true} instead of σ^{eff} and (b) explicitly written the temperature dependence. Augmentation of k^{true} by the factor 1.42 to give k^{eff} results in $k^{eff} = 8.22 \times 10^{-11}$, somewhat smaller than the 9×10^{-11} in Table I of Ref. 5, for an unknown reason.

5.5.2 Momentum-Transfer Cross-Sections for $U+O_2$.

The two momentum-transfer cross-sections given by Eqs. (102a) and (102b) are approximately an order-of-magnitude larger than the cross section for Reaction (103). At a relative velocity of 0.63 km/sec, the reaction cross-section is smaller than the two momentum-transfer cross-sections by respective factors of 14 and 8.2.

5.6 $U+O \rightarrow UO^+ + e$.

5.6.1 Results of Fite, Lo, and Irving [Ref. 20] and of Halle, Lo, and Fite [Ref. 27].

The effective cross-section measured by Fite et al. [Ref. 20, pp. 1236, 1239] for the associative ionization reaction

$$U+O \rightarrow UO^+ + e \qquad (108)$$

is

$$Q_1 = \sigma[U(O,e)UO^+]^{eff} = (97 \pm 20) \times Q_2 \qquad (109a)$$

$$= (1.63 \pm 0.43) \times 10^{-15} \ cm^2 \qquad (109b)$$

where

$$Q_2 = \sigma[U(O_2,e)UO_2^+]^{eff} = (1.68 \pm 0.27) \times 10^{-17} \ cm^2 . \qquad (110)$$

68

Similarly, by using the stated [Ref. 20, pp. 1240, 1248] ratio of true cross-sections (Q_1/Q_2) and reducing the effective cross-section Q_2' by the factor 1.42 to obtain the true cross-section Q_2, we have

$$Q_1 = \sigma[U(O,e)UO^+]^{true} = \frac{Q_1}{Q_2} Q_2 \qquad (111a)$$

$$= (1.21 \pm 0.30) \times 10^{-15} \, cm^2 \qquad (111b)$$

where

$$\frac{Q_1}{Q_2} = (103 \pm 20) \qquad (111c)$$

$$Q_2 = \sigma[U(O_2,e)UO_2^+]^{true} = (1.18 \pm 0.19) \times 10^{-17} \, cm^2 . \qquad (111d)$$

To obtain the revised effective cross-section $Q_{1,rev}'$, we write

$$Q_{1,rev}' = \sigma[U(O,e)UO^+]_{rev}^{eff} = (97 \pm 20) \times Q_{2,rev}' \qquad (112a)$$

$$= (3.89 \pm 0.96) \times 10^{-15} \, cm^2 \qquad (112b)$$

where the revised effective cross-section $Q_{2,rev}'$ from Ref. 27 is

$$Q_{2,rev}' = \sigma[U(O_2,e)UO_2^+]_{rev}^{eff} = (4.01 \pm 0.55) \times 10^{-17} \, cm^2 . \qquad (112c)$$

Similarly, to obtain the revised true cross-section $Q_{1,rev}$, we write

$$Q_{1,rev} = \sigma[U(O,e)UO^+]_{rev}^{true} = \frac{Q_1}{Q_2} Q_{2,rev} \qquad (113a)$$

$$\boxed{Q_{1,rev} = (2.90 \pm 0.69) \times 10^{-15} \, cm^2} \qquad (113b)$$

where

$$Q_{2,rev} = \sigma[U(O_2,e)UO_2^+]_{rev}^{true} = (2.82 \pm 0.39) \times 10^{-17} \, cm^2 . \qquad (113c)$$

Fite et al. [Ref. 20, Appendix A, p. 1247] presume that the same velocity independence of cross section that applies to associative ionization for the $U+O_2$ reaction also applies to associative ionization for the $U+O$ reaction. However, those authors do not state the velocity range for which this presumption may be valid.

The rate coefficient corresponding to Eq. (113b), from Eq. (79b) and for $n = 0$, is

$$k[U(O,e)UO^+]_{rev}^{true} = \sigma[U(O,e)UO^+]_{rev}^{true} \, \bar{g}(T) \, G_0$$

$$= 2.90 \times 10^{-15} \left[\frac{8kT}{\pi\mu}\right]^{1/2} \times 1$$

$$k[U(O,e)UO^+]_{rev}^{true} = 1.89 \times 10^{-10} \left[\frac{T}{300} \right]^{1/2} \quad \frac{cm^3}{molecule\,sec}$$ (114)

This rate coefficient differs from that in Table I of Ref. 5 in that we have (a) used σ_{rev}^{true} instead of σ_{rev}^{true} and (b) explicitly written the temperature dependence

5.6.2 Momentum-Transfer Cross-Sections for U+O.

From Eq. (40) and Table 9 in Section 2 (or equivalently, Eqs. (25b) and (26b)), we have two momentum-transfer cross-sections for the collision pair U+O,

$$\sigma(U+O)\big|_{(r^{-6})-pot.} = 9.79 \times 10^{-15}\, g_{km/sec}^{-2/3}\ cm^2$$ (115a)

$$\sigma(U+O)\big|_{Eff.(r^{-6})-pot.} = 6.41 \times 10^{-15}\, g_{km/sec}^{-2/3}\ cm^2\,.$$ (115b)

These two momentum-transfer cross-sections are about a half order-of-magnitude larger than the cross section for Reaction (97). If we consider a somewhat arbitrary value of 0.6 km/sec for the relative velocity, then the reaction cross-section $\sigma[U(O,e)UO^+]_{rev}^{true}$ given by Eq. (113b) is smaller than the two momentum-transfer cross-sections by respective factors of 4.8 and 3.1. These factors become unity at respective relative velocities of 4.8 and 3.1 km/sec.

5.7 SUMMARY OF CROSS SECTIONS AND RATE COEFFICIENTS FOR SELECTED URANIUM OXIDE REACTIONS.

In Table 26 we have collated suggested cross-sections and rate coefficients for the more important uranium oxide reactions, for which the following notes obtain.

Notes for Table 26: Suggested Cross Sections & Rate Coefficients
for Selected $[(UO_n)^{m+} + (O,O_2)]$-Reactions

---

a. "True" cross-section [Ref. 20]; revised [Ref. 27], Eq. (113b). Reaction rate coefficient is given in two-temperature form in Table 26 as well as one-temperature form; cf. Eq. (114). See Section 5.6 for details.

b. See Fig. 13. Velocity dependence [Ref. 4]; coefficient is determined by average value at $g = 4.74 \times 10^4$ cm/sec of (1) extrapolated value (1.18×10^{-14} cm^2) from Ref. 4 (cf. Eq. (81b) and Fig. 10) and (2) value (1.84×10^{-14} cm^2; cf. Eq. (85d)) inferred from Ref. 37 rate coefficient by assuming $g^{-1/2}$ velocity dependence from Ref. 4. See Section 5.2 for details.

c. See Fig. 14. Velocity dependence [Ref. 4]; coefficient is determined by average value at g = 4.73 x10^4 cm/sec of (1) extrapolated value (1.97 x 10^{-14} cm2) from Ref. 4 (cf. Eq. (91b) and Fig. 11) and (2) value (4.24 x10^{-14} cm2; cf. Eq. (95)) inferred from Ref. 19 rate coefficient by assuming $g^{-1.1}$ velocity dependence from Ref. 4. See Section 5.3 for details.

d. See Fig. 15. Velocity dependence [Ref. 68]; coefficient is determined by average value at g = 6.3 x10^4 cm/sec of (1) extrapolated value (1.58 x10^{-17} cm2) from Ref. 68 (cf. Eq. (101) and Fig. 12) and (2) value (true, revised: (1.68/1.42) x10^{-17} x 2.39 = 2.83 x 10^{-17} cm2; cf. Eq. (99b)) from Ref. 27. See Section 5.4 for details.

e. Subtract $\sigma[U(O_2, e)UO_2^+]^{true}_{revised}$ [Ref. 27] from the total cross-section $\sigma[U(O_2, X)Y]^{true}_{total}$ [Ref. 20]. See Section 5.5 for details.
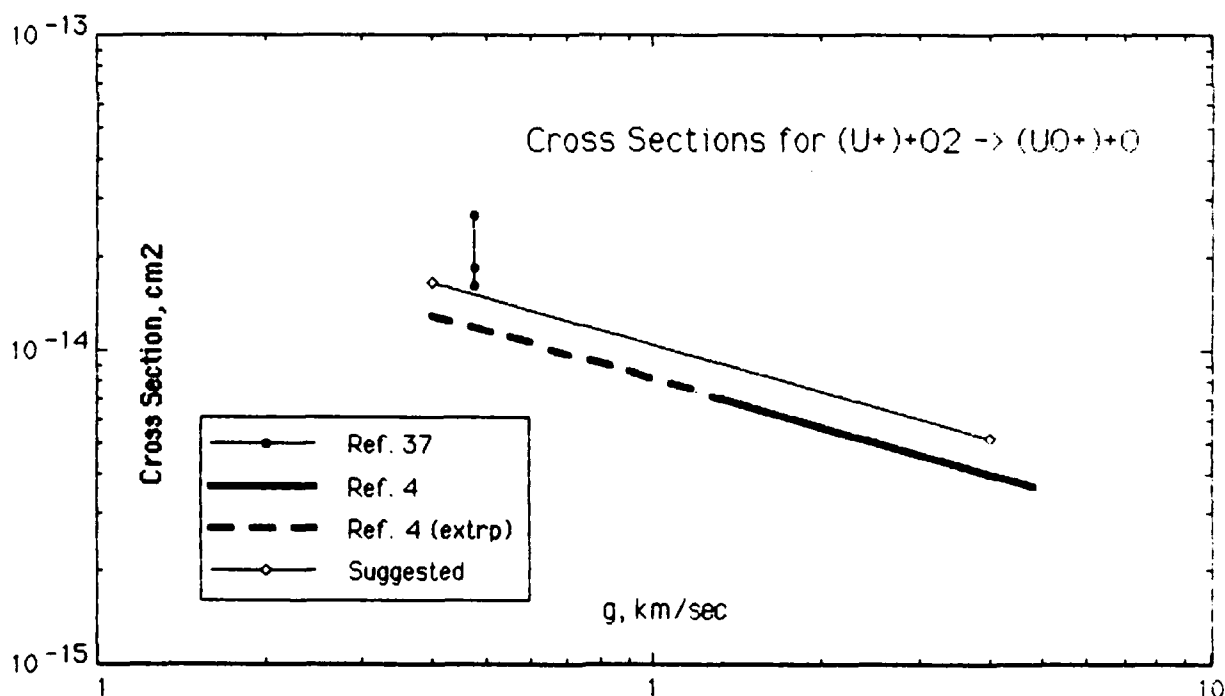
Figure 13. Comparison of our suggested velocity-dependent cross-section with experimental data for the reaction $U^+ + O_2 \rightarrow UO^+ + O$.

71
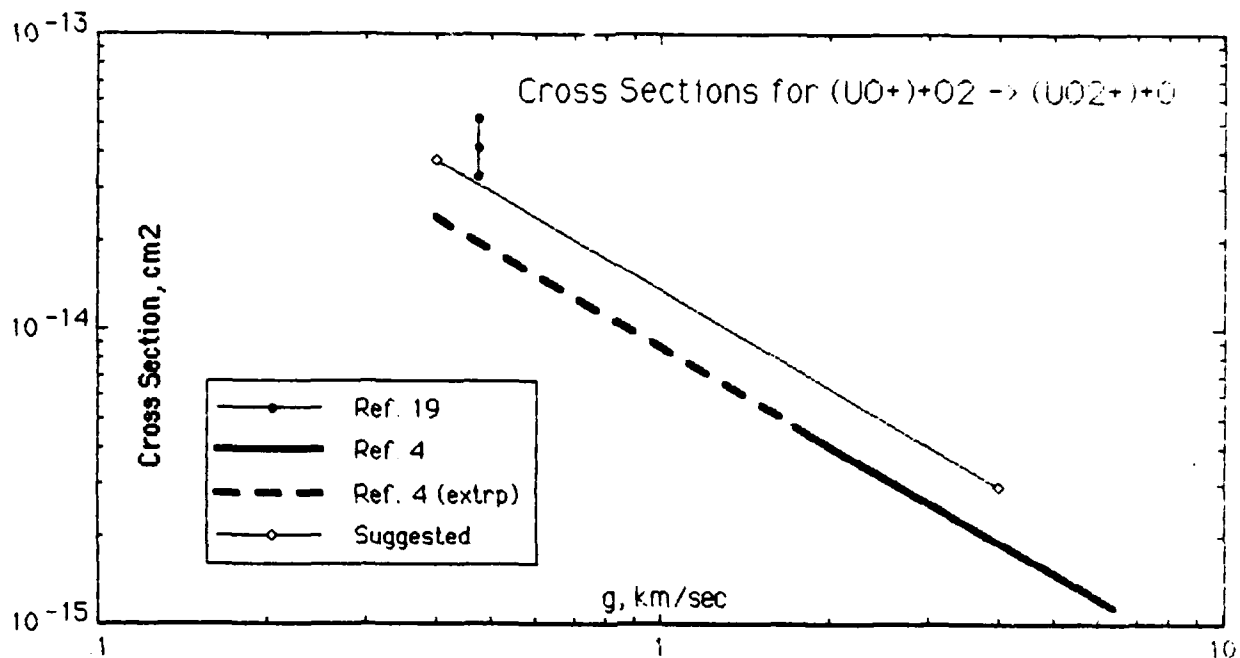
Figure 14. Comparison of our suggested velocity-dependent cross-section with experimental data for the reaction $UO^+ + O_2 \rightarrow UO_2^+ + O$.
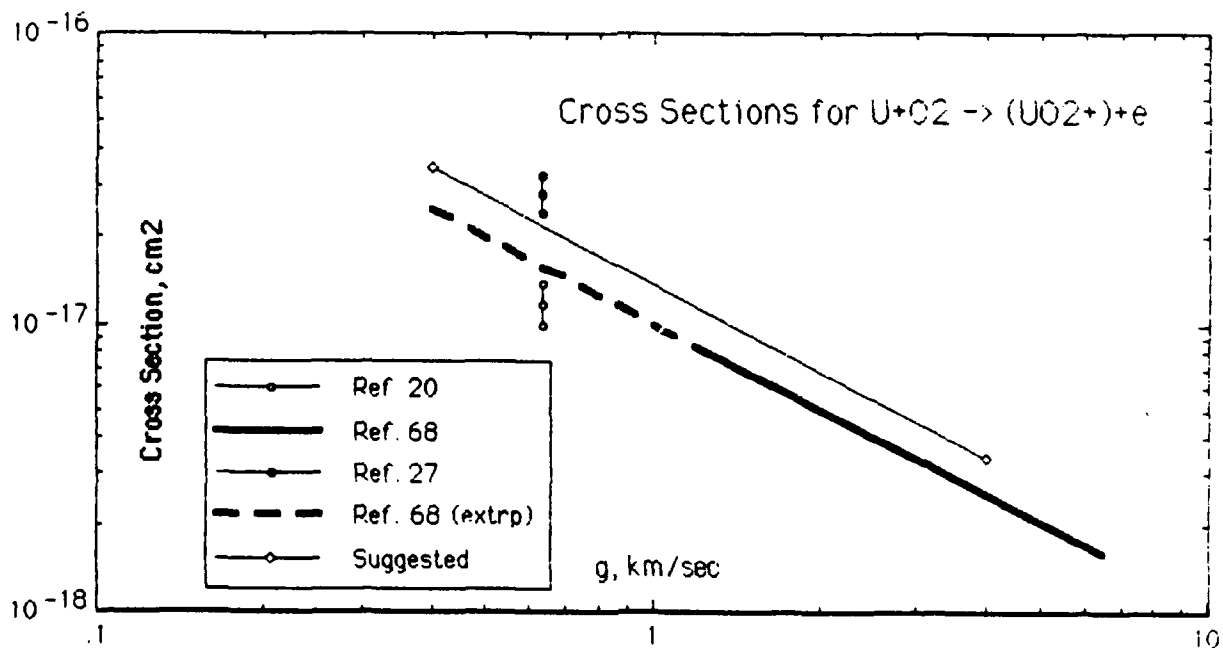
Figure 15. Comparison of our suggested velocity-dependent cross-section with experimental data for the reaction $U + O_2 \rightarrow UO_2^+ + e$.

Table 26 Suggested cross sections and rate coefficients for selected $[(UO_n)^{m+} + (O, O_2)]$-reactions

No.	Reaction	Cross Section cm^2	Note[*]	Rate Coefficient[††] cm^3/(molecule sec)
(1)	$U + O \rightarrow UO^+ + e$	$2.90×10^{-15}$	a	$\dfrac{T^*}{\mu} = \left[\dfrac{T_1}{238} + \dfrac{T_2}{16}\right]\dfrac{1}{1.66×10^{-24}}$ $\bar{g}(T^*) = [8\kappa T^*/\pi\mu]^{1/2}$ $\sigma_0(\bar{g}) = 2.90×10^{-15}$ $k(T^*) = \sigma_0(\bar{g})\bar{g}(T^*)$ $= 4.2×10^{-11}\left[\dfrac{T_1}{238} + \dfrac{T_2}{16}\right]^{1/2}$ For $T_1 = T_2 = T$, $k(T) = 1.9×10^{-10}\left[\dfrac{T}{300}\right]^{1/2}$
(2)	$U^+ + O_2 \rightarrow UO^+ + O$	$3.28×10^{-12}/g^{1/2}$	b	$k(T) = 7.0×10^{-10}\left[\dfrac{T}{300}\right]^{1/4}$
(3)	$UO^+ + O_2 \rightarrow UO_2^+ + O$	$4.32×10^{-9}/g^{11}$	c	$k(T) = 15×10^{-9}\left[\dfrac{T}{300}\right]^{-0.05}$
(4)	$U + O_2 \rightarrow UO_2^+ + e$	$1.38×10^{-12}/g$	d	$k(T) = \sigma_0(\bar{g})\bar{g}(T)G_1 = [1.38×10^{-12}/\bar{g}]\bar{g}×1$ $= 1.4×10^{-12}$
(5)	$U + O_2 \rightarrow UO + O$	$1.22×10^{-15}$	e	$k(T) = 5.8×10^{-11}\left[\dfrac{T}{300}\right]^{1/2}$

[*] See previous pages for notes

[††] g = relative velocity, cm/sec. μ = reduced mass

T_1 = U-temperature T_2 = O-temperature

73

SECTION 6

LIST OF REFERENCES

1   M. Abramowitz and I. Stegun, Handbook of Mathematical Functions, National Bureau of Standards Applied Mathematical Series 55, U. S. Government Printing Office, Washington, D. C., June 1964.

2   H. L. Anderson, Editor in Chief, Physics Vade Mecum, American Institute of Physics, New York, 1981.

3   D. H. Archer, "Requirements for Improved Infrared Prediction Capability. LWIR," DNA-5471F [MRC-R-583], 31 October 1980.

4   P. B. Armentrout and J. L. Beauchamp, "Reactions of U^+ and UO^+ with O_2, CO, CO_2, COS, CS_2, and D_2O," Chem. Phys. 50, 27 (1980).

5   R. A. Armstrong, "An Analysis of the Potential for LWIR Emission from Uranium and Aluminum Oxide After a Nuclear Burst," AFGL-TR-82-0064, 26 October 1981.

6   P. Banks, "Collision Frequencies and Energy Transfer. Electrons," Planet. Space Sci. 14, 1085 (1966).

7   P. M. Banks and G. Kockarts, Aeronomy, Parts A and B, Academic Press, New York, 1973.

8   D. R. Bates, Editor, Atomic and Molecular Processes, Academic Press, New York, 1962.

9   S. J. Bauer, Physics of Planetary Atmospheres, Springer-Verlag, New York, 1973.

10   W. P. Boquist, D. E. Overbye, R. A. Kiesling, and E. E. Eves, "Optical Measurements of High Altitude Barium Releases for Project Secede I," DASA 2368 [EG&G Report B-4092], 15 June 1970.

11   L. Brata, "Emission of Metallic Ions from Oxide Surfaces. I. – Identification of the Ions by Mobility Measurements," Proc. Roy. Soc., (London) A141, 454 (1933).

12   S. C. Brown, Basic Data of Plasma Physics, John Wiley & Sons, Inc., New York, 1959.

13   R. S. Burington, Compiler, <u>Handbook of Mathematical Tables and Formulas</u>, Handbook Publishers, Inc., Sandusky, Ohio. Second Edition, reprinted 1947.

14   S. Chapman and T. G. Cowling, <u>The Mathematical Theory of Non-Uniform Gases</u>, Cambridge University Press, London, 1939. (Reprinted 1960).

15   <u>COSPAR International Reference Atmosphere 1965</u>, North-Holland Publishing Co., Amsterdam, 1965.

16   A. Dalgarno, M. R. C. McDowell, and A. Williams, "The Mobilities of Ions in Unlike Gases," Phil. Trans. <u>A250</u>, 411 (1958).

17   E. A. Desloge, "Exchange of Energy between Gases at Different Temperatures," Phys. Fluids <u>5</u>, 1223 (1962).

18   D. F. Fairbanks and C. R. Wilke, "Diffusion Coefficients in Multicomponent Gas Mixtures," Ind. Eng. Chem. <u>42</u>, 471 (1950).

19   W. L. Fite and H. H. Lo, "Reactions of UO^+ with Atmospheric Gases," AFGL-TR-77-0029, January 31, 1977.

20   W. L. Fite, H. H. Lo, and P. Irving, "Associative Ionization in $U+O$ and $U+O_2$ Collisions," J. Chem. Phys. <u>60</u>, 1236 (1974).

21   J. H. M. Fu, "Pre-Striation Diffusion of an Artificial Cloud in the Ionosphere," p. 117 in Vol. 3 ("Theory") of Ref. 61.

22   J. H. M. Fu, E. P. Marram, T. B. Ponder, and J. R. Breedlove, "Photographic Data Reduction Report on Birdseed-I Barium Releases," EGG 1183-5003, 31 August 1971.

23   F. R. Gilmore, "Proposed Model for the Infrared Radiation from Metals and Metal Oxides Deposited by High-Altitude Nuclear Bursts, for Inclusion in ROSCOE," R & D Associates memorandum prepared for DNA Metal Oxide Subcommittee, 28 June 1982. (Unpublished).

24   F. R. Gilmore, "High-Altitude Metal Oxide Model for ROSCOE," Revision and extension of Ref. 23, 8 October 1982. (Unpublished).

25   I. S. Gradshteyn and I. M. Ryzhik, <u>Table of Integrals, Series, and Products</u>, Fourth Edition, Academic Press, New York, 1980.

26   D. E. Grey, Coordinating Editor, <u>American Institute of Physics Handbook,</u> McGraw-Hill Book Company, New York, 1957.

27   J. C. Halle, H. H. Lo, and W. L. Fite, "Associative Ionization of Uranium Atoms and Oxygen Molecules," J. Chem. Phys. <u>73</u>, 5681 (1980).

28   J. B. Hastad, <u>Physics of Atomic Collisions</u>, Butterworth, Inc., Washington D.C.,1964.

29   A. E. Hedin, "A Revised Thermospheric Model Based on Mass Spectrometer and Incoherent Scatter Data: MSIS-83," J. Geophys. Res. <u>88</u>, 10170 (1983).

30   A. E. Hedin, J. E. Salah, et al., "A Global Thermospheric Model Based on Mass Spectrometer and Incoherent Scatter Data. MSIS 1. N_2 Density and Temperature," J. Geophys. Res. <u>82</u>, 2139 (1977).

31   J. O. Hirschfelder, R. B. Bird, and E. L. Spotz, "The Transport Properties for Non-Polar Gases," J. Chem. Phys. <u>16</u>, 968 (1948).

32   A. R. Hochstim, Editor, <u>Kinetic Processes in Gases and Plasmas</u>, Academic Press, New York, 1969.

33   L. H. Holway, Jr., "Ambipolar Diffusion in the Geomagnetic Field," J. Geophys. Res. <u>70</u>, 3635 (1965).

34   K. P. Huber and G. Herzberg, <u>Molecular Spectra and Molecular Structure, IV. Constants of Diatomic Molecules</u>, Van Nostrand Reinhold Company, New York, 1979.

35   L. G. H. Huxley and R. W. Crompton, "The Motions of Slow Electrons in Gases," p. 349 in Ref. 8.

36   L. G. Jacchia, "Revised Static Models of the Thermosphere and Exosphere with Empirical Temperature Profiles," Smithsonian Astrophysical Observatory Special Report 332, 5 May 1971.

37   R. Johnson and M. A. Biondi, "Reaction Rates of Uranium Ions and Atoms with O_2 and N_2," J. Chem. Phys. <u>57</u>, 1975 (1972).

38   T. Kihara, M. H. Taylor, and J. O. Hirschfelder, Phys Fluids <u>3</u>, 715 (1960).

76

39   B. Kivel, "Study of Chemical Seeding Research," RADC-TR-69-298 [AVCO Everett Research Laboratory Report], July 1969.

40   I. L. Kofsky, J. L. Barrett, D. P. Villanucci, and C. A. Trowbridge, "Analysis of Infrared Effects-Simulation Experiments," DNA-TR-85-80, 31 December 1984.

41   C. Lathuillere, V.B. Wickwar, and W. Kofman, "Incoherent Scatter Measurements of Ion-Neutral Collision Frequencies and Temperatures in the Lower Thermosphere of the Auroral Region," J. Geophys. Res. 88, 10137 (1983).

42   J. C. Light, J. Ross, and K. E. Shuler, "Rate Coefficients, Reaction Cross Sections, and Microscopic Reversibility," p. 281 in Ref. 32.

43   J. V. Lincoln, Editor, "Geomagnetic and Solar Data [for January 1971]," J. Geophys. Res. 76, 3177 (1971).

44   L. M. Linson, "Coupling of Ion Clouds to the Neutral Wind," p. 1 in Vol. 3 ("Theory") of Ref. 61.

45   L. M. Linson and M. J. Baron, "Ion-Cloud Parallel Diffusion – Comparison of RF, Optical, and Theoretical Results," p. 161 in Vol. 1 ("Introduction, Experimental Results – RF Measurements") of Ref. 61.

46   L. M. Linson and D. C. Baxter, "Ion Cloud Modeling," DNA 4455F [SAI-77-918-LJ], 11 November 1977.

47   L. M. Linson and D. C. Baxter, "STRESS Ion Cloud Modeling," SAI-78-835-LJ, August 1978. (Unpublished).

48   L. M. Linson and D. C. Baxter, "Size, Shape, and Age of Ion Clouds," pp. 323-356 in Ref. 53.

49   L. M. Linson and J. B. Workman, "Formation of Striations in Ionospheric Plasma Clouds," J. Geophys. Res. 75, 3211 (1970).

50   T. Lumenello, J. Davis, and J. Freedman, "SECEDE-I Photographic and Spectrographic Data Reduction," TR B-4088 [EG&G-11183-520], September 1969.

51   E. A. Mason and H. W. Schamp, Jr., "Mobility of Gaseous Ions in Weak
        Electric Fields," AFOSR-TN-58-104 [University of Maryland Institute of
        Molecular Physics Report IMP-OSR-8], 13 February 1958.

52   E. A. Mason and H. W. Schamp, Jr., "Mobility of Gaseous Ions in Weak
        Electric Fields," Annals Phys. 4, 233 (1958).

53   D. R. McDaniel, Compiler, "Proceedings of the STRESS Data Review
        Meeting," 29-30 November 1977, DNA 4620T, June 1978.

54   D. R. McDaniel, Compiler, "Proceedings of the PLACES Preliminary Data
        Review Meeting, 20 and 21 May 1981," DNA 5848P, 1 July 1981.

55   E. W. McDaniel, Collision Phenomena in Ionized Gases, John Wiley & Sons,
        Inc., New York, 1964.

56   E. W. McDaniel and E. A. Mason, The Mobility and Diffusion of Ions in
        Gases, John Wiley & Sons, Inc., New York, 1973.

57   H. H. Michels, "Theoretical Determination of Metal Oxide f-Numbers,"
        AFWL-TR-74-239, May 1975.

58   J. H. Mitchell and K. E. W. Ridler, "The Speed of Positive Ions in Nitrogen,"
        Proc. Roy. Soc., (London) A146, 911 (1934).

59   L. Monchick and E. A. Mason, "Transport Properties of Polar Gases," J.
        Chem. Phys. 35, 1676 (1961).

60   D. R. Parsignault, R, W. Brooke, R. D Bucknam, W. H. G. Lewin, P. Osepa, S
        A. Rappaport, W. P. Reidy, W. H. Sheehan, O.Shepard, and T. F. Zehnpfennig,
        "Rocket-Borne Uranium Vapor Release," DNA-TR-87-29 [Visidyne VI-
        962], 20 February 1987.

61   "Proceedings of the 1971 Technical Planning Session," SRI International,
        (Unpublished).

62   "Project SECEDE — A Review," DASIAC/DoD Nuclear Information and
        Analysis Center, General Electric Company — TEMPO, (Unpublished).

63   J. A. Ratcliffe, An Introduction to the Ionosphere and Magnetosphere,
        Cambridge University Press, Cambridge, 1972.

64   A. Simon, "Growth and Stability of Artificial Ion Clouds in the Ionosphere," J. Geophys. Res. 75, 6287 (1970).

65   R. E. Stoeckly, R. W. Stagat, and R. W. Kilb, "Collisional Momentum and Energy Transfer Rates for Two-Fluid Nuclear-Burst Simulations," DNA 3827T [MRC-R-181], 25 July 1975.

66   R. E. Walker, N. deHaas, and A. A. Westenberg, "Measurements of Multicomponent Diffusion Coefficients for the CO_2-He-N_2 System Using the Point Source Technique," J. Chem. Phys. 32, 1314 (1960).

67   R. H. Wand, "Electron-to-Ion Temperature Ratio from Radar Thompson Scatter Observations," J. Geophys. Res. 75, 829 (1970)

68   C. E. Young, P. M. Dehmer, R. B. Cohen, L. G. Pobo, and S. Wexler, "Chemi-ionization Reactions in Accelerated Uranium – O_2 Crossed Molecular Beams," J. Chem. Phys. 64, 306 (1976).

69   K. S. Yun and E. A. Mason, "Collision Integrals for the Transport Properties of Dissociating Air at High Temperatures," Phys. Fluids, 5, 380 (1962).

APPENDIX A

RELATION BETWEEN DIFFERENT EXPRESSIONS FOR THE DIFFUSION COEFFICIENT AND MOBILITY

A.1 THE PROBLEM.

In the (weakly-ionized) plasma physics literature one sees the (ordinary) ion diffusion coefficient D and ion mobility $\mathcal{K}$ (sometimes written as μ, which here is reserved for reduced mass) written as

$$D = \frac{kT}{mv} \tag{A1a}$$

$$\mathcal{K} = \frac{e}{mv} = \frac{eD}{kT} \tag{A2a}$$

by, e.g., Refs. 33, 21, and 2 (Book, p. 266), or as

$$D = \frac{kT}{m}\tau \tag{A1b}$$

$$\mathcal{K} = \frac{e\tau}{m} = \frac{eD}{kT} \tag{A2b}$$

by, e.g., Refs. 49, 46, and 64.

On the other hand, elsewhere, for both binary and multicomponent gases, one sees the diffusion coefficient written differently than Eqs.(A1a) and (A1b):

<u>Binary Gas.</u> In a binary gas consisting of particles with masses m_i and m_k and with concentrations n_i and n_k, the diffusion coefficient [Ref. 7, Pt. B, p. 39, Eq. (15.27); equivalent to Dalgarno's Eq. (5), p. 644 in Ref. 8] is

$$D_{ik} = \frac{3\pi}{32 Q_{Dik}(n_i + n_k)}\left(\frac{8kT}{\pi \mu_{ik}}\right)^{1/2} \tag{A3}$$

where Q_{Dik} is an average diffusion (or momentum-transfer) cross-section given by

$$Q_{Dik} = \frac{1}{2}\int_0^\infty x^2 \sigma_{Dik}(x) e^{-x}\,dx \tag{A4a}$$

with

$$x = \frac{\mu_{ik} g^2}{2kT},$$ (A4b)

$$\mu_{ik} = m_i m_k / (m_i + m_k),$$ (A4c)

and g being the relative speed of the two types of particles.

Multicomponent Gas. Dalgarno [Ref. 8, p. 649, referencing Hirshfelder et al. (1954)] states that when the concentration of one of the components is very small compared with those of the others, the simplified formula for the diffusion coefficient of the rare component (D_i) is given by

$$D_i^{-1} = \sum_k f_k D_{ik}^{-1},$$ (A5)

where f_k is the fractional concentration of the kth particles. (Note: D_{ik} must be evaluated for n_k equal to n_{total}. This fact is more readily recognized from sources other than Dalgarno, such as Refs. 18 and 66.)

We now reconcile these different expressions for the diffusion coefficient.

A.2 RECONCILIATION.

First, we assume there is no question about relating the collision time τ to the collision frequency ν by

$$\tau = 1/\nu$$ (A6)

(cf. Ref. 7, p. 186, Eq. 9.14)). Next, we assume we are interested in an average collision frequency, $\bar{\nu}_{Lik}$, corresponding to an average momentum-transfer cross-section, obtained by averaging over a Maxwellian distribution of velocities. (We assume only one temperature obtains, for simplicity – the argument is extendable to the two-temperature case.) This $\bar{\nu}_{Lik}$ is to be the effective collision frequency in the laboratory, related to the collision frequency $\bar{\nu}_{ik}$ in the center-of-mass system [Ref. 7, p. 190, Eq. (9.40)] by

$$\bar{\nu}_{Lik} = \frac{m_k}{m_i + m_k} \bar{\nu}_{ik},$$ (A7)

where $\bar{\nu}_{ik}$ is given [Ref. 7, p. 189 (Eqs. (9.33), (9.34), (9.35), & (9.36)), with a reference to Ref. 6] by

$$\bar{v}_{ik} = \tfrac{4}{3} n_k \bar{g}_{ik} Q_{Dik} \tag{A8a}$$

with

$$\bar{g}_{ik} = \left(\frac{8kT}{\pi \mu_{ik}}\right)^{1/2} \tag{A8b}$$

and

$$Q_{Dik} = \frac{1}{c^6} \int_0^\infty g_{ik}^5 \sigma_D(g_{ik}) e^{-g_{ik}^2/c^2} \, dg_{ik} \tag{A8c}$$

$$c^2 = \frac{2kT}{\mu_{ik}}. \tag{A8d}$$

Thus, by collating expressions, we find the diffusion coefficient as given by Eq. (A1a) for a binary gas becomes

$$D = \frac{kT}{mv} \Rightarrow \frac{kT}{m_i \bar{v}_{Lik}} \tag{A9a}$$

$$= \frac{kT}{m_i} \frac{m_i + m_k}{m_k} \frac{1}{\bar{v}_{ik}} \tag{A9b}$$

$$= \frac{kT}{\mu_{ik}} \frac{1}{\bar{v}_{ik}} \tag{A9c}$$

$$= \frac{kT}{\mu_{ik}} \frac{3}{4 n_k \bar{g}_{ik} Q_{Dik}} \tag{A9d}$$

$$= \frac{3}{4} \frac{kT}{\mu_{ik} n_k} \left(\frac{\pi \mu_{ik}}{8kT}\right)^{1/2} \frac{1}{Q_{Dik}} \tag{A9e}$$

$$= \frac{3\pi}{32} \frac{1}{n_k Q_{Dik}} \left(\frac{8kT}{\pi \mu_{ik}}\right)^{1/2} \tag{A9f}$$

which is the same expression we have for D_{ik} in Eq. (A3) if $n_i \ll n_k$.

Thus, by this correspondence the proper expression for the τ in Eqs. (A1b) and (A2b) for a binary gas is

$$\tau = \frac{1}{v} \Rightarrow \frac{1}{\bar{v}_{Lik}} = \frac{m_i}{kT} D_{ik} \tag{A10a}$$

$$\tau = \frac{3}{4} \frac{m_i}{\mu_{ik} n_k Q_{Dik}} \left(\frac{\pi \mu_{ik}}{8kT}\right)^{1/2}. \tag{A10b}$$

A.3 PARAMETERS SPECIALIZED FOR THREE POTENTIALS.

We now want to specialize the expressions for Q_0, τ, $\mathcal{K}$, and D for the polarization, (r^{-6}), and (hybrid) effective (r^{-6}) potentials.

A.3.1 Q_{Dik}, The Mean Momentum-Transfer Cross-Section.

A.3.1.1 Polarization Potential. For a polarization-potential interaction, the velocity-dependent momentum-transfer cross-section for singly-charged ions is [Ref. 7, Pt. A, p. 218]

$$\sigma_{Dik} = 2.21\pi (\alpha_k e^2 / \mu_{ik} g_{ik}^2)^{1/2} \tag{A11a}$$

$$= 2.59 \times 10^{-9} [\alpha_k' / \mu(A_{ik}) g_{ik}^2]^{1/2}, \tag{A11b}$$

where α_k is the polarizability of the neutral target particle, α_k' is in units of 10^{-24} cm^3, μ_{ik} is the reduced mass of the ion and neutral, $\mu(A_{ik})$ is in atomic mass units, e is the electronic charge, and g_{ik} is the relative speed of the ion and neutral. By using Eq. (A4b), we find that Eq. (A11a) becomes

$$\sigma_{Dik} = 2.21\pi (\alpha_k e^2 / 2kT)^{1/2} / \sqrt{x}, \tag{A12}$$

so that Eq. (A4a) becomes

$$Q_{Dik} = \frac{2.21\pi}{2} \left(\frac{\alpha_k e^2}{2kT}\right)^{1/2} \Gamma(5/2) \tag{A13a}$$

where [Ref. 1, p. 255]

$$\Gamma(n) = \int_0^\infty x^{n-1} e^{-x} dx \tag{A14a}$$

$$\Gamma(5/2) = [(1 \times 3)/2^2] \Gamma(1/2) = 1.3293. \tag{A14b}$$

Thus,

$$Q_{Dik}\big|_{\text{pol.pot.}} = \frac{2.21\pi \Gamma(5/2)}{2} \left(\frac{\alpha_k e^2}{2kT}\right)^{1/2}. \tag{A13b}$$

$$= 1.33 \times 10^{-13} (\alpha_k' / T)^{1/2}. \tag{A13c}$$

A.3.1.2 (r^{-6})-Potential. The asymptotic low-energy momentum-transfer cross-section for the r^{-6} potential,

$$\phi(r) \Rightarrow -2\varepsilon_o (r_m / r)^6, \tag{A15}$$

obtained by combining Eqs. (5), (1c), and (12) in Section 2, is

$$\sigma(g_{ik}) = \pi D^2 S^{(1)}(\kappa) \tag{A16a}$$

$$= C \left(\frac{r_m^6 \varepsilon_o (eV)}{\mu_{ik} g_{ik}^2} \right)^{1/3} \tag{A16b}$$

$$= C' \left(\frac{r_m^6 \varepsilon_o (eV)}{\mu(A_{ik}) g_{ik}^2} \right)^{1/3} \tag{A16c}$$

$$C = 0.4342 \times (3 \times 1.60 \times 10^{-12})^{1/3} \times 4\pi \tag{A16d}$$

$$= 9.204 \times 10^{-4} \tag{A16e}$$

$$C' = 7.773 \times 10^4 . \tag{A16f}$$

By using Eq. (A4b), we find Eq. (A16b) becomes

$$\sigma_{Dik} = \frac{C}{x^{1/3}} \left(\frac{r_m^6 \varepsilon_o}{2kT} \right)^{1/3} \tag{A16g}$$

so that Eq. (A4a) becomes

$$Q_{Dik} = \frac{C \, \Gamma(8/3)}{2} \left(\frac{r_m^6 \varepsilon_o}{2kT} \right)^{1/3} \tag{A17a}$$

where [Ref. 1, p. 255]

$$\Gamma(8/3) = [(2 \times 5)/(3^2)] \, \Gamma(2/3) = 1.5046 . \tag{A18}$$

Thus

$$Q_{Dik} \big|_{(r^{-6})-pot} = 6.92 \times 10^{-4} \left(\frac{r_m^6 \varepsilon_o}{2kT} \right)^{1/3} \tag{A17b}$$

A.3.1.3 <u>Effective (r^{-6})-Potential.</u> As discussed in detail with respect to $(Ba^+ + N_2)$-collisions in Appendix C, we want to introduce an effective (r^{-6})-potential determined by requiring the equalities of mobilities (at STP conditions) based on (a) an effective (r^{-6})-potential and on (b) the polarization potential. This requirement is equivalent to an equality of mean momentum-transfer cross-sections (at STP conditions) based on the same two potentials, since the mobility is (inversely) proportional to the mean momentum-transfer cross-section. To determine this effective (r^{-6})-potential, we equate the right-hand members of Eqs. (A13c) and (A17b), set T to 273.15 K ($= T_{STP}$), and solve for the parameter $(r_m^6 \varepsilon_o)^{1/3}$:

$$(r_m^6 \varepsilon_o)^{1/3} \big|_{Eff. (r^{-6})-pot.} = 4.94 \times 10^{-16} (\alpha_k')^{1/2} . \tag{A19}$$

Note that determining the parameter $(r_m^6 \varepsilon_o)^{1/3}$ in this manner results in its having no dependence on any property of the incident ion i. However, the velocity-dependent momentum-transfer cross-section still has a reduced mass factor. Use of Eq. (A19) in (A16b,c) gives

$$\sigma(g_{ik})\big|_{\text{Eff.} (r^{-6})\text{-pot.}} = C_{\text{Eff.}} \frac{(\alpha'_k)^{1/2}}{(\mu_{ik} \, g_{ik}^2)^{1/3}} \tag{A20a1}$$

$$= C_{\text{Eff.}} \frac{(\alpha'_k)^{1/2}}{[\mu(A_{ik}) \, g_{ik}^2]^{1/3}} \tag{A20a2}$$

with

$$C_{\text{Eff.}} = 4.55 \times 10^{-19} \tag{A20a3}$$

$$C_{\text{Eff.}} = 3.84 \times 10^{-11} \, . \tag{A20a4}$$

Use of Eq. (A19) in (A17b) gives

$$Q_{Dik}\big|_{\text{Eff.} (r^{-6})\text{-pot.}} = 5.25 \times 10^{-14} (\alpha'_k)^{1/2} (T)^{-1/3} \, . \tag{A20b}$$

A.3.1.4 <u>Polarization Potential and Effective (r^{-6})-Potential.</u> From Eqs. (A20) and (A13c) we have

$$Q_{Dik}\big|_{\text{Eff.} (r^{-6})\text{-pot.}} = \left(\frac{T}{T_{\text{STP}}}\right)^{1/6} Q_{Dik}\big|_{\text{pol.pot.}} \tag{A21a}$$

$$T_{\text{STP}} = 273.15 \, \text{K.} \tag{A21b}$$

Hence, from Eqs. (A21) and (A13c), we have

$$Q_{Dik}\big|_{\text{Eff.} (r^{-6})\text{-pot.}} = 1.33 \times 10^{-13} \left(\frac{T}{T_{\text{STP}}}\right)^{1/6} \left(\frac{\alpha'_k}{T}\right)^{1/2} \, . \tag{A22}$$

We can combine Eqs. (A13c) and (A22) by writing

$$Q_{Dik}\big|_{\beta} = 1.33 \times 10^{-13} \left(\frac{T}{T_{\text{STP}}}\right)^{\beta} \left(\frac{\alpha'_k}{T}\right)^{1/2} \, \text{cm}^2 \tag{A23a}$$

$$\beta = \begin{cases} 0, & \text{polarization potential} \\ 1/6, & \text{effective } (r^{-6})\text{-potential.} \end{cases} \tag{A23b}$$

A.3.2 τ, The Collision Time.

Substituting Eqs. (A17b) and (A23) into (A10b) gives

$$\tau_{ik}\big|_{(r^{-6})\text{-pot.}} = \frac{1.90 \times 10^{-7}}{n_k} \frac{A_i}{[\mu(A_{ik})]^{1/2} (r_m^6 \, \varepsilon_o)^{1/3}} \left(\frac{T_{\text{STP}}}{T}\right)^{1/6} \tag{A24}$$

$$\tau_{ik}\big|_{\beta} = \frac{3.88 \times 10^{8}}{n_k} \frac{A_i}{[\mu(A_{ik}) \alpha'_k]^{1/2}} \left(\frac{T_{\text{STP}}}{T}\right)^{\beta} \tag{A25a}$$

$$\beta = \begin{cases} 0, & \text{polarization potential} \\ 1/6, & \text{effective } (r^{-6})\text{-potential.} \end{cases} \qquad (A25b)$$

A.3.3 $\mathscr{K}$, The Mobility.

A.3.3.1 <u>Polarization Potential.</u> From Eqs. (A2), (A9f), and (A13b), we have

$$\mathscr{K}_{ik}\big|_{\text{pol.pot.}} = \frac{n_l}{n_k} \, \mathscr{K}_{ik}^{\text{STP}}\big|_{\text{pol.pot.}} \qquad (A26a)$$

$$\mathscr{K}_{ik}^{\text{STP}}\big|_{\text{pol.pot.}} = \frac{13.8}{[\mu(A_{ik})\alpha_k']^{1/2}} \, \frac{\text{cm/sec}}{\text{volt/cm}} \qquad (A26b)$$

$$n_l = 2.69 \times 10^{19} \ \text{cm}^{-3} \qquad (A26c)$$

Equation (A26b) is equivalent to that given by Dalgarno [Ref. 8, p. 652 or Ref. 16],

$$\mathscr{K}^{\text{STP}} = \frac{35.9}{[\mu(A)\alpha]^{1/2}} \, \frac{\text{cm/sec}}{\text{volt/cm}} \qquad (A27)$$

where α is in atomic units (a_0^3) instead of 10^{-24} cm^3 as for our α', the reduced mass $\mu(A)$ is in units of the proton mass, and $\mathscr{K}^{\text{STP}}$ is referred to a constant gas density of 2.69×10^{19} cm^{-3}.

A.3.3.2 <u>(r^{-6})-Potential.</u> From Eqs. (A2), (A9f), and (A17b), we have

$$\mathscr{K}_{ik}\big|_{(r^{-6})\text{-pot.}} = \frac{n_l}{n_k}\left(\frac{T_{\text{STP}}}{T}\right)^{1/6} \mathscr{K}_{ik}^{\text{STP}}\big|_{(r^{-6})\text{-pot.}} \qquad (A28a)$$

$$\mathscr{K}_{ik}^{\text{STP}}\big|_{(r^{-6})\text{-pot.}} = \frac{6.82 \times 10^{-15}}{[\mu(A_{ik})]^{1/2}(r_m^6 \varepsilon_o)^{1/3}} \, \frac{\text{cm/sec}}{\text{volt/cm}} . \qquad (A28b)$$

A.3.3.3 <u>Polarization Potential and Effective (r^{-6})-Potential.</u> From Eqs. (A2), (A9f), and (A23) we have

$$\mathscr{K}_{ik}\big|_{\beta} = \frac{n_l}{n_k}\left(\frac{T_{\text{STP}}}{T}\right)^{\beta} \mathscr{K}_{ik}^{\text{STP}} \qquad (A29a)$$

$$\mathscr{K}_{ik}^{\text{STP}} = \mathscr{K}_{ik}^{\text{STP}}\big|_{\text{pol.pot.}} = \mathscr{K}_{ik}^{\text{STP}}\big|_{\text{Eff.}(r^{-6})\text{-pot.}} \qquad (A29b)$$

$$\beta = \begin{cases} 0, & \text{polarization potential} \\ 1/6, & \text{effective } (r^{-6})\text{-potential.} \end{cases} \qquad (A29c)$$

A.3.3.4 <u>Collation of Ba⁺ Theoretical Mobilities at STP Conditions.</u> The parameters for Ba⁺ theoretical mobility (and diffusion coefficient, presented below) are collated in Table 27. For values of α', see, e.g., Ref. 7, Pt. A, p. 219. These parameters are used in Eq. (A26b) to obtain the Ba⁺ theoretical mobilities in Table 28. As discussed in Appendix C, the theoretical value for the Ba⁺ mobility in N_2 is larger than the experimental value by only about four percent.

Table 27. Parameters for Ba⁺ theoretical mobility and diffusion coefficient in atmospheric species.

k	α'_k	$i = Ba^+$	
		$\mu(A_{ik})$	$[\mu(A_{ik})\,\alpha'_k]^{1/2}$
O	0.79	14.33	3.36
N_2	1.76	23.26	6.40
O_2	1.59	25.95	6.42

Table 28. Ba⁺ mobilities in atmospheric species at STP conditions. (Based on Eq. (A26b) and properties in Table 27.)

Species k	$\mathscr{K}^{STP}(Ba^+, k)$, [(cm/sec)/(volt/cm)] (either polarization or effective (r^{-6})-potential)
O	4.10
N_2	2.16
O_2	2.15

A.3.4 D, The Diffusion Coefficient.

From Eqs. (A5) and (A2) we have

$$D_i^{-1} = \sum_k f_k\, D_{ik}^{-1} \qquad (A30a)$$

$$= \frac{e}{300\,kT} \sum_k f_k\, \mathscr{K}_{ik}^{-1} \qquad (A30b)$$

A.3.4.1 <u>(r^{-6})-Potential.</u> From Eqs. (A28) and (A30b) we have

$$D_i|_{(r^{-6})\text{-pot}} = \frac{15.8}{n_{tot}} \left(\frac{T_{STP}}{T}\right)^{1/6} \frac{T}{\sum_k f_k [\mu(A_{ik})]^{1/2} (r_m^6 \varepsilon_o)_{ik}^{1/3}} \quad \frac{cm^2}{sec} \qquad (A31)$$

A.3.4.2 <u>Polarization Potential and Effective (r^{-6})-Potential.</u> From Eqs. (A29) and (A26b) we have

$$D_i|_\beta = \frac{3.21 \times 10^{16}}{n_{tot}} \left(\frac{T_{STP}}{T}\right)^\beta \frac{T}{\sum_k f_k [\mu(A_{ik}) \alpha_k]^{1/2}} \quad \frac{cm^2}{sec} \qquad (A32a)$$

$$\beta = \begin{cases} 0, & \text{polarization potential} \\ 1/6, & \text{effective } (r^{-6})\text{-potential.} \end{cases} \qquad (A32b)$$

A.3.4.3 <u>Working Formula for Ba$^+$ Diffusion Coefficient.</u> The parameters necessary to apply Eq. (A32) to Ba$^+$ are collated in Table 27 and applied to Eq. (A32) to obtain Eq. (A33). Results of evaluating Eq. (A33) for a range of altitudes are given in Table 34.

$$D_{Ba^+}|_\beta = \frac{3.21 \times 10^{16}}{n_{tot}} \left[\frac{T_{STP}}{T}\right]^\beta \frac{T}{3.36 f_0 + 6.40 f_{N_2} + 6.42 f_{O_2}} . \qquad (A33)$$

APPENDIX B

ION-NEUTRAL COLLISIONS IN MULTICOMPONENT GAS

B.1 COMMENTARY ON SELECTED LITERATURE FORMULAS FOR COLLISION TIME.

Linson & Workman [Ref. 49, Eq. (2a)] state that

"... the ion-neutral collision time, τ, is

$$\tau = 4.5 \times 10^9 / N_n \ , \ \text{sec} \tag{B1}$$

where N_n is the atmospheric neutral density in cm^{-3} .... A typical ionospheric temperature of 1000 K has been taken for the barium ions. The value of τ was obtained from the temperature-corrected measurement of the mobility

$$\mu = e\tau / M \tag{B2}$$

of barium ions in nitrogen by *Mitchell and Ridler* [Ref. 58] and reprinted by *Brown* [Ref. 12]."

We believe there are two shortcomings in Eq. (B1), due to improperly (a) correcting for the ionospheric temperature of about 1000 K and (b) treating mobilities in a multicomponent gas. (This latter statement is equivalent to objecting to treating O_2 (which doesn't matter) and O (which does matter) as if they were N_2.)

The LW-70 authors apparently became aware of the first shortcoming because a later paper by Linson and Baron [Ref. 45] states that the ion-neutral collision time is

$$\tau_i = 9 \times 10^9 / N_n \ . \tag{B3}$$

An improved but still slightly incorrect formula, related to Eq. (B3), is presented by Linson & Baxter [Ref. 46, p. 58] and reproduced here:

"An expression for the collision time, $\tau = 1/\nu$, can be obtained from measurements of the mobility of barium ions in nitrogen gas [Ref. 58] resulting in

$$\tau = 8.6 \times 10^{15} / \bar{n}_n \ \text{sec} \qquad (4.54) \tag{B3a1}$$

where $\bar{n}_n$ is an effective neutral concentration in particles/m^3,

$$\bar{n}_n = n_{N_2} + n_{O_2} + 0.8 \, n_0. \qquad (4.55) \tag{B3a2}$$

In deriving Eq. (4.54) it has been assumed that the collision cross section varies inversely as the square root of the temperature and that the collision cross section for oxygen molecules and atoms is the

same as it is for nitrogen molecules. The fact that the lighter oxygen atoms are less efficient in stopping a heavier barium ion is expressed by the appropriate Langevin factor,

$$\left[1+M_{Ba}/M_{N_2}\right]^{1/2}\left[1+M_{Ba}/M_O\right]^{-1/2} \approx 0.8 ,$$

where M_{N_2} and M_O are the masses of the nitrogen molecule and oxygen atom respectively."

The proper way to obtain the collision time in a multicomponent neutral gas mixture can be done in at least a couple of (equivalent) ways. In Section B.2 we compute it in terms of mobilities; here, we show another quite direct way, by summing the collision frequencies for the ion in the various neutral gases.

Summation of the collision frequencies, under the assumption of the polarization-potential interaction, has been used frequently, including a recent paper by Lathuillere, Wickwar, and Kofman [Ref. 41], from which we reproduce the relevant portion. (In the Ref. 41 Eq. (4) we have corrected the typographical error in an exponent, changing it from 10^{-11} to 10^{-9}.)

"Neutral density and collision frequency are connected by

$$\bar{v}_{in} = 2.59\times10^{-9}\, n_n \left(\frac{\alpha_o}{\mu(i,n)}\right)^{1/2} \tag{1}$$

[$Banks\ and\ Kockarts$ [Ref. 7]], where $\bar{v}_{in}$ is the collision frequency for momentum transfer between ion species i and neutral species n, measured in the center of mass frame; n_n is the number density of neutral species n, $\mu(i,n)$ is the ion-neutral reduced mass (in atomic mass units), and α_o is the neutral gas atomic polarizability (in units of 10^{-24} cm^3).

"The ion-neutral collision frequency, v_{in}, used in the calculation of the incoherent scatter spectrum is the momentum transfer collision frequency measured in the laboratory frame:

$$v_{in} = \frac{m_n}{m_i + m_n}\, \bar{v}_{in} \tag{2}$$

where m_i and m_n are the ion and neutral particle masses (in atomic mass units), respectively. Combining (1) and (2) and summing over the three principal neutral species in the E region, we obtain

$$v_{in} = K\,N \tag{3}$$

for each ion species, where N in the total neutral density,

$$K = 2.59\times10^{-9}\,(1/m_i)[1.76^{1/2}\,\mu(i,N_2)^{1/2}\%(N_2)$$
$$+1.59^{1/2}\,\mu(i,O_2)^{1/2}\%(O_2)+0.79^{1/2}\,\mu(i,O)^{1/2}\%(O)] \tag{4}$$

and %(n) represents the percentage of neutral species n in the neutral gas."

To obtain explicit numbers, we write

$$\tau_{in} = 1/\nu_{in}$$

$$= \frac{A_i}{2.59 \times 10^{-9}} \left[\sqrt{1.76 \mu_{i,N_2}} \, [N_2] + \sqrt{1.59 \mu_{i,O_2}} \, [O_2] + \sqrt{0.79 \mu_{i,O}} \, [O] \right]^{-1}$$

$$= \frac{137.4}{2.59 \times 10^{-9}} \left[6.40 [N_2] + 6.42 [O_2] + 3.36 [O] \right]^{-1}$$

$$= \frac{8.29 \times 10^9}{[N_2] + [O_2] + 0.525 [O]} \quad \text{for polarization potential} \qquad (B3b)$$

which we believe to be the proper version of Eqs. (4.54) and (4.55) in Ref. 46 (our Eqs. (B3a1) and (B3a2)).

B.2 FORMULAS FOR MOBILITY, COLLISION TIME, AND DIFFUSION COEFFICIENT IN A MULTICOMPONENT GAS.

Dalgarno [Ref. 8, p. 659] notes, from the theory of Chapman and Cowling [Ref. 14], that the mobility $\mathcal{K}$ (a symbol used here in preference to μ as in Eq. (B2), since we reserve μ for reduced mass) of an ion in a multicomponent gas is given by

$$\mathcal{K}^{-1} = \sum_k f_k \, \mathcal{K}_k^{-1} \qquad (B4)$$

(known as Blanc's law), where f_k is the fraction of the kth particles ($f_k = n_k / n_{total}$) and $\mathcal{K}_k$ is the mobility of the ion in the kth gas. In using Eq. (B4) it is important that $\mathcal{K}_k$ be evaluated for the total number density. (See the related comment with respect to Eq. (A5).)

Thus, to compute an effective ion-neutral collision time (τ) for an ion in a multicomponent gas, one should use

$$\tau^{-1} = \frac{e}{m} \mathcal{K}^{-1} = \frac{e}{m} \sum_k f_k \, \mathcal{K}_k^{-1}. \qquad (B5)$$

We now specialize Eq. (B5) for two different interaction potentials, polarization and effective r^{-6}. By using Eq. (A29) we get

$$\tau\big|_\beta = \frac{m\, n_i}{e\, n_{tot}}\left[\frac{T_{STP}}{T}\right]^\beta \frac{1}{\sum_k [f_k / \mathscr{K}_{ik}^{STP}]} \qquad (B6a)$$

$$\beta = \begin{cases} 0, & \text{polarization potential} \\ 1/6, & \text{effective } (r^{-6})\text{-potential}. \end{cases} \qquad (B6b)$$

For Ba$^+$, Eq. (B6) becomes

$$\tau\big|_\beta = \frac{3.83\times10^9}{n_{tot}}\left[\frac{T_{STP}}{T}\right]^\beta \frac{1}{(f_O/4.10)+(f_{N_2}/2.16)+(f_{O_2}/2.15)} \qquad (B7)$$

where we have used values for $\mathscr{K}^{STP}(Ba^+,k)$ from Table 27.

The effective ion-neutral diffusion coefficient is also properly defined by [Ref. 7, Pt. B, p. 164]

$$D = \frac{kT}{m_i}\frac{1}{\sum_k \nu_{ik}}. \qquad (B8)$$

B.3 COMPARISONS OF Ba$^+$ COLLISION TIME.

The CIRA-65 Model-6 1800-hr [Ref. 15] atmosphere is of special interest in Appendix D for comparisons being made there. Selected properties of that atmosphere for the 140- to 300-km altitude range are given in Table 31 and have been used in evaluating the Ba$^+$ collision time according to several formulas presented here, with results in Table 29. At 200-km altitude, e.g., our procedure, per Eq. (B7), gives 1.18 sec and 0.935 sec respectively for the polarization potential and effective (r^{-6})-potential, whereas treating the O and O$_2$ as N$_2$ in Eq. (B7) – in the spirit of the Ref. 45 equation – gives 0.954 sec and 0.752 sec, respectively; our collision times are longer by a factor of 1.24. Again at 200-km altitude, in comparison with Ref. 45 (our Eq. (B3)), our values differ by respective factors of 1.13 and 0.899; in comparison with Ref. 46 (our Eq. (B3a)), by factors of 1.09 and 0.866.

Table 29. Ba$^+$ collision times in CIRA-65 Model-6 1800-hr atmosphere per several formulas. (See Table 31 for atmospheric properties.)

Altitude	Collision Time τ, sec			
km	Pol. Pot.	Eff. (r^{-6})-Pot.	LB-71	LB-77
140	1.03 E-01	8.87 E-02	1.00 E-01	1.00 E-01
160	2.96 E-01	2.44 E-01	2.78 E-01	2.82 E-01
180	6.38 E-01	5.12 E-01	5.79 E-01	5.92 E-01
185	7.47 E-01	5.96 E-01	6.72 E-01	6.92 E-01
200	1.18 E+00	9.35 E-01	1.04 E+00	1.08 E+00
220	2.01 E+00	1.57 E+00	1.70 E+00	1.80 E+00
240	3.23 E+00	2.50 E+00	2.64 E+00	2.82 E+00
260	4.96 E+00	3.83 E+00	3.92 E+00	4.24 E+00
280	7.39 E+00	5.67 E+00	5.66 E+00	6.18 E+00
300	1.07 E+01	8.22 E+00	7.97 E+00	8.80 E+00
	Eq. (B7)	Eq. (B7)	Eq. (B3)	Eq. (B3a)

APPENDIX C

Ba AND Ba⁺ COLLISIONS WITH ATMOSPHERIC SPECIES

C.1 (Ba+O)-COLLISIONS: MOMENTUM-TRANSFER CROSS-SECTION.

For such collisions we are aware of only one (simple) approach for estimating the momentum-transfer cross-section, that described for atom-atom collisions in Section 2.1.1. For relative speeds g below a few times 10^5 cm/sec, the asymptotic form of the momentum-transfer cross-section based on the r^{-6} potential is given by Eq. (A16c), where r_m is the radius at which the minimum energy $(-\varepsilon_o)$ occurs in the Lennard-Jones (12,6)-potential. For (Ba+O)-collisions we adopt the potential parameters from Huber and Herzberg [Ref. 34, p. 72]:

$$\varepsilon_o \approx 5.79 \, eV \tag{C1a}$$

$$r_m \approx r_e = 1.9397 \, \text{Å} \tag{C1b}$$

and the reduced mass number from Table 27. Then, from Eq. (A16c) we have

$$\sigma(Ba+O)\big|_{(r^{-6})\text{-pot.}} = 2.16 \times 10^{-11} \, g^{-2/3} \, cm^2 \tag{C2a}$$

$$= 1.00 \times 10^{-14} \, g_{km/sec}^{-2/3} \, cm^2. \tag{C2b}$$

Equation (C2) is plotted as the long-dash line in Fig. 16. (Equation (C2) is very close to what we found for (U+O)-collisions, based on the (r^{-6})-potential, in Section 2.3.2: $2.11 \times 10^{-11} \, g^{-2/3}$.) It will be explained later that our final suggestion for the momentum-transfer cross-section for (Ba+O)-collisions is not Eq. (C2) but Eq. (C4).

C.2 (Ba⁺+O)-COLLISIONS: MOMENTUM-TRANSFER CROSS-SECTION.

For such collisions we are aware of, and consider, two (simple) approaches for estimating the momentum-transfer cross-section. Unaware of a strong basis for choosing between them, we will offer a compromise, which will lead us to modify our formula for (Ba+O)-collisions.

C.2.1 Polarization Potential.

For a polarization-potential interaction, the momentum-transfer cross-section is given by Eq. (A11b), which, with parameters from Table 27, gives
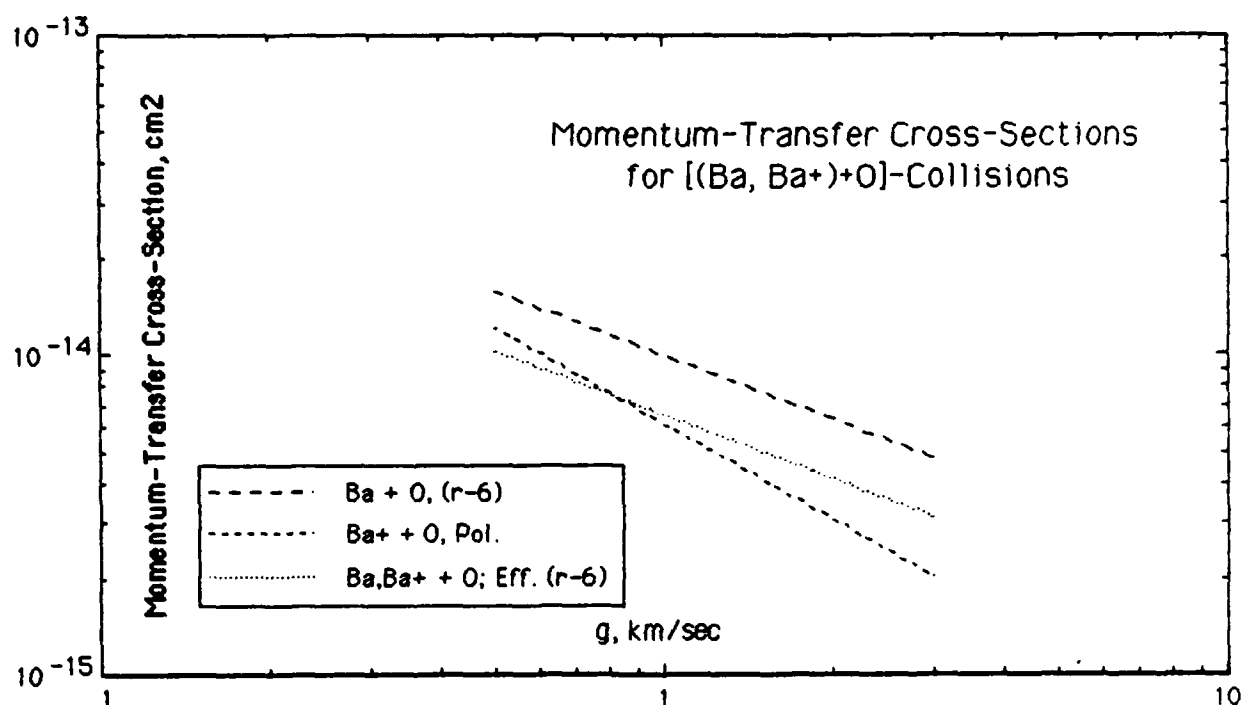
Figure 16. Velocity-dependent momentum-transfer cross-sections for (Ba+O)-collisions, based on (r^{-6})- and effective (r^{-6})-potentials and for (Ba$^+$+O)- collisions, based on polarization and effective (r^{-6})-potentials.

$$\sigma(Ba^+ + O)\big|_{pol.pot.} = 6.08 \times 10^{-10}\, g^{-1}\ cm^2 \qquad\qquad (C3a)$$

$$= 6.08 \times 10^{-15}\, g^{-1}_{km/sec}\ cm^2. \qquad\qquad (C3b)$$

Equation (C3) is plotted as the short-dash line in Fig. 16.

C.2.2 (r^{-6})-Potential.

In Section 2 we indicated a basis for reservations about the applicability of the polarization potential for UO_n^{m+}-collisions, especially for the higher velocities ($\leq$ 5 km/sec) being considered by LANL personnel early in these studies. We have a similar reservation with respect to Ba$^+$ collisions. The parameter γ in the (12,6,4)-potential [cf. Section 2.1.2.2] is a measure of the relative strength of the r^{-6} and r^{-4} energies. For $\gamma = 1$, the (12,6)-potential obtains; for $\gamma = 0$, the (12,4)-potential obtains.

Not aware of potential parameters being available for BaO$^+$, we tentatively assume they can be approximated by those for BaO, given by Eqs. (C1a) and (C1b)

C-2

In that case, γ would be equal to 0.954, close to the value (0.960) we found for UO^+ [Section 2.2.2.3] Such a value for γ suggests the importance of the r^{-6} term compared with the r^{-4} term. If one ignored the r^{-4} term completely, and also adopted the BaO potential parameters for BaO^+, then Eq. (C2) would be an approximate expression for the momentum-transfer cross-section for (Ba^++O)-collisions based on a "quasi-realistic" potential. (Note that Eq. (C2) is extremely close to what we found for (U^++O)-collisions in Section 2.1.2.3, $2.15 \times 10^{-11} \times g^{-2/3}$.)

C.2.3 A Compromise (?): An Effective (r^{-6})-Potential.

Note that:
(a) The experimental mobility of Ba^+ in N_2 [Powell and Brata, unpublished [Ref. 58]; see Section C.3.2] can be predicted to within about four percent by use of the polarization potential (see Section C.3).
(b) A similar situation may hold for (Ba^++O)-collisions.
(c) There are reservations about the applicability of the polarization potential at the higher velocities.
(d) There is concern about Eq. (C2) giving a larger cross-section for $(Ba+O)$-collisions than that given by Eq. (C3) for (Ba^++O)-collisions at (room) thermal energies.

In view of these considerations, we use Eq. (A19) in Eq. (A16c), with parameters evaluated from Table 27, to get our final expression for the momentum-transfer cross-section for $[(Ba,Ba^+),O]$-collisions,

$$\sigma[(Ba,Ba^+)+O]\big|_{\text{Eff.}(r^{-6})\text{-pot.}} = 1.40 \times 10^{-11} \, g^{-2/3} \text{ cm}^2 \qquad (C4a)$$
$$= 6.50 \times 10^{-15} \, g_{\text{km/sec}}^{-2/3} \text{ cm}^2. \qquad (C4b)$$

Equation (C4) is plotted as the dotted line in Fig. 16.

C.3 (Ba^++N_2)-COLLISIONS: MOBILITY.

C.3.1 Introduction.

We are unaware of any potential parameters for (Ba^++N_2)-collisions. However, there is a mobility measurement which we will compare with a theoretical value based on the polarization-potential interaction. Owing to reservations about the applicability of the polarization-potential interaction at the higher velocities — if we extrapolate to N_2 our considerations of (Ba^++O)-collisions — we will use the theoretical mobility based on the polarization potential (essentially equivalent to the experimental mobility) to set the

parameter $(r_m^6 \epsilon_o)^{1/3}$ in the asymptotic low-energy cross-section based on the (r^{-6}) potential.

C.3.2 Experimental Mobility.

The mobility in nitrogen of various ions has been reported by, e.g., Brata [Ref. 11] and by Mitchell and Ridler [Ref. 58]. A graph of mobility versus ion mass number (erroneously attributed to Ref. 11) is shown in Fig. 10.17 of Hasted [Ref. 28]; basically the same graph (but slightly edited), shown in Fig. 3.20 of Brown [Ref. 12] (and also in Fig. 7m-87 of Grey [Ref. 26]) and correctly attributed to Ref. 58, is reproduced here as Fig. 17. A similar graph does appear in Fig. 4 of Ref. 11, but Ba+ does not appear in it. The only comment about Ba+ made in Ref. 58 is reproduced below:

"... those [mobilities of various ions in nitrogen] previously examined [by Tyndall, Powell, and Brata] ... including Ba+ at 2.23 obtained by Powell and Brata previously unpublished ... ."
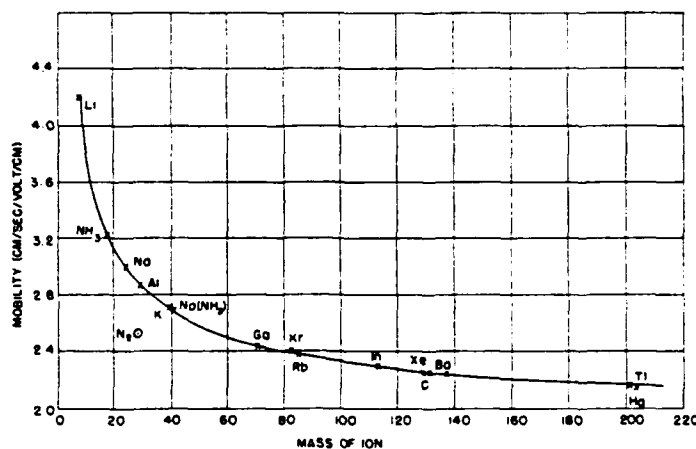
Fig. 3. 20. Mobility in nitrogen of various ions as a
function of mass at 1 atmosphere pressure.

J. H. Mitchell and K. E. W. Ridler, Proc. Roy. Soc.
(London) A146, 911 (1934).

Figure 17. Reduced mobility in N_2 of various ions as a function
of their mass number (from Brown [Ref. 12, p. 62]).

The temperature is not stated in Refs. 28, 12, 26, or 58; Ref. 11 variously refers to 20 °C, 17 °C, and NTP. We will assume the temperature to be room temperature, taken as $T \approx 293$ K.

From Eqs. (A2b), (A9f), and (A13) – or from Eq. (29a) – we see that, for the polarization-potential interaction, the mobility is inversely proportional to the number density of the gas, or equivalently proportional to the ratio of the temperature to the pressure. Hence, to adjust the experimental value of Ba$^+$ mobility to STP conditions, we write

$$\mathscr{K}^{STP}_{exp}(Ba^+, N_2) = \mathscr{K}_{exp}(Ba^+, N_2) \frac{T_{STP}}{T_{exp}} \frac{p_{exp}}{p_{STP}}$$

$$= 2.23 \frac{273}{293} \frac{1}{1}$$

$$= 2.08 \ (cm/sec)/(volt/cm) \tag{C5}$$

C.3.3 Theoretical Mobility.

C.3.3.1 <u>Polarization Potential.</u> From Eq. (A26b) and Table 27 we have

$$\mathscr{K}^{STP}(Ba^+, N_2)\big|_{pol.pot.} = 2.16 \ (cm/sec)/(volt/cm), \tag{C6}$$

as given in Table 28. That the value in Eq. (C6) differs from that in Eq. (C5) by less than four percent is, perhaps, remarkable. The essential agreement could probably justify regarding the mobility of Ba$^+$ in N$_2$ (for the temperature in the experiment) as being properly based on the polarization-potential interaction.

C.3.3.2 <u>Effective (r^{-6})-Potential.</u> We now determine an effective value of the parameter $(r_m^6 \varepsilon_o)^{1/3}$ such that

$$\mathscr{K}^{STP}(Ba^+, N_2)\big|_{(r^{-6})-pot.} = \mathscr{K}^{STP}(Ba^+, N_2)\big|_{pol.pot.} \tag{C7}$$

(From a practical viewpoint it matters little whether we use the theoretical value based on the polarization-potential interaction or the experimental value. We choose the theoretical value to simplify some subsequent formulas.) Thus, from Eq. (A19), we have

$$(r_m^6 \varepsilon_o)^{1/3}\big|_{eff.(Ba^+,N_2)\,mobility} = 4.94 \times 10^{-16} (1.76)^{1/2}$$

$$= 6.55 \times 10^{-16} \ cm^2 \ eV^{1/3} \tag{C8}$$

and from Eqs. (A28b) and (C8),

$$\mathscr{K}^{STP}(Ba^+, N_2)\Big|_{Eff.\,(r^{-6})-pot.} = \frac{6.82\times10^{-15}}{(23.26)^{1/2}\times6.55\times10^{-16}}$$
$$= 2.16\,(cm/sec)/(volt/cm).\qquad(C9)$$

C.4 (Ba^++O_2)-COLLISIONS: MOBILITY.

We follow the procedure used for (Ba^++O)-collisions but limit our considerations to mobility. Thus, from Eq. (A19) we have

$$(r_m^6\,\varepsilon_o)_{eff.}^{1/3}\Big|_{(Ba^+,O_2)\,mobility} = 4.94\times10^{-16}\,(1.59)^{1/2}$$
$$= 6.23\times10^{-16}\,cm^2\,eV^{1/3}\qquad(C10)$$

and from Eqs. (28b) and (C10) we have

$$\mathscr{K}^{STP}(Ba^+, O_2)\Big|_{Eff.\,(r^{-6})-pot} = \frac{6.82\times10^{-15}}{(25.95)^{1/2}\times6.23\times10^{-16}}$$
$$= 2.15\,(cm/sec)/(volt/cm).\qquad(C11)$$

APPENDIX D

AMBIPOLAR DIFFUSION COEFFICIENT – A LIMITED COMPARISON OF EXPERIMENTAL AND THEORETICAL RESULTS FOR SOME BARIUM RELEASES

D.1 THEORETICAL.

The ambipolar diffusion coefficient is usually defined (cf., e.g., Dalgarno [Ref. 8, p. 660]; McDaniel [Ref. 55, p. 513]; Fu [Ref. 21]) as

$$D_a = \frac{D_i \, \mathcal{K}_e + D_e \, \mathcal{K}_i}{\mathcal{K}_i + \mathcal{K}_e} \tag{D1}$$

where the ion and electron mobilities $\mathcal{K}_i$ and $\mathcal{K}_e$ are both positive numbers.

With use of the (Einstein) expressions relating mobility and diffusion coefficient (cf. Eq. (A2a)),

$$D_i = (kT_i / e) \, \mathcal{K}_i \tag{D2a}$$

$$D_e = (kT_e / e) \, \mathcal{K}_e, \tag{D2b}$$

Eq. (D1) becomes

$$D_a = \frac{D_i \, D_e (T_i + T_e)}{D_i T_e + D_e T_i}. \tag{D3}$$

Equation (D3) is the form in which the ambipolar diffusion coefficient appears, e.g., in Holway [Ref. 33, Eq. (18)].

If one combines Eqs. (D1) and (D2) and then assumes $\mathcal{K}_e \gg \mathcal{K}_i$ due to the electron's small mass and its concomitant larger contribution to the conductivity, one has

$$D_a = \frac{D_i (1 + T_e / T_i)}{1 + \mathcal{K}_i / \mathcal{K}_e} \tag{D4a}$$

$$\approx D_i (1 + T_e / T_i), \tag{D4b}$$

where Eq. (D4b) is (or essentially is) the form for the ambipolar diffusion coefficient presented in some atmospheric physics texts, e.g., Banks and Kockarts [Ref. 7, Pt. B, p. 164], Ratcliffe [Ref. 63, p. 108], and Bauer [Ref. 9, p. 97].

D.2 MODEL ATMOSPHERE PROPERTIES.

D.2.1 Neutral Particles.

Later we will need selected neutral-particle densities for two model atmospheres presented in Tables 30 and 31.

The CIRA-1965 Model-6 1800-hr [Ref. 15] atmosphere (cf. Table 31) appears to be the model atmosphere used by at least some members (see, e.g., Ref. 46, p. 23) of the SECEDE community as being appropriate for the solar-flux conditions during the second half of January 1971 when the SECEDE-II events occurred.

Table 30. Selected properties for CIRA-65, Model-5, 0600-hr.

h, km	T, K	cm^{-3}		
		[O]	[N$_2$]	[O$_2$]
190	823	4.25 E+09	4.83 E+09	5.45 E+08
200	852	3.33 E+09	3.32 E+09	3.45 E+08
210	877	2.63 E+09	2.19 E+09	2.23 E+08
220	898	2.11 E+09	1.51 E+09	1.46 E+08

h, km	cm^{-3}	f[O]	f[N$_2$]	f[O$_2$]
	n(total)			
190	9.62 E+09	0.442	0.502	0.056
200	6.99 E+09	0.476	0.475	0.049
210	5.04 E+09	0.522	0.434	0.044
220	3.77 E+09	0.560	0.401	0.039

Table 31. Selected properties for CIRA-65, Model-6, 1800-hr.

h, km	T, K	cm^{-3}		
		[O]	[N$_2$]	[O$_2$]
140	662	1.98 E+10	6.05 E+10	9.48 E+09
150	779	1.36 E+10	3.49 E+10	5.16 E+09
160	878	9.36 E+09	2.02 E+10	2.81 E+09
180	1029	5.49 E+09	8.92 E+09	1.13 E+09
185	1058	4.93 E+09	7.54 E+09	9.39 E+08
200	1135	3.59 E+09	4.55 E+09	5.33 E+08
220	1210	2.49 E+09	2.52 E+09	2.74 E+08
240	1264	1.79 E+09	1.47 E+09	1.49 E+08
250	1286	1.54 E+09	1.14 E+09	1.12 E+08
260	1304	1.33 E+09	8.85 E+08	8.37 E+07
280	1333	9.96 E+08	5.46 E+08	4.84 E+07
300	1355	7.58 E+08	3.43 E+08	2.85 E+07

Table 31. Selected properties for CIRA-65, Model-6, 1800-hr. (Cont'd)

h, km	n(total) cm^{-3}	f[O]	f[N$_2$]	f[O$_2$]
140	8.98 E+10	0.220	0.674	0.106
150	5.37 E+10	0.253	0.650	0.096
160	3.23 E+10	0.289	0.624	0.087
180	1.56 E+10	0.353	0.574	0.073
185	1.34 E+10	0.368	0.562	0.070
200	8.67 E+09	0.413	0.525	0.062
220	5.28 E+09	0.471	0.477	0.052
240	3.41 E+09	0.526	0.430	0.044
250	2.79 E+09	0.552	0.408	0.040
260	2.29 E+09	0.578	0.386	0.036
280	1.59 E+09	0.626	0.343	0.031
300	1.13 E+09	0.672	0.303	0.025

D.2.2 Electron- to Ion-Temperature Ratio.

Linson et al., guided by results in Wand [Ref. 67], have used the following prescription for the ratio of electron temperature to ion temperature:

$$\frac{T_e}{T_i} = \begin{cases} 1.0 + \dfrac{h-130}{80}\,0.6, & 130 \le h\text{(km)} \le 210 \\[2ex] 1.6 - \dfrac{h-210}{90}\,0.4, & 210 \le h\text{(km)} < 300. \end{cases} \tag{D5}$$

Equation (D5) appears to be an approximate fit to the ratio T_e/T_i (for a period spanning an evening twilight) appearing in Fig. 3c of Ref. 67, reproduced here as Fig. 18.

Figure 32 in Bauer [Ref. 9], showing T_e and T_i for different solar-cycle conditions, is reproduced here as Fig. 19; the time of day is not specified, but it is presumably daytime (noon?). We have collated in Table 32 values of T_e and T_i (and the ratio T_e/T_i) at 200-km altitude read from Fig. 19.

Table 32. Temperatures at 200-km altitude per Bauer [Ref. 9, Fig. 32]

	A (Solar Max)	B (Intermediate)	C (Solar Min; Mag. Act.)
T_e	1125	1450	1950
T_i	700	775	875
T_e/T_i	1.61	1.87	2.23
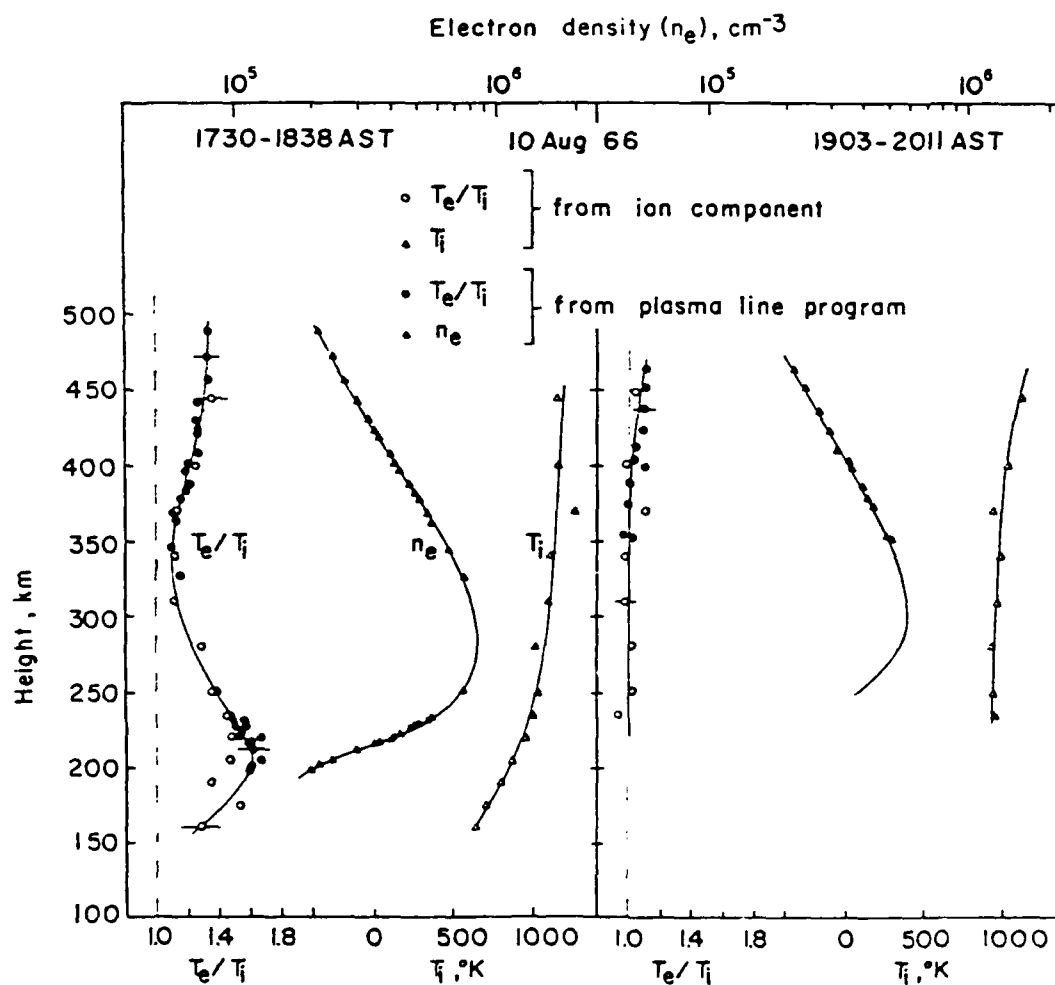
Fig. 3c.

Figure 18.   Electron and ion temperatures versus altitude for 1730-1838
AST, 10 August 1966 (from Wand [Ref. 67]).
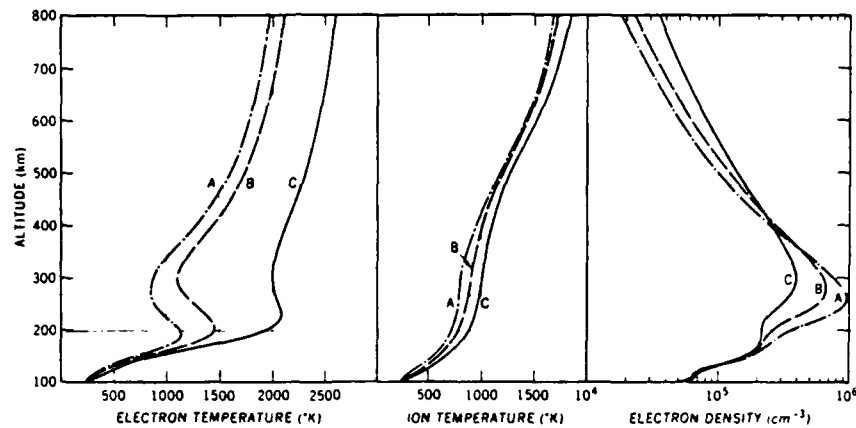
Fig. 32. Electron and ion temperatures in the terrestrial ionosphere for different conditions. Also shown are the corresponding electron density profiles. Curves A reflect a high peak electron density (e.g., solar maximum) and high atomic oxygen concentration at the lower boundary; curves C reflects a low peak electron density (e.g., solar minimum) and an atomic oxygen concentration reduced by 50 % while curves B reflects and intermediate condition. Similarly, curves C are also representative of a situation occurring during magnetic storms. (After Herman and Chandra)

Figure 19.   Electron and ion temperatures versus altitude
              for different solar-flux conditions (from
              Bauer [Ref. 9]).

The smoothed solar flux at 10.7-cm wavelength is shown, for the period from 1958 to 1968, in Fig. 6 of Jacchia [Ref. 36], reproduced here as Fig. 20. The general trend of the same flux ($F_{10.7}$) is shown in Fig. 1 of Hedin et al. [Ref. 30], reproduced here as Fig. 21. From Figs. 20 and 21, one would judge $\bar{F}_{10.7} \approx 110$ at the date (10 Aug 66) corresponding to the data in Fig. 18. (It would be of interest to compare this value with the daily values for August 1966, but those data are not readily available. Solar data for an approximate period including 1966 through September 1970 are not in the J. Geophys. Res. but were published in "Solar-Geophysical Data," U. S. Dept. of Commerce, Boulder, Colorado, 80302. Data for October 1970 are in J. Geophys. Res. 76, 1097 (1 Feb 71), with subsequent data following regularly.)

Solar flux data for January 1971 are given in Table 33. The average for the last half of January 1971,

$$\frac{1}{16} \sum_{i=16\,\text{Jan}\,71}^{i=31\,\text{Jan}\,71} F'_{10.7} = 173.3 , \tag{D6}$$

is somewhat higher than the average for the month, 162.6, and considerably higher than the value ($\approx$152) shown as the "general trend of F_{107}" in Fig. 1 of Ref. 30 (our Fig. 21).
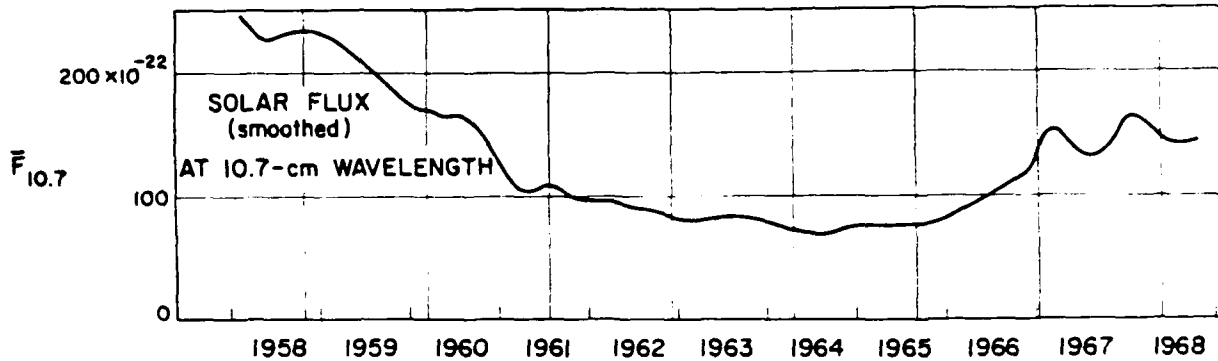
Figure 20.   Mean 10.7-cm solar flux index for the period 1958-1968 (from Jacchia [Ref. 36]).
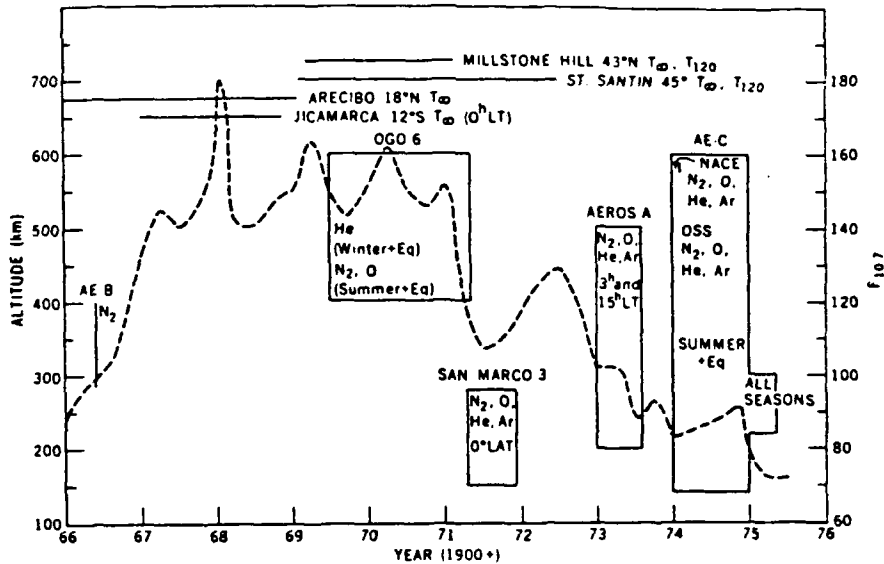
Fig. 1. MSIS model data coverage in altitude and year-day of year coordinates. Also shown, as the dashed line, is the general trend in the $F_{10.7}$ index during this period.

Figure 21.   Mean 10.7-cm solar flux index for the period 1966-1975 (from Hedin et al. [Ref. 30]).

Generally speaking, the data in Fig. 18 are for a relatively low value of $\bar{F}_{107}$; at higher values of $\bar{F}_{107}$ one would probably expect lower values of the ratio T_e/T, , based on the trend from Fig. 18 (and Table 32).

Table 33. Observed solar flux at 2800 MHz during January 1971 [Ref 43]

Day	$\bar{F}_{107}$	Day	$\bar{F}_{107}$	Day	$\bar{F}_{107}$
1	135.0	11	154.1	21	184.6
2	139.4	12	155.6	22	186.4
3	139.3	13	153.2	23	188.8
4	145.0	14	159.2	24	182.7
5	151.1	15	158.9	25	174.0
6	151.9	16	161.6	26	170.2
7	155.3	17	160.4	27	171.9
8	154.2	18	165.6	28	171.3
9	158.1	19	171.3	29	165.7
10	157.3	20	174.8	30	168.0
				31	175.2

D.3 COMPARISONS.

D.3.1 Kivel [Ref. 39].

For *Dogwood* (h = 191 km [Ref. 62]), the neutral cloud grows with a diffusion coefficient $D \approx 0.1$ km^2/sec. The ambipolar diffusion coefficient for the ion cloud along the Earth's magnetic field is $D_{\parallel} \approx 0.2$ km^2/sec.

Comments. The value 0.2 km^2/sec for $D_{\parallel}$ is larger than the 0 136 km^2/sec and 0.11 km^2/sec also reported for *Dogwood* respectively by Lumenello et al. [Ref. 50] and by Boquist et al. [Ref. 10] in following Sections D.3.2 and D.3.3

To make predictions to compare with the quoted *Dogwood* (and *Apple*) ambipolar diffusion coefficients, we need an atmosphere. For convenience and simplicity, we use Figs. 20 and 21 to read respectively $\bar{F}_{107} \approx 145$ and $\bar{F}_{107} \approx 142$ (in units of 10^{-22} W/(m^2 cyc/sec)] for May 1968. (*Apple* occurred on 2 May 68; *Dogwood*, 13 May 68.) These values of $\bar{F}_{107}$ lead us to use Model-5 (for which $\bar{F}_{107}$ =150) in CIRA-1965 [Ref 15]. For 0600 hrs, we have atmospheric data in Table 30; results for diffusion coefficients are given in Table 34. The ordinary diffusion coefficient D, for Ba$^+$ was evaluated from Eq. (A33), the ambipolar diffusion coefficient $D_{\parallel}$ from Eq. (D4b), and T_e / T_i from Eq. (D5). The value 0.124 km^2/sec for the effective (r^{-6})-potential at 191-km altitude in Table 34 does not agree well with the value 0.2 km^2/sec quoted by Kivel, but does agree well with

the values 0.136 and 0.11 quoted respectively by Lumenello et al. and by Boquist et al. (Sections D.3.2 and D.3.3)

Table 34. Ba$^+$ diffusion coefficients for CIRA-65, Model-5, 0600-hr

h	D_i, km^2/sec			$D_{\parallel}$, km^2/sec			
km	Pol.	Eff. (r^{-6})	$1+T_e/T_i$	Pol.	Eff. (r^{-6})	LB-71	LB-77
190	5.84 E-02	4.86 E-02	2.45	0.143	0.119	0.114	0.129
191			2.46	0.149	0.124	0.119	0.125
194			2.48	0.167	0.139	0.133	0.140
196			2.49	0.181	0.150	0.143	0.151
200	8.43 E-02	6.98 E-02	2.52	0.212	0.176	0.167	0.177
201			2.53	0.221	0.183	0.174	0.184
204			2.55	0.250	0.207	0.195	0.207
205			2.56	0.260	0.216	0.203	0.216
207			2.58	0.283	0.234	0.219	0.233
210	1.23 E-01	1.01 E-01	2.60	0.320	0.264	0.246	0.263
215			2.58	0.375	0.309	0.286	0.306
220	1.72 E-01	1.41 E-01	2.56	0.440	0.361	0.332	0.357
(1)	(2)	(3)	(4)	(5)	(6)	(7)	(8)
	Eq. (A33)	Eq. (A33)	Eq. (D5)	Col. 2 × Col.4 ⇓ (D4b)	Col. 3 × Col. 4 ⇓ (D4b)	Eq. (D7) (D8a) (D5) ⇓ (D10a)	Eq.(D7) (B3a) (D5) ⇓ (D10b)

D.3.2 Lumenello, Davis, and Freedman [Ref. 50].

Measured diffusion coefficients of the ion cloud parallel to the field were 0.238 km^2/sec for *Apple* (h = 196 km) and 0.136 km^2/sec for *Dogwood* (188 km, or 191 km per Table I in Ref. 62).

Comments. For *Apple*, the interpolated value 0.150 km^2/sec for the effective (r^{-6})-potential at 196 km in Table 34 does not agree well with the value 0.238 km^2/sec quoted by Lumenello et al. [Ref. 50]

For *Dogwood*, the value 0.136 km^2/sec quoted by Lumenello et al [Ref 50] is (a) smaller than the 0.2 km^2/sec reported by Kivel (Section D.3.1), (b) larger than the 0.11 km^2/sec reported by Boquist et al. (Section D.3.3), and (c) slightly larger than the 0.124 km^2/sec computed for the effective (r^{-6})-potential at 191-km altitude in Table 34.

Although the report by Lumenello et al. [Ref. 50] is an EG&G report, it is not referenced in the later EG&G report by Boquist et al. [Ref. 10].

D.3.3 Boquist, Overbye, Kiesling, and Eves [Ref. 10].

These authors report a value of 0.11 km^2/sec for $D_\parallel$ for both *Apple* and *Dogwood*, each occurring during morning twilight.

Comments. For *Dogwood*, the value 0.11 km^2/sec is (a) less than the 0.2 km^2/sec reported by Kivel (Section D.3.1), (b) less than the 0.136 km^2/sec reported by Lumenello et al. (Section D.3.2), and (c) less than the computed values (Table 34) for $D_\parallel$ of 0.124 km^2/sec and 0.149 km^2/sec respectively for the effective (r^{-6})-potential and polarization potential.

For *Apple*, the value 0.11 km^2/sec is (a) less than the value 0.238 km^2/sec reported by Lumenello et al. (Section D.3.2) and (b) the computed values (Table 34) for $D_\parallel$ of 0.150 km^2/sec and 0.181 km^2/sec respectively for the effective (r^{-6})-potential and polarization potential.

D.3.4 Fu, Marram, Ponder, and Breedlove [Ref. 22].

The data in Table 35 have been collated from Tables 1, 2, and 8 of Ref. 22

Comments. Why is $D_\parallel$ (*Titmouse*) so small? Why is $D_\parallel$ (*Titmouse*) < $D_\parallel$ (*Sapsucker*), since h(*Sapsucker*) < h(*Titmouse*) ?

Why is $D_\parallel$ (*Mulberry*) so small? Why is $D_\parallel$ (*Mulberry*) < $D_\parallel$ (*Kumquat*), since h(*Kumquat*) < h(*Mulberry*) ?

D.3.5 Linson and Baron [Ref. 45].

This short paper includes the statements:
"... Beyond 20 sec, the ion cloud expands by ambipolar diffusion parallel to the magnetic field. An ambipolar diffusion coefficient of D = 0.1 km^2/sec at 185-km altitude is consistent with an ion-neutral

Table 35. BIRDSEED and PRE-SECEDE data from Fu et al. [Ref. 22]

$\bar{F}_{107}$[a]	Date	Name	Altitude km	Time UT	$D_{\parallel}$ km²/sec
		BIRDSEED			
≈152	26 May 70	*Sapsucker*[b]	204±3	0552:25	0.3
≈152	6 June 70	*Titmouse*[b]	210±5	0555:25	0.2
		PRE-SECEDE			
≈145	5 Sep 69	*Kumquat*[c]	194		0.26
≈145	6 Sep 69	*Lime*[c]	201.5		0.29
≈145	13 Sep 69	*Mulberry*[c]	195.8		0.13

[a] As read by the writer from the "general trend $F_{10.7}$" in Fig. 1 of Ref. 30 (see our Fig. 21).

[b] The results for these events are the primary purpose of Ref. 22.

[c] The results for these events are included in Ref. 22 for comparison purposes.

collision time of

$$\tau_i = 9 \times 10^9 \, N_n^{-1}$$

where N_n is the neutral density in cm^{-3}, with an electron-plus-ion temperature of 2300 °K."

"Excellent agreement between the radar data and theoretical expressions is obtained for the first 10 minutes, indicating that the value for $D_{\parallel}$ (0.1 km²/sec) is appropriate at early times for these two [*Spruce* and *Olive*] releases."

Comments. The quoted value, 0.1 km²/sec at 185-km altitude, appears to be in contradiction with a later value, 0.15 km²/sec at 185-km altitude, quoted by Linson [Ref. 44, p. 5].

It is desirable to understand why 185-km altitude is selected for a quoted $D_{\parallel}$ when explicit results are given (on the next page of Ref. 45) for *Spruce* and *Olive* (at altitudes of 187.3 and 193.4 km, per Ref. 62, Table 1, p. 3). Could it be that the text should have referred to *Olive Pit* (at 185 km) instead of *Olive*?

We should like to verify the 0.1 km^2/sec by using formulas likely to have been used by Ref. 45. Thus, by combining Eqs. (A1) and (D4b) we have

$$D_{\parallel} = \frac{k\,(T_i + T_e)}{m_i\,v_i} = \frac{k\,(T_i + T_e)}{m_i}\,\tau_i\,,\tag{D7}$$

from the Ref. 45 text,

$$\tau_i = 9\times10^9/N_n\tag{D8a}$$

$$T_i + T_e = 2300\ K,\tag{D8b}$$

and for 185-km altitude in Table 31,

$$N_n = 1.34\times10^{10}\ cm^{-3}.\tag{D8c}$$

Hence,

$$D_{\parallel} = 0.093\ km^2/sec,\tag{D9}$$

which is only seven percent smaller than the quoted 0.1 km^2/sec.

If, instead of using Eq. (D8b) for the temperatures, we use for T_i the neutral gas temperature of 1054 K at 185-km altitude in Table 31 and Eq. (D5) giving a value of 1.41 for the ratio T_e/T_i, we then obtain $D_{\parallel} = 0.104\times10^{10}$ km^2/sec

In Section B.1 we disagree with the use of Eq. (B3) ($=$Eq. (D8a)) for the collision time — though the disagreement is more in principle than in practice, specially with consideration of the improved formula in Ref. 46. The proper formula is given by Eq. (B7) (or by Eq. (B3b), explicitly for the polarization potential), with (interpolated) results from Table 31 giving $\tau_i = 0.747$ and $\tau_i = 0.596$ respectively for collisions based on the polarization and effective (r^{-6})-potentials. Evaluation of Eq. (D8a) ($=$Eq. (B3)) with use of Eq. (D8c) gives $\tau_i = 0.67$ sec, a value intermediate to what we would propose by factors of 0.90 and 1.13 for the polarization and effective (r^{-6})-potentials.

Use of the ordinary diffusion coefficient in Table 36 for 185 km and use of Eq. (D5) for the temperature ratio give values for $D_{\parallel}$ of 0.12 and 0.092 km^2/sec respectively for the polarization and effective (r^{-6})-potentials.

D.3.6 Linson [Ref. 44].

This paper [p. 5] states :
"... appropriate ambipolar diffusion coefficient $D_{\parallel} = 0.04, 0.15,$ and 0.7 for the three altitudes [150, 185, and 250 km]."

Comments. It is not clear whether these are theoretical or experimental values.

Instead of 0.15 km²/sec as quoted here for 185 km, Ref. 45 quotes 0.1 km²/sec.

Our computed values are given in Columns 5 and 6 of Table 36. As a set, the better agreement with the Ref. 44 values is for those obtained with the polarization potential.

In Table 36 we also record the values of $D_\parallel$ computed from Eqs. (D7) and (D8a) [... Eq. (B3)], i.e., the Ref. 45 prescription, and with T_e/T_i given by Eq. (D5).

$$D_\parallel = 5.45 \times 10^5 \frac{T_i}{N_n} \left[1 + \frac{T_e}{T_i} \right], \quad km^2/sec. \tag{D10a}$$

Similarly, we record in Table 36 the values of $D_\parallel$ computed from Eqs (D7) and (B3a), i.e., the Ref. 46 prescription, and with T_e/T_i given by Eq. (D5):

$$D_\parallel = 5.20 \times 10^5 \frac{T_i}{[N_2]+[O_2]+0.8[O]} \left[1 + \frac{T_e}{T_i} \right], \quad km^2/sec. \tag{D10b}$$

We see that the results from Eq. (D10b) agree slightly better with the Ref. 44 values than do those from Eq. (D10a).

D.3.7 Summary Table and Comments.

A summary of all the comparisons is provided in Table 37.

In the Linson-Baron [Ref. 45] and Linson-Baxter [Ref. 46] formulas for the coefficient for ambipolar diffusion along the magnetic field,

$$D_\parallel = \frac{kT_i}{m_i} \left[1 + \frac{T_e}{T_i} \right] \tau_{in}, \tag{11}$$

the expression for the ion-neutral collision time τ_{in}, given by Eq. (B3) [Ref 45] and Eq. (B3a) [Ref. 46] – which is nominally based on the experimental mobility of Ba⁺ in N_2 – improperly accounts for O and O_2 if a polarization-potential interaction is assumed. Correction of this relatively small error by properly accounting for the polarizabilities of O_2 (which actually does not matter) and O (which does matter) does not significantly change the overall comparison between theoretical values of the ambipolar diffusion coefficient $[D_{\parallel, pol.pot.}]$ based on the polarization potential and (sometimes ambiguous or uncertain) experimental values $[D_{\parallel, exp}]$ derived from 12 Ba-releases. Values of the ambipolar diffusion coefficient $[D_{\parallel, Eff. (r^{-4})-pot.}]$ computed from an effective (r^{-6})-potential – which are about 79% to 85% of $D_{\parallel, pol.pot.}$ for ionospheric ion temperatures ranging from 1135 K to 750 K – are (accidentally) very nearly the same as those obtained with the Ref. 46 formula for

Table 36. Ba$^+$ diffusion coefficients for CIRA-65, Model-6, 1800-hr.

| h | $D_\perp$, km^2/sec | | $1+T_e/T_i$ | $D_\parallel$, km^2/sec | | | | |
km	Pol.	Eff. (r^{-6})		Pol.	Eff. (r^{-6})	Ref. 44	Ref. 45	Ref. 46
140	4.13 E-03	3.56 E-03	2.08	0.009	0.007		0.008	0.008
150	8.28 E-03	6.95 E-03	2.15	0.018	0.015	0.04	0.017	0.017
160	1.58 E-02	1.30 E-02	2.23	0.035	0.029		0.033	0.033
180	3.97 E-02	3.19 E-02	2.38	0.095	0.076		0.085	0.088
185	4.80 E-02	3.83 E-02	2.41	0.116	0.092	0.15	0.104	0.107
200	8.17 E-02	6.44 E-02	2.53	0.207	0.163		0.180	0.188
220	1.48 E-01	1.16 E-01	2.56	0.379	0.296		0.319	0.337
240	2.48 E-01	1.92 E-01	2.47	0.612	0.474		0.499	0.532
250	3.13 E-01	2.42 E-01	2.42	0.757	0.585	0.7	0.607	0.652
260	3.94 E-01	3.03 E-01	2.38	0.937	0.722		0.738	0.794
280	5.98 E-01	4.59 E-01	2.29	1.37	1.05		1.05	1.14
300	8.83 E-01	6.76 E-01	2.20	1.94	1.49		1.44	1.59
(1)	(2)	(3)	(4)	(5)	(6)	(7)	(8)	(9)
	Eq. (A33)	Eq. (A33)	Eq. (D5)	Col. 2 x Col.4 ⇓ (D4b)	Col. 3 x Col. 4 ⇓ (D4b)		Eq. (D7) (D8a) (D5) ⇓ (D10a)	Eq. (D7) (B3a) (D5) ⇓ (D10b)

one of the model atmospheres used. An overall comparison of $D_{\parallel,\,Eff.\,(r^{-6})-pol.}$ with $D_{\parallel,\,exp.}$ is about the same as for $D_{\parallel,\,pol.pol.}$, so that a strong preference cannot be established on this basis, unless one should have reasons (unknown to the writer) to select or exclude certain experimental data.

It would be desirable to determine whether or not there exists a definitive set of experimental values for all the Ba-releases, including the six evening twilight Ba-releases for Project STRESS (*Anne*, early December 1976; *Betty*, *Carolyn*, *Dianne*, *Ester*, and *Fern* in late February and March 1977 [Ref. 47 (substantially in Ref. 48)]. Reference 53, while providing an overview of Project STRESS, gives no information regarding early-time ambipolar diffusion coefficients, since the interest was in late-time striations. A similar comment applies to Project PLACES [Ref. 54].

Table 37. Summary of measured and predicted Ba⁺ diffusion coefficients for barium releases

	Release		$D_\parallel$(exp.), km²/sec			$D_\parallel$(theory), km²/sec			
		Alt.							
Date	Name	km	Value	Reference	T_e/T_i	LB-71	LB-77	Pol.	Eff.r⁻⁶
SECEDE I (Arecibo, Puerto Rico)						CIRA-65, Model-5, 0600-Hr			
2 May 68	*Apple*	196	0.238	Lumenello et al. [Ref. 50]					
			0.11	Boquist et al. [Ref. 10]	1.49	0.14	0.15	0.18	0.15
13 May 68	*Dogwood*	191	0.2	Kivel [Ref. 39]					
			0.136	Lumenello et al. [Ref. 50]					
			0.11	Boquist et al. [Ref. 10]	1.46	0.12	0.12	0.15	0.12
PRE-SECEDE (White Sands, New Mexico)									
5 Sep 69	*Kumquat*	194	0.26	Fu et al. [Ref. 22]	1.48	0.13	0.14	0.17	0.14
6 Sep 69	*Lime*	201.5	0.29	Fu et al.	1.53	0.17	0.18	0.22	0.18
13 Sep 69	*Mulberry*	195.8	0.13	Fu et al.	1.49	0.14	0.15	0.18	0.15
BIRDSEED (Kauai, HI)					Alt.				
26 May 70	*Sapsucker*	204±3	0.3	Fu et al. ↓	201	1.53	0.17	0.18	0.22	0.18
					204	1.55	0.19	0.21	0.25	0.21
					207	1.58	0.22	0.23	0.28	0.23
6 Jun 70	*Titmouse*	210±5	0.2	Fu et al. ↓	205	1.56	0.20	0.22	0.26	0.22
					210	1.60	0.25	0.26	0.32	0.26
					215	1.58	0.29	0.31	0.37	0.31
SECEDE-II (Eglin, Florida)						CIRA-65, Model-6, 1800-Hr			
21 Jan 71	*Olive*	193.4	0.1	Linson & Baron [Ref. 45]	1.48	0.14	0.15	0.16	0.13
1 Feb 71	*Spruce*	187.3	0.1	Linson & Baron [Ref. 45]	1.43	0.11	0.12	0.13	0.10
16 Jan 71	*Nutmeg*	150	0.04	Linson [Ref. 44]	1.15	0.017	0.017	0.017	0.015
29 Jan 71	*Olive Pit*	185	0.15	Linson [Ref. 44]	1.41	0.10	0.11	0.12	0.092
26 Jan 71	*Redwood*	250	0.7	Linson [Ref. 44]	1.42	0.61	0.65	0.76	0.58

Eq (D5) (D10a) (D10b) (D4b) (D4b)

APPENDIX E

RELATIVE SPEED FOR MONOENERGETIC BEAM IN A MAXWELLIAN GAS

E.1 APPROXIMATE FORMULAS.

In developing the energy loss rate for a particle traversing a Maxwellian gas (Section 3.3.1), we were not initially aware of a literature formula for the mean relative speed between a monoenergetic beam and the particles of a traversed Maxwellian gas. We expediently started with the formula for the relative speed for the particles of two separate Maxwellian speed distributions [Ref 6; Ref 7, Pt. A, p. 189] and adapted it to the current need by assuming that the beam speed (V_b) was the rms speed corresponding to the fictitious temperature assigned to the beam (T_b^{fict}), i.e.,

$$\tfrac{3}{2} k T_b^{fict} = \tfrac{1}{2} M_b V_b^2 . \tag{E-1}$$

Note that the relative speed for two Maxwellian gases (cf. Eq. (48b) in Section 3.2.2) is just the square root of the sum of the squares of the mean speeds for the two individual gases. Thus, as the temperature of one gas approaches zero, the relative speed tends toward the mean speed of the second gas. Owing to this fact, we now express the relative speed of the beam traversing the Maxwellian gas ($\bar{g}_{bg}$) in units of the mean speed of the Maxwellian gas ($\bar{V}_g$) and generalize the relation of V_b to T_b^{fict}, i.e.,

$$\bar{g}_{bg} / \bar{V}_g \approx [1 + \alpha_b R^2]^{1/2} , \tag{E-2a}$$

$$\alpha_b = \begin{cases} (8/3\pi) & \text{for } V_b \Rightarrow \text{rms speed corresponding to } T_b^{fict} \\ 1 & \text{for } V_b \Rightarrow \text{mean speed corresponding to } T_b^{fict} \end{cases} \tag{E-2b}$$

$$R = V_b / \bar{V}_g . \tag{E-2c}$$

E.2 EXACT FORMULA.

Fite et al. [Ref. 20, Appendix A.C] have derived the formula for the distribution of relative speed (v_r) for a monoenergetic particle of speed w passing through a Maxwellian gas,

$$f(v_r, w) \, dv_r = \left[\frac{2\beta^{3/2}}{\pi^{1/2}} \right] \exp[-\beta(v_r^2 + w^2)] \frac{\sinh(2v_r \beta w)}{\beta w} v_r \, dv_r \tag{E-3a}$$

where

$$v_r > 0$$

and β, the inverse square of the most probable speed, is

$$\beta = M_g / 2kT_g . \tag{E-3b}$$

The mean relative speed would, of course, be defined as

$$\bar{V}_r = \int_0^\infty V_r \, f(V_r, w) \, dV_r \tag{E-4}$$

A formula for the mean relative speed is presented in Ref. 20, without intermediate steps. However, one of the terms in the formula contains the error function with the obviously incorrect (dimensional) argument $[\beta^{1/2} - w]$, whereas elsewhere in the formula the (dimensionless) product $x \equiv \beta^{1/2} w$ appears. Thus, one would expect that the argument of the error function should probably be x, a surmise consistent with the equations in Appendix B of Ref. 20 and with formula 3.562.5 on p. 365 of Ref. 25:

$$\int_0^\infty x^2 \exp(-\beta x^2) \sinh(\gamma x) \, dx = \left[\frac{\pi^{1/2}(2\beta + \gamma^2)}{8\beta^{5/2}} \right] \exp\left[\frac{\gamma^2}{4\beta} \right] \mathrm{Erf}\left[\frac{\gamma}{2\beta^{1/2}} \right] + \frac{\gamma}{4\beta^2} . \tag{E-5}$$

Hence, one can write

$$\bar{g}_{bg} \equiv \bar{V}_r = \frac{1}{(\pi\beta)^{1/2}} \left[\frac{\pi^{1/2}}{2x} (1 + 2x^2) \mathrm{Erf}(x) + \exp(-x^2) \right] . \tag{E-6}$$

If one introduces the mean speed of the gas ($\bar{V}_g$),

$$\bar{V}_g = \left[\frac{8kT_g}{\pi M_g} \right]^{1/2} , \tag{E-7}$$

then

$$x^2 = \beta w^2 = \frac{4}{\pi} R^2 \tag{E-8a}$$

and

$$(\pi\beta)^{-1/2} = \bar{V}_g / 2 \tag{E-8b}$$

with

$$R = w / \bar{V}_g . \tag{E-8c}$$

Thus,

$$\bar{g}_{bg} / \bar{V}_g = 0.5 \left[\frac{\pi^{1/2}}{2x} (1 + 2x^2) \mathrm{Erf}(x) + \exp(-x^2) \right] . \tag{E-9}$$

It is readily shown, by using the series expansion of Erf(x) given as Formula 7.1.6 in Ref. 1, that

$$\frac{1}{x} \text{Erf}(x) \xrightarrow[x \to 0]{} \frac{2}{\pi^{1/2}}.$$

(E-10)

Hence,

$$\bar{g}_{bg} / \bar{V}_g \xrightarrow[x \to 0]{} 1.$$

(E-11)

E.3 COMPARISON OF APPROXIMATE AND EXACT RESULTS.

Hence, the exact and both of the approximate formulas give the same result at very low beam-speeds ($R \to 0$). At very high beam-speeds, the exact formula for $\bar{g}_{bg} / \bar{V}_g$ gives R; the general approximate expression, Eq. (E-2a), gives $\alpha_b^{1/2} R$, so that the first approximate formula [Eq. (E-2b1)] gives the slightly smaller value of $(8/3\pi)^{1/2} R$ ($= 0.921 R$) and the second approximate formula [Eq. (E-2b2)] gives R. Results from evaluating the exact and two approximate formulas for R = 0(0.1)3(1)10 are given in Table 38. For low beam-speeds ($R \leq 1$) the first approximate-formula results are in excellent agreement with the exact results, but the second approximate-formula results provide a better overall fit to the exact results.

Table 38. Comparison of two approximate methods with the exact method of computing relative speed for monoenergetic beam in (ambient) Maxwellian gas.

	Relative speed, $\bar{g}_{bg}/\bar{V}_g$				Relative speed, $\bar{g}_{bg}/\bar{V}_g$		
	Approximate Eq.		Exact Eq.		Approximate Eq.		Exact Eq.
R	(E-2b1)	(E-2b2)	(E-9)	R	(E-2b1)	(E-2b2)	(E-9)
0.0	1.0000	1.0000	1.0000	1.9	2.0160	2.1471	2.1066
0.1	1.0042	1.0050	1.0042	2.0	2.0965	2.2361	2.1963
0.2	1.0168	1.0198	1.0169	2.1	2.1779	2.3259	2.2870
0.3	1.0375	1.0440	1.0378	2.2	2.2602	2.4166	2.3785
0.4	1.0657	1.0770	1.0666	2.3	2.3431	2.5080	2.4707
0.5	1.1010	1.1180	1.1029	2.4	2.4268	2.b.00	2.5636
0.6	1.1426	1.1662	1.1462	2.5	2.5110	2.6926	2.6571
0.7	1.1899	1.2207	1.1961	2.6	2.5958	2.7857	2.7510
0.8	1.2423	1.2806	1.2518	2.7	2.6810	2.8792	2.8454
0.9	1.2991	1.3454	1.3129	2.8	2.7667	2.9732	2.9402
1.0	1.3597	1.4142	1.3787	2.9	2.8528	3.0676	3.0354
1.1	1.4238	1.4866	1.4487	3.0	2.9393	3.1623	3.1309
1.2	1.4907	1.5620	1.5224	4.0	3.8185	4.1231	4.0982
1.3	1.5603	1.6401	1.5993	5.0	4.7139	5.0990	5.0785
1.4	1.6321	1.7205	1.6789	6.0	5.6176	6.0828	6.0654
1.5	1.7058	1.8028	1.7609	7.0	6.5263	7.0711	7.0561
1.6	1.7813	1.8868	1.8449	8.0	7.4381	8.0623	8.0491
1.7	1.8583	1.9723	1.9307	9.0	8.3519	9.0554	9.0436
1.8	1.9365	2.0591	2.0180	10.0	9.2673	10.0499	10.0393

Relative speed is in units of the ambient mean speed. R is the ratio of beam speed to ambient mean speed.

MAXWELLIAN ENERGY DISTRIBUTION

The (dimensionless) Maxwellian differential energy distribution function $f(\xi)$ is

$$f(\xi) = 2\sqrt{\frac{\xi}{\pi}}\exp(\xi), \qquad \xi \equiv \frac{\frac{1}{2}MV^2}{kT}. \qquad (\text{F1a,1b})$$

The integral distribution $F(\xi)$ is

$$F(\xi) = \int_0^\xi f(\xi')\,d\xi' = -f(\xi) + \text{Erf}\left[\sqrt{\xi}\right] \qquad (\text{F2})$$

where $\text{Erf}(x)$ is the error function,

$$\text{Erf}(x) = \frac{2}{\sqrt{\pi}}\int_0^x \exp(-t^2)\,dt. \qquad (\text{F3})$$

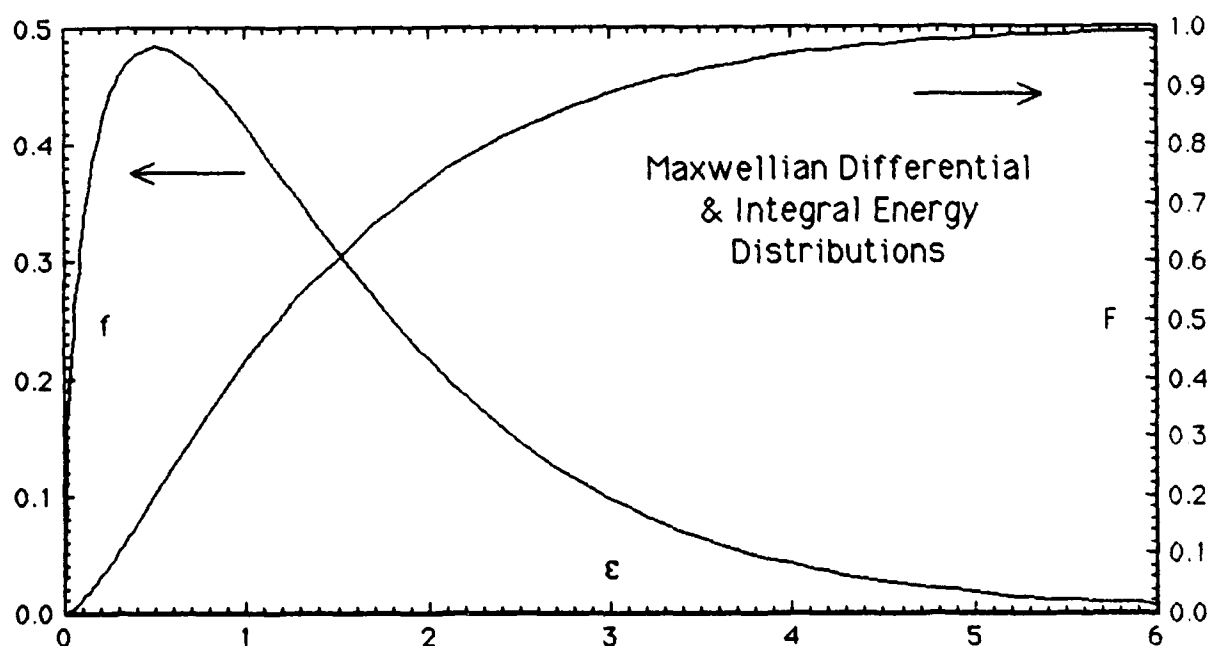Figure 22 shows the differential and integral distribution functions.

Figure 22. Differential $[f(\varepsilon)]$ and integral $[F(\varepsilon)]$ Maxwellian energy distributions.

DISTRIBUTION LIST

DNA-TR-88-37

DEPARTMENT OF DEFENSE

ASSISTANT TO THE SECRETARY OF DEFENSE
ATOMIC ENERGY
    ATTN: EXECUTIVE ASSISTANT

DEFENSE INTELLIGENCE AGENCY
    ATTN: RTS-2B

DEFENSE NUCLEAR AGENCY
    ATTN: PRPD R YOHO
    ATTN: RAAE A MARDIGUIAN
    ATTN: RAAE K SCHWARTZ
    ATTN: RAAE L WITTWER
    ATTN: RAAE S BERGGREN
4 CYS ATTN: TITL

DEFENSE TECHNICAL INFORMATION CENTER
2 CYS ATTN: DTIC/FDAB

STRATEGIC AND THEATER NUCLEAR FORCES
    ATTN: DR E SEVIN

STRATEGIC DEFENSE INITIATIVE ORGANIZATION
    ATTN: DR O JUDD
    ATTN: EN
    ATTN: PTN C GIESE
    ATTN: PTP COL RIVA
    ATTN: PTP LTC SEIBERLING
    ATTN: TN
2 CYS ATTN: TNS MAJ IMKER

DEPARTMENT OF THE ARMY

U S ARMY FOREIGN SCIENCE & TECH CTR
    ATTN: DRXST-SD

U S ARMY MISSILE COMMAND
    ATTN: AIAMS-S/B J GAMBLE

U S ARMY NUCLEAR & CHEMICAL AGENCY
    ATTN: MONA-NU

U S ARMY STRATEGIC DEFENSE CMD
    ATTN: CSSD-H-SA
    ATTN: CSSD-H-SA/R SMITH
    ATTN: CSSD-IN-T M POPE

DEPARTMENT OF THE AIR FORCE

AIR FORCE GEOPHYSICS LABORATORY
    ATTN: OP/A RATKOSKY
    ATTN: OP/W BLUMBERG
    ATTN: OPE/H GARDINER
    ATTN: SUL

AIR FORCE OFFICE OF SCIENTIFIC RSCH
    ATTN: AFOSR/NC
    ATTN: AFOSR/NP

DEPARTMENT OF ENERGY

LAWRENCE LIVERMORE NATIONAL LAB
    ATTN: A GROSSMAN

    ATTN: G SIMONSON
    ATTN: H KRUGER

LOS ALAMOS NATIONAL LABORATORY
    ATTN: MS P364

SANDIA NATIONAL LABORATORIES
    ATTN: CODE 9014 R BACKSTROM
    ATTN: ORG 9114
    ATTN: TECH LIB
    ATTN: 2000

DEPARTMENT OF DEFENSE CONTRACTORS

AERODYNE RESEARCH, INC
    ATTN: C KOLB

AEROSPACE CORP
    ATTN: C CREWS
    ATTN: C RICE
    ATTN: G LIGHT

BERKELEY RSCH ASSOCIATES, INC
    ATTN: J WORKMAN

EOS TECHNOLOGIES, INC
    ATTN: B GABBARD

INSTITUTE FOR DEFENSE ANALYSES
    ATTN: E BAUER

JAMIESON SCIENCE & ENGINEERING
    ATTN: J JAMIESON

KAMAN SCIENCES CORP
    ATTN: DASIAC
    ATTN: E CONRAD
    ATTN: G DITTBERNER

LOCKHEED MISSILES & SPACE CO, INC
    ATTN: J HENLEY
    ATTN: R SEARS

MISSION RESEARCH CORP
    ATTN: R ARMSTRONG

MISSION RESEARCH CORP
    ATTN: D ARCHER

PHOTOMETRICS, INC
    ATTN: I L KOFSKY

PHYSICAL RESEARCH, INC
    ATTN: T STEPHENS

PHYSICAL RESEARCH, INC
    ATTN: J DEVORE

PHYSICAL SCIENCES, INC
    ATTN: G CALEDONIA

R & D ASSOCIATES
    ATTN: F GILMORE

SCIENCE APPLICATIONS INTL CORP
2 CYS ATTN: D HAMLIN

SCIENCE APPLICATIONS INTL CORP
    ATTN. E HYMAN

TECHNOLOGY INTERNATIONAL CORP
    ATTN: W BOQUIST

UNITED TECHNOLOGIES RESEARCH CTR
    ATTN: H MICHELS

VISIDYNE, INC
    3 CYS ATTN: J CARPENTER